Mfsd8 regulates growth and multicellular development in *Dictyostelium discoideum*

A Thesis Submitted to the Committee of Graduate Studies in Partial Fulfillment of the Requirements for Degree of Master of Science in the Faculty of Arts and Science

TRENT UNIVERSITY
Peterborough Ontario, Canada
© Copyright by Shyong Quan Yap 2021
Environmental and Life Science M.Sc. Graduate Program
January 2022

Abstract

Mfsd8 regulates growth and multicellular development in *Dictyostelium discoideum*

Shyong Quan Yap

The neuronal ceroid lipofuscinoses (NCLs), commonly known as Batten disease, are a family of inherited neurodegenerative lysosomal storage disorders. CLN7 disease is a subtype of NCL that is caused by mutations in the *MFSD8* gene. *MFSD8* encodes a lysosomal transmembrane protein that is predicted to play a role in transporting small substrates across membranes. However, little is known about its role and substrate specificity. Previous work identified an ortholog of human *MFSD8* in the social amoeba *Dictyostelium discoideum* and reported its localization to endocytic compartments. In this study, the effects of *mfsd8* loss during *Dictyostelium* growth and multicellular development were further characterized. *Dictyostelium mfsd8*$^-$ cells displayed increased rates of proliferation and pinocytosis in liquid media. During growth, loss of *mfsd8* altered lysosomal enzymatic activities and reduced the intracellular and extracellular levels of autocrine proliferation repressor A. *mfsd8*$^-$ cells grown on a lawn of bacteria formed plaques in a shorter period of time compared to WT cells, providing additional support for the enhanced growth of *mfsd8*$^-$ cells. Upon starvation, the aggregation of *mfsd8*$^-$ cells was delayed, and *mfsd8*$^-$ cells formed more mounds that were smaller in size, which may be attributed to the reduced cell-substrate adhesion and altered lysosomal enzymatic activities observed for *mfsd8*$^-$ cells. Following aggregation, tipped mound formation was delayed, however, loss of *mfsd8* did not affect the timing of slug/finger and fruiting body formation. Additionally, slug migration was reduced in *mfsd8*$^-$ cells. These aberrant phenotypes, excluding fruiting body formation, were effectively or partially rescued when Mfsd8-GFP was introduced into *mfsd8*$^-$ cells. Overall, these results show that Mfsd8

plays a role in regulating growth and developmental processes in *Dictyostelium* via lysosomal-associated functions.

Keywords: NCLs, Batten disease, lysosomes, *Dictyostelium discoideum*, CLN7, MFSD8, AprA, Cln3, Cln5, CtsD

Acknowledgements

Research is the discovery of the unknown and I am grateful to be a part of the scientific world, unraveling mysteries one experiment at a time to piece together this gigantic jigsaw puzzle. Doing research has most certainly been a humbling experience for me.

First and foremost, I would like to offer my utmost gratitude to my supervisor, Dr. Robert Huber, for the opportunity to conduct research in his lab. His support and guidance have helped me grow professionally as a researcher in many aspects such as critical thinking, writing, and public speaking. His availability, speedy response to emails and reassurance have been very helpful and comforting especially during the pandemic.

I would also like to thank my committee members, Dr. Carolyn Kapron and Dr. Erin Morrison, for their time and constructive feedback during my committee meetings. Their assistance has refined and solidified the structure of my thesis. Dr. Huber, Dr. Kapron, and Dr. Morrison have also been very accommodating and considerate of my timeline to graduate which I am very grateful for.

I am thankful for my mentors, Sabateeshan Mathavarajah and Meagan McLaren, who have been great role models and have inspired me to pursue this area of research. They have taught me various techniques and skills in the Huber lab. Their patience and guidance are highly appreciated. I am also grateful to the current Huber lab members, Megan Aoki, William Kim, Morgan Wilson-Smillie and Aruban Thanabalasingam for being great researchers, motivators, and excellent company, especially during long days in the lab.

Finally, I would also like to thank my family and friends for their unconditional love, support, and encouragement that they have provided me throughout my time as a Master student. They have uplifted me when lab work gets rough and constantly show their support even when they are 8000 miles away. Lastly, I want to give a special shout out to my sister, Evelynn Yap, for always taking care of me and making sure that I am mentally, emotionally, and physically well.

Table of Contents

List of Tables

List of Figures

List of Abbreviations

ABC	ATP-binding cassette
AcbA	Acyl Coenzyme A binding protein,
AprA	Autocrine proliferation repressor A
ATP13A2	ATPase Cation Transporting 13A2
bsr	Blasticidin resistance
cAMP	3',5'-cyclic adenosine monophosphate
Car	cAMP receptor
CB	Conditioned starvation buffer
CF	Counting factor
CfaD	Counting factor associated protein A
CLN	Ceroid neuronal lipofuscinosis protein
CM	Conditioned growth media
CMF	Conditioned media factor
CotB	Spore coat protein SP70
CprA	Cysteine protease 1
CrlA	cAMP receptor-like A
CSPα	Cysteine string protein α
CTSD/CD	Cathepsin D
CTSF	Cathepsin F
DNAJC5	DnaJ homolog subfamily C member 5
ER	Endoplasmic reticulum
G418	Geneticin

GFP	Green fluorescent protein
GFP-Mfsd8	N-term GFP tagged Mfsd8
GSK-3	Glycogen synthase kinase 3
GWDI	Genome Wide *Dictyostelium* Insertion
Gα5	G-protein α 5
HRP	Horseradish peroxidase
KCTD7	Potassium Channel Tetramerization Domain Containing 9
LSD	Lysosomal storage disorder
MEFs	Mouse embryonic fibroblasts
MFS	Major Facilitator Superfamily
MFSD8	Major Facilitator Superfamily Domain 8
Mfsd8-GFP	C-term GFP tagged Mfsd8
mTOR	mammalian/mechanistic target of rapamycin
mTORC	mTOR Complex
NCLs	Neuronal ceroid lipofuscinoses
p80	Protein 80
PFKFB3	6-phosphofructo-2-kinase/fructose-2,6-bisphosphatase-3
PGRN	Progranulin
PI3K/Akt	Phosphoinositide-3-kinase–protein kinase B/Akt
PPT1	Palmitoyl thioesterase 1
REMI	Restriction Enzyme Mediated Integration
RHEB	Ras Homolog, MTORC1 Binding
SAPs	Sphingolipid activator proteins

SCMAS	Subunit c of mitochondrial ATP synthase
SDF-2	Spore differentiation factor 2
SM	Sussman Maurice
TBCK	TBC1 domain-containing kinase
TORC1	TOR complexes 1
TORC2	TOR complexes 2
TPP1	Tripeptidyl peptidase 1
VatC	Vacuolar ATPase subunit C

1. Introduction

1.1 Lysosomes in the endomembrane system

The endomembrane system of a eukaryotic cell is a dynamic network of membranous components that allows for the compartmentalization of various functions and processes (Søreng et al., 2018; Wang, 2014). The interconnected network comprises the nuclear envelope, endoplasmic reticulum (ER), Golgi apparatus, endosomes, lysosomes, vesicles, and plasma membrane (Søreng et al., 2018; Wang, 2014). Through the aid of vesicles, these organelles interact dynamically to mediate fundamental processes including the synthesis, processing, trafficking, degradation, and secretion of biomolecules (Søreng et al., 2018; Wang, 2014).

Lysosomes function at the intersection between the endocytic, autophagic and secretory pathways (Ferguson, 2019). Intracellular and extracellular cargo is delivered to the lysosomes for degradation through the autophagic and endocytic pathways, respectively (Ferguson, 2019). Meanwhile, the secretory pathway replenishes the lysosome with newly synthesized lysosomal proteins from the ER (Ferguson, 2019). Aligned with its role in cellular waste disposal, lysosomes house hydrolases in an acidic environment that is maintained by the activity of ATP-dependent proton pumps (Hu et al., 2015). Macromolecules as well as unwanted cellular components and organelles are degraded by these enzymes and then recycled back into the cells for other purposes (e.g., energy production or building blocks for biosynthetic pathways) (Hu et al., 2015). Beyond their degradative and recycling role, lysosomes are also involved in secretion (Buratta et al., 2020). Lysosomal exocytosis is a process whereby lysosomal contents are released into the extracellular milieu upon fusion with the plasma membrane and this process is critical for cellular clearance and plasma membrane repair (Buratta et al., 2020). Apart from its secretory role, this acidic organelle

also facilitates ion homeostasis within its lumen as well as in other organelles (e.g., ER and mitochondria) through membrane contact sites (Trivedi et al., 2020).

In addition, lysosomes also serve as signaling hubs for cellular metabolism via the mechanistic/mammalian target of rapamycin (mTOR) signaling pathway (Laplante & Sabatini, 2009; Mony et al., 2016). In mammalian cells, the serine/threonine kinase mTOR exists in two structurally and functionally distinct signaling complexes, mTOR Complex 1 (mTORC1) and mTOR Complex 2 (mTORC2) (Fu & Hall, 2020). The presence of growth factors and amino acids stimulates the phosphoinositide-3-kinase–protein kinase B/Akt (PI3K/Akt) proliferation signaling pathway, which activates mTORC1 and its recruitment to the lysosome (Laplante & Sabatini, 2009; Puertollano, 2014). Subsequently, essential growth regulators are phosphorylated by active mTORC1 which ultimately leads to the upregulation of macromolecular synthesis, fueling cell growth (Laplante & Sabatini, 2009; Puertollano, 2014). On the other hand, when nutrients are depleted, mTORC1 activity is repressed and its dissociation from the lysosomes activates autophagy, induces lysosomal biogenesis, and promotes the formation of autophagosomes, to meet the energy demands of the cell (Laplante & Sabatini, 2009; Puertollano, 2014). Interestingly, studies have found that, under prolonged periods of starvation, mTORC1 can be reactivated by simple metabolites such as amino acids that are generated through autophagy (Yu et al., 2010). mTORC1 reactivation is accompanied by a process known as autophagic lysosome reformation (ALR), where functional lysosomes are regenerated from autophagosomes (Puertollano, 2014). While activated mTORC1 resides at the lysosomes during nutrient-rich conditions, mTORC2 appears to localize to various subcellular locations, including the plasma membrane and subpopulations of endosomal vesicles, and its activity is dependent on its localization (Fu & Hall, 2020). Besides its well-established role in regulating the actin cytoskeleton, accumulating evidence

suggests that, upon growth factor stimulation, mTORC2 works upstream of mTORC1 activity by facilitating the phosphorylation of Akt in the PI3K/Akt proliferation signaling pathway (Fu & Hall, 2020; Saxton & Sabatini, 2017). Although the functional significance of mTORC2 association with lysosomes has not been well established, recent work revealed that lysosomal positioning influences the reactivation of mTORC2 and Akt signaling upon serum replenishment and mTORC2 activity is necessary for lysosomal acidification (Jia & Bonifacino, 2019; Monteith et al., 2018). Given that lysosomes play a plethora of roles within the cell, perturbations in lysosomal functions can result in broad detrimental effects and such defects have been implicated in many human diseases including neurodegenerative diseases and lysosomal storage disorders (LSDs) (Bonam et al., 2019).

LSDs are a heterogenous group of inherited metabolic diseases, with estimated incidences ranging from 1 in 5,000 human live births for common forms of LSDs to 1 in 250,000 human live births for rare forms of LSDs (Platt et al., 2018). LSDs are caused by mutations in genes encoding for lysosomal hydrolases and membrane proteins as well as proteins involved in trafficking, and non-lysosomal proteins (Platt et al., 2018). Mutations in these genes are responsible for over 70 different inherited LSDs including Fabry disease, Gaucher disease, Tay-Sachs disease, and the neuronal ceroid lipofuscinoses (NCLs) (Platt et al., 2018) (Table 1). In these diseases, there is an excessive accumulation of certain substrates in lysosomes as a result of aberrant lysosomal function (i.e., defects in processing and degradation of these substrates) (Platt et al., 2018). Consequently, substrate accumulation ultimately leads to cell death and manifests as clinical abnormalities in organs such as the brain and heart (Platt et al., 2018). However, the precise mechanisms underlying substrate accumulation and how it leads to cellular and organ pathology observed in LSDs is still largely unknown.

Table 1. List of diseases caused by mutations in lysosomal enzymes

Disease	Enzyme	Accumulation of material
Gaucher disease	β-glucosidase	Glucocerebroside and glucosylsphingosine
α-mannosidosis	α-mannosidase	Mannose-rich oligosaccharides
GM1 gangliosidosis mannosidosis	β-galactosidase	GM1 ganglioside, keratan sulfate and oligosaccharides
Fabry disease	α-galactosidase	Globotriaosylceramide (Gb_3), lipopigment aggregates, α-synculein
Mucolipidosis type II (and type III)	β-N-glucosaminidase	Mutilamellar bodies, lipofusin, glycans, gangliosides
CLN1	Ppt1	Lipidated thioesters and saposins A and D
CLN2	Tpp1	Subunit c of mitochondrial ATP synthase
CLN10	CtsD	Saposins A and D
CLN13	CtsF	Unknown

1.2 The neuronal ceroid lipofuscinoses (NCLs)

The NCLs, commonly referred to as Batten disease, are a family of inherited neurodegenerative LSDs that affect population groups in all ethnicities (Mole & Coleman, 2015). The estimated worldwide incidence rates of Batten disease range from 2 of 100,000 human live births in the United States to 13 of 100,000 human live births in Newfoundland, Canada (Moore et al., 2008; Williams, 2011). These disorders are characterized histopathologically by the lysosomal accumulation of ceroid lipofuscin, specifically in the neuronal cells of the brain and retina (Radke et al., 2015). The accumulated lipofuscin is composed of sphingolipid activator proteins (SAPs) A and D and/or subunit c of mitochondrial ATP synthase (SCMAS) and its composition varies between the different NCL subtypes (Haltia, 2006). As the lipofuscin accumulates within the lysosomes, it impacts cellular trafficking, ultimately resulting in

neuroinflammation and neuronal loss (Platt, 2018). NCL patients suffer from epileptic seizures, progressive vision loss, a decline in mental and motor capacities and premature death (Schulz et al., 2013).

Mutations in 13 distinct genes have been linked to the NCLs (*CLN1*-*CLN8, CLN10*-*CLN14*) with each gene causing a different NCL subtype (e.g., mutations in *CLN1* causes CLN1 disease) (Mole & Cotman, 2015) (Table 2). CLN15 disease was recently classified as a new NCL subtype, which is caused by mutations in the *TBCK* (TBC1 domain-containing kinase) gene (Beck-Wödl et al., 2018). The NCL proteins localize to compartments of the endomembrane system (Cárcel-Trullols et al., 2015). CLN1/PPT1 (palmitoyl protein thioesterase 1), CLN2/TPP1 (tripeptidyl peptidase 1), CLN5 (ceroid lipofuscinosis neuronal 5), CLN10/CTSD (cathepsin D) and CLN13/CTSF (cathepsin F) localize to the lysosomal lumen, CLN3 (ceroid lipofuscinosis neuronal 3), CLN7/MFSD8 (major facilitator superfamily domain-containing 8) and CLN12/ATP13A2 (ATPase 13A2) are lysosomal transmembrane proteins, CLN6 (ceroid lipofuscinosis neuronal 6) and CLN8 (ceroid lipofuscinosis neuronal 8) reside in the ER, CLN4/DNAJC5 (DNAJC5, DnaJ heat shock protein family member)/CSPα (cysteine string protein α) and CLN14/KCTD7 (potassium channel tetramerization domain-containing 7) are cytosolic proteins associated with vesicular membranes, and CLN11/PGRN (progranulin) is a secreted glycoprotein (Cárcel-Trullols et al., 2015). While their functions and localizations differ, there is growing evidence showing the interaction between these proteins, pointing to the possibility that they may be involved in shared biological pathways (Huber, 2020; Persaud-Sawin et al., 2007). Notably, lysosomal dysfunction, such as impaired autophagic pathway and dysregulated lysosomal acidification, has been reported in all NCL subtypes (Mukherjee et al.,

2019). Nonetheless, despite intense research efforts, the physiological functions of these NCL proteins and how their deficiency leads to NCL pathology remain elusive.

To date, there is still no cure for the NCLs. Recent advances have successfully developed a treatment for CLN2 disease. The clinically approved drug known as Cerliponase alfa, which is a recombinant human proenzyme of TPP1, has been shown to be effective in slowing the progression of CLN2 disease (Schulz et al., 2018). Furthermore, pre-clinical and clinical trials for treatment of CLN1, CLN2, CLN3 and CLN6 disease using gene therapy show promising results (Rosenberg et al., 2019). Nevertheless, a few treatment approaches have been proposed for each NCL subtype and clinical trials for these treatments are well underway (Rosenberg et al., 2019). These studies highlight the need for and importance of elucidating the functions of NCL genes to develop therapeutic strategies for this family of neurodegenerative disorders.

Table 2. List of genes linked to the NCLs and their function and respective homologs in *Dictyostelium discoideum*

NCL gene	Associated disease(s)	Alternate name; function	*Dictyostelium* homolog
CLN1	CLN1 disease, infantile NCL	PPT1; Palmitoyl thioesterase	Ppt1
CLN2	CLN2 disease, Late-infantile NCL	TPP1; Serine protease	Tpp1
CLN3	CLN3 disease, Juvenile NCL	Transmembrane protein of unknown function	Cln3
CLN4	CLN4 disease, Adult autosomal, Kuf's diseases, Parry disease	DNAJC5/CSPα; Hsc70 co-chaperone	Ddj1
CLN5	CLN5 disease, Late-infantile NCL (Finnish variant)	Glycoside hydrolase	Cln5
CLN6	CLN6 disease, Early juvenile or late-infantile NCL	Transmembrane protein of unknown function	No homolog
CLN7	CLN7 disease, Late-infantile NCL (Turkish variant)	MFSD8; Transmembrane protein of unknown function	Mfsd8
CLN8	CLN 8 disease, Late-infantile NCL, progressive epilepsy with mental retardation	Trafficking receptor	No homolog
CLN10	CLN10 disease, Congenital neonatal and late-infantile NCL	CTSD; aspartic protease	CtsD
CLN11	CLN11 disease, Adult-onset NCL	PGRN; secreted glycoprotein	Grn
CLN12	CLN12 disease, Juvenile-infantile NCL	ATP13A2; transmembrane protein of unknown function	Kil2
CLN13	CLN13 disease, Adult-Kufs type B	CTSF; cysteine protease	CprA
CLN14	CLN14 disease, Infantile NCL	KCTD7; CUL3-E3 ubiquitin ligase linker	Kctd9

1.3 CLN7 disease

One of the NCL subtypes that is currently untreatable is ceroid lipofuscinosis neuronal 7 (CLN7) disease, a recessively inherited late-infantile variant of NCL (Elleder et al., 2011). The onset of disease symptoms usually begins between the ages of 1.5 and 6 years, with early symptoms such as epilepsy and development regression followed by ataxia, a rapid decline in mental and motor function, vision failure, myoclonus, and speech impairment, leading to premature death (Elleder et al., 2011; Kousi et al., 2009). CLN7 disease is caused by defects in the *CLN7* gene, also known as *MFSD8* (Elleder et al., 2011; Kousi et al., 2009). As of 2020, a total of 46 CLN7 disease-causing mutations have been identified in *MFSD8* (https://www.ucl.ac.uk/drupal/site_ncl-disease/mutation-and-patient-database). In post-mortem CLN7 disease patients, high amounts of SCMAS have been detected immunohistochemically in brain, heart and skeletal muscle (Elleder et al., 2011). Neural degeneration and storage accumulation have also been reported in the retinas of CLN7 disease patients (Elleder et al., 2011).

The *MFSD8* gene is ubiquitously expressed, albeit in low amounts, in various human tissues including skeletal muscle, lung, brain and heart (Siintola et al., 2007). *MFSD8* encodes a 518-amino acid, 58 kDa polytopic integral membrane protein that contains 12 transmembrane domains (Siintola et al., 2007). MFSD8 belongs to the major facilitator superfamily (MFS) of transporter proteins and the members of the MFS are predicted to transport small substrates such as ions, sugars, nucleosides, amino acids, and drugs across membranes using chemiosmotic ion gradients (Pao et al., 1998; Saier et al., 2016; Siintola et al., 2007). At present, the substrate specificity of MFSD8 remains unknown.

Human MFSD8 contains two *N*-glycosylation sites in positions N371 and N376 and a N-terminal dileucine motif that targets the protein to lysosomes (Sharifi et al., 2010; Steenhuis et al.,

2010; Steenhuis et al., 2012). Upon arrival to the lysosomes, MFSD8 is proteolytically cleaved twice by lysosomal cysteine proteases, in which one of the proteolytic events is mediated by cathepsin L (Steenhuis et al., 2012). The N- and C-terminal fragments generated by the two proteolytic events are then released into the extracellular space (Steenhuis et al., 2012). Biochemical analyses revealed the presence of endogenous MFSD8 in the membrane proteome of purified human and rat lysosomes (Bagshaw et al., 2005; Schröder et al., 2007). Colocalization studies further confirmed the localization of MFSD8 to late endosomes and lysosomes in cultured mouse hippocampal neurons, COS-1 fibroblast-like cells, *HeLa* cervical cancer cells, *Drosophila melanogaster* as well as in the lower eukaryote *Dictyostelium discoideum*, showing that its localization is evolutionarily conserved (Huber et al., 2020; Mohammed et al., 2017; Sharifi et al., 2010; Siintola et al., 2007). Interestingly, among the missense mutations tested, none of them affected the trafficking and localization of MFSD8, implying that mutations in *MFSD8* alter the function or structure of the protein instead of its localization (Kousi et al., 2009; Siintola et al., 2007). Together, these studies suggest that MFSD8 acts as a lysosomal transporter of an unknown substrate.

Mounting evidence has linked the role of MFSD8 to lysosomal-associated functions. In mammalian models, loss of *MFSD8* alters the levels of soluble lysosomal enzymes including NCL proteins such as CLN1, CLN5 and CLN10, which is indicative of lysosomal dysfunction (Brandenstein et al., 2016; Danyukova et al., 2018; von Kleist et al., 2019). Moreover, impaired lysosomal exocytosis and motility were apparent in immortalized cerebellar neuronal progenitor cells isolated from *Cln7*$^{-/-}$ mice (von Kleist et al., 2019). Mutant mouse models also displayed impaired autophagy, reduced cell survival and defects in mTORC1 signalling (Brandenstein et al., 2016; Danyukova et al., 2018; Lopez-Fabeul et al., 2020; von Kleist et al., 2019). Furthermore, in

Drosophila, loss of *Cln7* affects synapse size and function due to dysregulation of TOR signaling, which may further exacerbate the neurological decline observed in CLN7 disease (Connolly et al., 2019). Despite significant research progress, the function of the MFSD8 protein and how its loss leads to defects in lysosomal function and NCL pathology remain hitherto unclear.

Model organisms, such as mouse (*Mus musculus*), nematode (*Caenorhabditis elegans)*, fruit fly (*Drosophila melanogaster),* zebrafish (*Danio rerio*) and budding (*Saccharomyces cerevisiae*) and fission yeast (*Saccharomyces pombe*), have been used extensively in NCL research with the aim to uncover the functions of NCL proteins and the pathways they regulate (Cárcel-Trullols et al., 2015; Huber, 2020; Myre et al., 2018). Their genomes encode orthologs of some, if not all, NCL proteins (Huber, 2016). In addition, large animal models with mutations in *MFSD8* recapitulate key behavioral and neuropathological phenotypes seen in patients with CLN7 disease (Ashwini et al., 2016; Faller et al., 2016; Guo et al., 2015; McBride et al., 2018). These animal models include Japanese macaques (*Macaca fuscata*), Chinese Crested Dog and Chihuahuas (Ashwini et al., 2016; Faller et al., 2016; Guo et al., 2015; McBride et al., 2018). In light of recent research advances, the simple eukaryote, *Dictyostelium discoideum,* is now recognized as a powerful model organism for studying a variety of biological processes and functions of proteins associated with human diseases including the NCLs (Huber, 2016; Huber, 2020; Mathavarajah et al., 2017).

1.4 *Dictyostelium discoideum* as a CLN7 disease model

The social amoeba, *Dictyostelium discoideum,* undergoes a unique 24-hour life cycle that is tightly regulated by various extracellular signals (Consalvo et al., 2019; Fey et al., 2007; Loomis, 2014) (Fig 1B). During growth, single cells ingest bacteria by phagocytosis and divide mitotically

(Fey et al., 2007). Depletion of nutrients triggers dramatic transcription changes within *Dictyostelium* cells, which sets off a cascade of signaling pathways, resulting in the initiation of multicellular development (Mathavarajah et al., 2017). In response to starvation, cells chemotactically aggregate towards pulses of cyclic AMP (cAMP) to form a multicellular aggregate, known as a mound (Mathavarajah et al., 2017). Cells within mounds begin to differentiate into two specialized cell types, pre-spore and pre-stalk cells. The mound undergoes several morphological changes to form a finger that eventually falls over to form a migrating slug (Mathavarajah et al., 2017). During culmination, pre-spore and pre-stalk cells terminally differentiate to form a fruiting body composed of a stalk of dead vacuolated cells that support a mass of spores (Mathavarajah et al., 2017). When nutrients are made available again, the spores germinate and the life cycle re-starts (Mathavarajah et al., 2017).

Over the past few years, *Dictyostelium* has been gaining traction as an excellent model system for studying human diseases (Francione et al., 2011; Huber, 2016; Mathavarajah et al., 2017; Maniak, 2011). The rapid *Dictyostelium* life cycle, along with its genetic tractability, permits the study of mutational effects on a wide range of dynamic biological processes, all within 24 hours (Mathavarajah et al., 2017). Additionally, due to this species' conserved biological processes, findings from *Dictyostelium* can be easily translated to mammalian systems (Mathavarajah et al., 2017). Unlike budding and fission yeast, nematode, and fruit fly, the *Dictyostelium* genome encodes orthologs of 11 of the 13 NCL proteins (*CLN1-CLN5, CLN7, CLN10-CLN14*) (Huber, 2016) (Table 2). As a result, *Dictyostelium* presents as an ideal model system to study the cellular and developmental defects caused by mutations in NCL-like genes as well as the interactions between NCL proteins (Huber, 2016; Mathavarajah et al., 2017). For instance, recent work has linked the role of *Dictyostelium* Cln5 to autophagy and revealed its

interaction with other NCL-like proteins including Tpp1, CtsD and CprA (homolog of human CTSF) (Huber & Mathavarajah, 2018a; McLaren et al., 2021). Based on these studies, this amoeba is undoubtedly a good and versatile model system for NCL research.

The *Dictyostelium* genome encodes an ortholog of *MFSD8* (gene: *mfsd8,* protein: Mfsd8; DDB0307149) that has 29% exact identity and 47% similar identity to human MFSD8 (Huber et al., 2020; Rot et al., 2009). The *mfsd8* gene spans one exon and encodes a 498-amino acid, 55 kDa protein (Huber et al., 2020). *mfsd8* mRNA expression increases during the early stages of development and reaches peak levels after 8 hours (https://dictyexpress.research.bcm.edu/landing/) (Huber et al., 2020; Rot et al., 2009) (Fig 1A). Expression then decreases dramatically during the mid-stages of development and increases slightly between 20 to 24 hours (Huber et al., 2020) (Fig 1A). Based on its expression profile, Mfsd8 is predicted to play an important role in chemotaxis, aggregation and fruiting body formation. Furthermore, proteomic analysis using high-resolution mass spectrometry showed that Mfsd8 localizes to macropinosomes (Journet et al., 2011). Nonetheless, the role of Mfsd8 in *Dictyostelium* has not been explored in-depth until recently.

Through sequence analysis, Huber et al. (2020) showed that the N-terminal dileucine-based lysosomal targeting signal sequence in human MFSD8 is partially conserved in the *Dictyostelium* Mfsd8. Accordingly, akin to findings in mammalian models, *Dictyostelium* Mfsd8 localizes to late endosomes and acidic intracellular compartments (Huber et al., 2020; Sharifi et al., 2010; Siintola et al., 2007). Interactome analysis using mass spectrometry revealed that Mfsd8 interacts with proteins that are linked to pathways that regulate nuclear architecture, cell polarity and movement, protein folding, lipid and glucose metabolism, and ion transporters during growth (Huber et al., 2020). During starvation, Mfsd8-interactors are associated with all the processes revealed for

growth-stage interactors except for lipid metabolism (Huber et al., 2020). Additionally, pull-down assays showed that Mfsd8 interacts with proteins that have been linked to Cln3 and Cln5 function, namely CtsD, another NCL protein (Huber et al., 2020). Further western blot analysis confirmed the interaction between Mfsd8 and CtsD during growth conditions (Huber et al., 2020). Using a *mfsd8* knockout mutant (*mfsd8*$^{-}$), Huber et al. (2020) also demonstrated that Mfsd8 influences the secretion of Cln5 and CtsD. However, the role of Mfsd8 during both growth and development were not addressed in this study.

1.5 Aims, hypotheses and rationale

Lysosomes play an important role during each stage of the *Dictyostelium* life cycle. Within the cells, lysosomal enzymes are differentially expressed during the life cycle (Fig 2) (Rot et al., 2009). Several lysosomal enzymes, namely α-mannosidase, β-glucosidase, N-acetylglucosaminidase, acid phosphatase, leucine aminopeptidase, alanine transaminase, and proteases, are upregulated and secreted during growth and early development, highlighting the importance of these enzymes in regulating growth, chemotaxis, and aggregation (Burns et al., 1981; Dimond et al., 1981; Rossomando et al., 1978). Additional support of these findings came from the observation that 80% of the mutants with defective lysosomal enzyme secretion were arrested at the aggregation stage of development (Ebert et al., 1990). Furthermore, Dimond et al. (1973) showed that gene mutants for N-Acetyl glucosaminidase showed little accumulation of the enzyme and, as a result, formed small migrating slugs with reduced migration. Hence, the regulation and secretion of lysosomal enzymes is critical throughout the *Dictyostelium* life cycle.

Like mammalian cells, nutrient depletion induces autophagy and promotes the formation of autophagosomes in *Dictyostelium* via the inhibition of TORC1 activity (Kosta et al., 2004).

During development, *Dictyostelium* cells are highly reliant on autophagy, which takes place in the lysosomes where the cell's own components are broken down for energy production and simple metabolites required for aggregation and terminal differentiation (Otto et al., 2003). Non-recycling roles of autophagy include regulation of the later stages of *Dictyostelium* development. For instance, autophagy is involved in the formation of vacuolated dead stalk cells, which precedes stalk cell differentiation (Uchikawa et al., 2011). Consequently, autophagy mutants display abnormal developmental phenotypes (e.g., multi-tipped mounds) (Otto et al., 2003). Taken together, these studies reveal that normal lysosomal function is essential for both cellular and developmental processes in *Dictyostelium*.

Given the localization of *Dictyostelium* Mfsd8 to endocytic compartments as well as findings indicating lysosomal dysfunction in other CLN7 disease models, in the present study, I hypothesize that *Dictyostelium* Mfsd8 plays a critical role in regulating lysosomal function. I predict that cellular and developmental processes in *Dictyostelium,* such as cell proliferation, pinocytosis, aggregation and development, will be affected due to altered lysosomal function caused by *mfsd8* deficiency. Therefore, this study aims to investigate the role of Mfsd8 during *Dictyostelium* growth and development. Findings from this study could provide insight into the links between *mfsd8*-deficiency and CLN7 disease pathology in relation to lysosomal dysfunction. As many biological pathways are conserved in *Dictyostelium*, findings from this study can also be easily translated to mammalian models of CLN7 disease. Furthermore, by delineating the function of Mfsd8, this study could aid in developing therapeutic strategies for CLN7 disease.

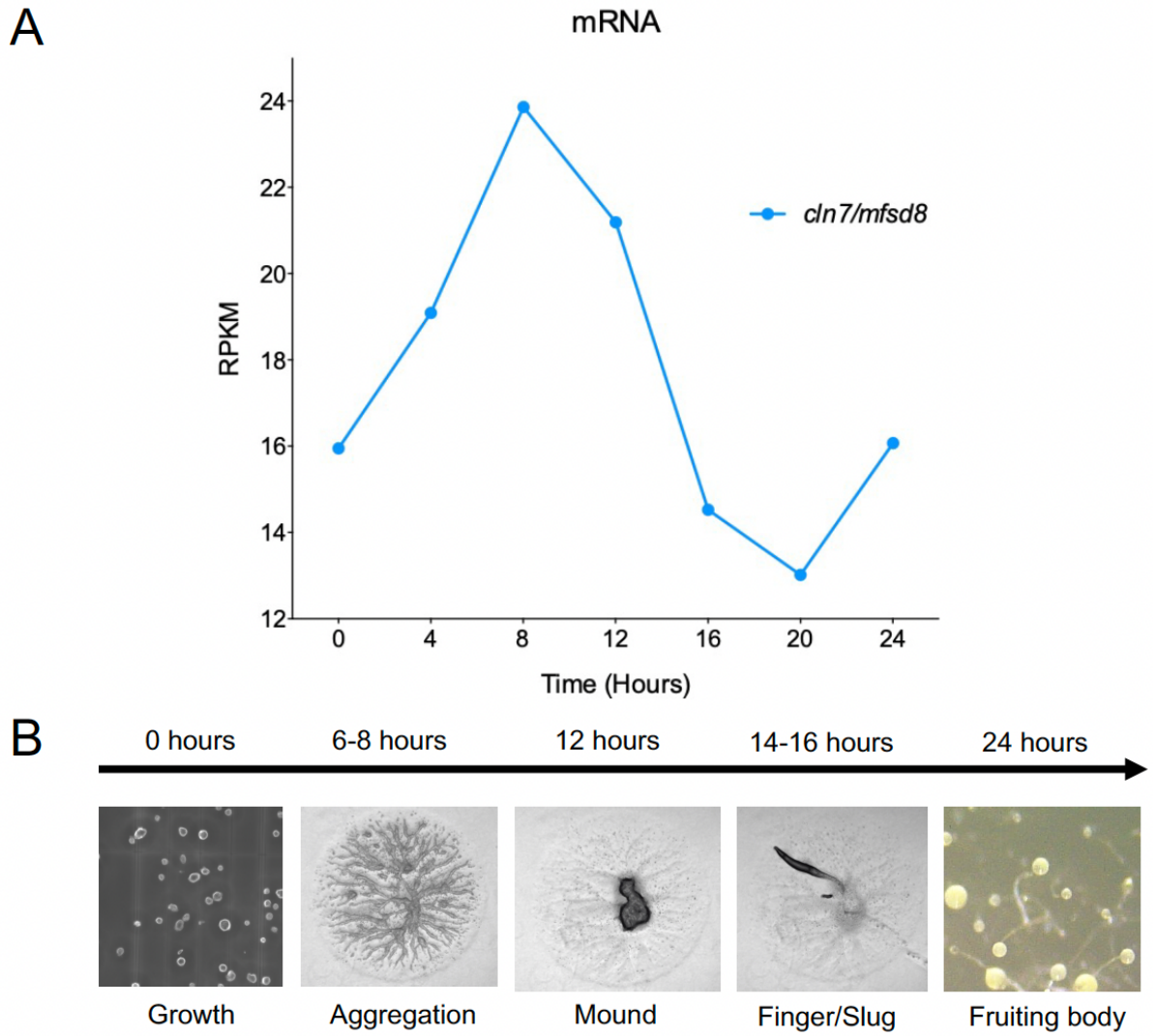

Figure 1. Gene expression analysis of *mfsd8* during the *Dictyostelium* life cycle. (A) Gene expression profile of *cln7/mfsd8* during the *Dictyostelium* life cycle obtained from dictyExpress (https://dictyexpress.research.bcm.edu/landing/) (Rot et al., 2009). RPKM, Reads per kilo base per million mapped reads. (B) Timeline showing the unique 24-hour *Dictyostelium* life cycle that consists of a unicellular growth phase and a multicellular developmental phase. In the presence of nutrients, *Dictyostelium* cells feed on bacteria and divide mitotically. Depletion of the food source prompts multicellular development. Upon starvation, cells chemotactically aggregate towards pulses of cyclic AMP to form a multicellular aggregate, known as a mound. Cells within mounds then differentiate into two specialized cell types, pre-spore and pre-stalk cells. The mound undergoes several morphological changes to form a finger, which eventually topples over to form a migrating slug. During culmination, pre-spore and pre-stalk cells terminally differentiate to form a fruiting body, which is composed of a stalk of dead vacuolated cells that support a mass of spores. When nutrients are made available again, the spores germinate and the life cycle re-starts. Images were taken at different magnifications.

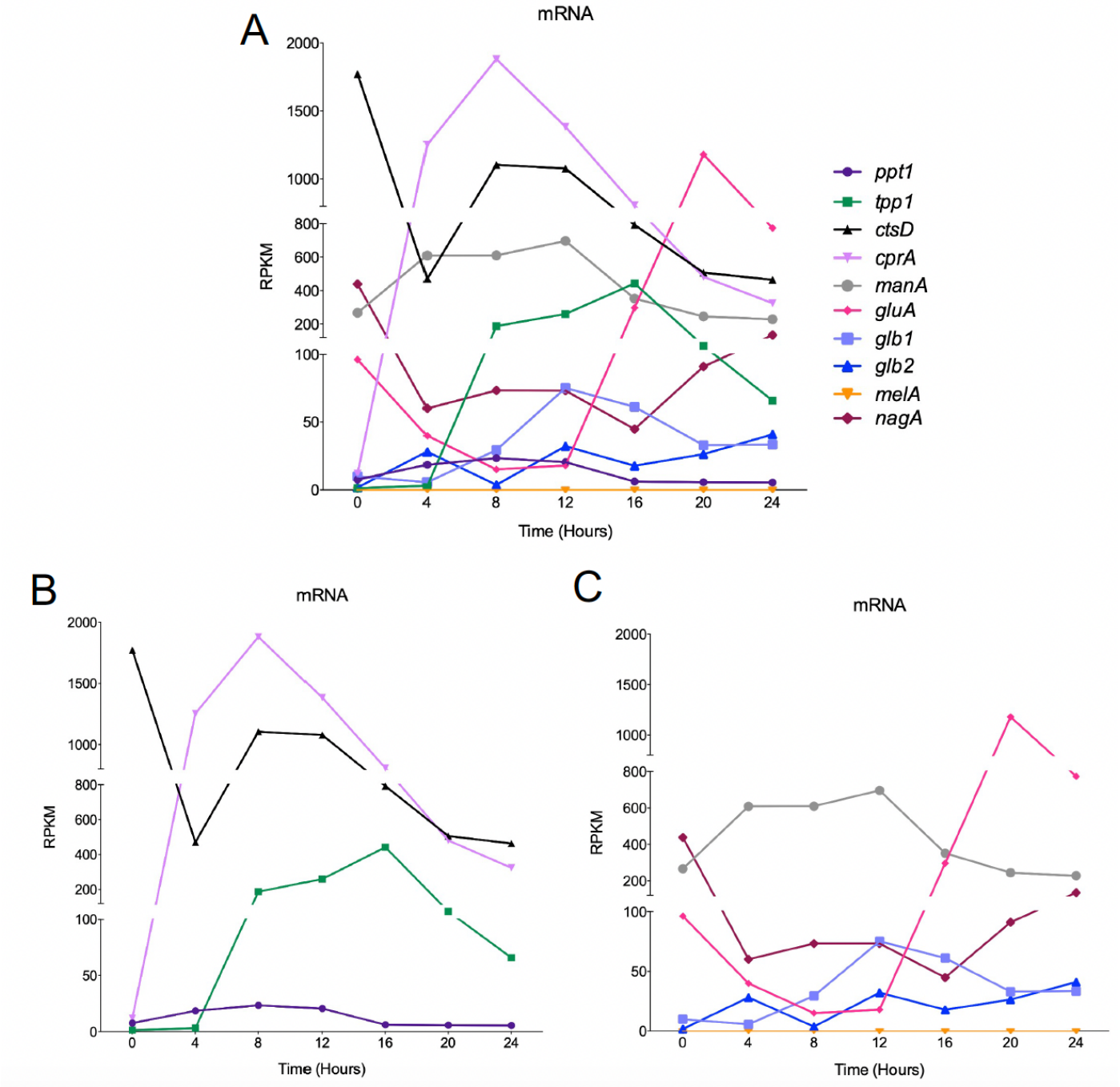

Figure 2. Gene expression analysis of lysosomal enzymes in *Dictyostelium* (A) Gene expression profile of all the homologs of lysosomal enzymes examined in the study. RNA-seq data was obtained from dictyExpress (https://dictyexpress.research.bcm.edu/landing/) and replotted in Excel (Rot et al., 2009). Genes were grouped together according to lysosomal enzymes that are associated with the NCLs and those that are not. (B) Expression profiles of homologs of NCL lysosomal enzymes. *ppt1* encodes for palmitoyl-protein thioesterase 1, *tpp1* encodes for tripeptidyl peptidase 1, *ctsD* encodes for cathepsin D and *cprA* encodes for cysteine proteinase A. (C) Expression profiles of homologs of lysosomal enzymes that are not associated with the NCLs. *gluA* encodes for β-glucosidase, *manA* encodes for α-mannosidase A, *glb1* and *glb2* encode for β-galactosidase 1 and β-galactosidase 2, *melA* encodes for putative α-galactosidase, *nagA* encodes for N-Acetyl glucosaminidase. RPKM, Reads per kilo base per million mapped reads.

2. Materials and Methods

2.1 Cell Culture, chemicals, media, and antibodies

AX4, the parental line of *mfsd8*$^{-}$ cells, was obtained from the Dicty Stock Center and hereafter will be referred to as the wild-type (WT) cell line (Fey et al., 2013). The *mfsd8*$^{-}$ cell line was purchased from the Genome Wide *Dictyostelium* Insertion (GWDI) bank via the Dicty Stock Center (https://remi-seq.org) (Fey et al., 2013). All cell lines were grown on Sussman Maurice (SM) agar with *Klebsiella aerogenes* and maintained at 21°C (Fey et al., 2007). Cells were also grown axenically in HL5 supplemented with ampicillin (100 µg/mL) and streptomycin sulfate (300 µg/mL) at 21°C on a rotary shaker at 150 rpm (Bioshop, Burlington, ON, CA) (Fey et al., 2007). *mfsd8*$^{-}$ cells carrying a blasticidin S resistance (bsr) cassette were selected using blasticidin S hydrochloride (10 µg/mL) (Bioshop, Burlington, ON, CA) (Faix et al., 2013). Cells carrying the extrachromosomal vector pDM323 (C-term GFP-fusion) were selected using Geneticin (G418, 25 µg/mL) (Bioshop, Burlington, ON, CA) (Levi et al., 2000; Veltman et al., 2009). Cells were harvested in mid-log phase of growth (1-5 x 10^6 cells/mL) for experiments described below (Fey et al., 2007).

HL5 and low-fluorescence HL5 were purchased from Formedium (Hunstanton, Norfolk, UK). KK2 buffer (0.7 g/L of anhydrous K_2HPO_4, 2.2 g/L of anhydrous KH_2PO_4, pH 6.5) was used as the starvation buffer. 2-N-morpholinoethanesulfonic acid (MES) was purchased from Fisher Scientific Company (Ottawa, ON, CA). Mouse monoclonal anti-VatC (224–256-2) and mouse monoclonal anti-p80 (H161) were purchased from the Developmental Studies Hybridoma Bank (University of Iowa, Iowa City, IA, USA). Mouse monoclonal anti-β-actin was purchased from Santa Cruz Biotechnology Incorporated (Santa Cruz, CA, USA), while rabbit polyclonal anti-GFP

was purchased from Fisher Scientific Company (Ottawa, ON, CA). Rabbit polyclonal anti-AprA was provided as a gift by Dr. Richard Gomer (Texas A&M University, College Station, TX, USA). Horseradish peroxidase (HRP)-conjugated and Alexa Fluor-conjugated secondary antibodies were purchased from New England Biolabs (Whitby, ON, CA) and Fisher Scientific Company (Ottawa, ON, CA), respectively. Enzyme substrates were purchased from different suppliers and listed in Table 3.

2.2 *Dictyostelium* transformation

The expression construct for Mfsd8 fused to a C-terminal GFP tag (Mfsd8-GFP) was generated in a previous study using the C-term GFP fusion plasmid pDM323 (Huber et al., 2020). In this study, this construct was transformed into freshly germinated *mfsd8*$^{-}$ cells (Gaudet et al., 2007). Briefly, *mfsd8*$^{-}$ cells (1×10^{8} cells/mL) were collected and washed twice with ice cold E buffer (10 mM $NaPO_4$, 5b0 mM sucrose, pH 6.1). Cells were mixed with plasmid DNA in a prechilled electroporation cuvette (Fisher Scientific Company, Ottawa, ON, Canada) and pulsed with two 1.0 V surges using a MicroPulser electroporator (Bio-Rad Laboratories Limited, Mississauga, ON, CA), after which time the cuvette was incubated on ice for 5 minutes. 100 mM $CaCl_2$ and 100 mM $MgCl_2$ were added to the electroporated cells to a final concentration of 1 mM each. G418 (25 μg/mL) was added to transformed cells the next day to select for transformants (Gaudet et al., 2007). The recovery line, *mfsd8*$^{-}$ + Mfsd8-GFP, was then validated using western blotting and immunolocalization. The following primary and secondary antibodies were used for western blotting: anti-GFP (1:1000), anti-β-actin (1:1000), and HRP-conjugated secondary antibodies (1:2000). The following primary and secondary antibodies were used for immunolocalization: anti-VatC (1:50), anti-p80 (1:50), and anti-mouse Alexa Fluor 555 (1:100).

Cells were also lysed, separated by SDS-PAGE and analyzed by western blotting. *mfsd8*$^{-}$ + Mfsd8-GFP cells were used in conjunction with WT and *mfsd8*$^{-}$ for assays described in the sections below.

2.3 Cell proliferation, pinocytosis and cell size analyses

To examine cell proliferation, cells in the mid-log phase of growth were washed thrice with fresh HL5 (Huber et al., 2014). Cells were then diluted to 1–2 × 10^5 cells/mL in HL5 and incubated at 21°C and 150 rpm (Huber et al., 2014). Cell concentrations were measured every 24 hours over a 144-hour growth period using a hemocytometer (Huber et al., 2014). Results were obtained from 5 independent experiments.

The pinocytosis assay was conducted using a method described elsewhere (Huber et al., 2014; Rivero & Makiak, 2006). Briefly, cells in the mid-log phase of growth were placed in HL5 at a density of 5 x 10^6 cells/mL. 100 µL of a 20 mg/mL FITC-dextran (70,000 M_r) stock solution was added to the 5 mL suspension and cells were incubated for 120 minutes at 150 rpm. 500 µL of cells were collected every 15 minutes, washed twice with ice-cold Sorenson's buffer (2 mM Na_2HPO_4, 14.6 mM KH_2PO_4, pH 6.0) and lysed with 1 mL of pinocytosis lysis buffer (50 mM Na_2HPO_4, pH 9.3, 0.2% Triton-X). Lysates were added to separate wells of black bottom 96-well plates and fluorescence was measured using a BioTek Synergy HTX plate reader (excitation 470 nm, emission 515 nm) (BioTek Instruments Incorporated, Winooski, VT, USA). Results were obtained from 3 independent experiments. The data were corrected for background signals and expressed as the mean % fluorescence change relative to the 0-minute time point.

The cell area was measured as an indicator of cell size as area would change with the shape of the cells. Briefly, cells in the mid-log phase of growth were deposited onto a hemocytometer. Cells were imaged with a Nikon Ts2R-FL inverted microscope equipped with a Nikon 10 Digital

Sight Qi2 monochrome camera (Nikon Canada Incorporated Instruments Division, Mississauga, ON, CA). The area of each individual cell was quantified using ImageJ/Fiji. Results were obtained from 5 independent experiments and placed into different ranges of cell area. The data were expressed as the mean % of total cells analyzed. Statistical significance was assessed in GraphPad Prism 8 (GraphPad Software Incorporated, La Jolla, CA, USA) using two-way ANOVA followed by Bonferroni's multiple comparison test. A p-value < 0.05 was considered significant.

2.4 Protein secretion analysis

To assess the effect of *mfsd8*-deficiency on the intracellular and extracellular levels of AprA, cells were grown axenically in HL5 and harvested after 24, 48, and 72 hours of growth (Huber et al., 2014). Cells were lysed with Nonidet P40 (NP40) lysis buffer (50 mM Tris–HCl pH 8.0, 150 mM sodium chloride, 0.5% NP40) supplemented with a Pierce™ protease inhibitor tablet (Thermo Fisher Scientific, Whitby, ON, CA). Conditioned media (CM) were collected and standardized based on cell number (1×10^6 total). Whole cell (WC) lysates (10 µg) and equal volume of samples of CM were separated by SDS-PAGE and analyzed by western blotting. The following primary and secondary antibodies were used: anti-AprA (1:1000), anti-β-actin (1:1000), and HRP-conjugated secondary antibodies (1: 2000). Identified bands of WC lysates and samples of CM were quantified using ImageJ/Fiji. Intracellular AprA protein levels were normalized against β-actin levels.

To assess whether there is a defect in global protein secretion during growth, samples of CM were separated by SDS-PAGE and stained using the Pierce™ Silver Stain Kit (Thermo Fisher Scientific, Whitby, ON, CA). Each lane was quantified using ImageJ/Fiji. Results were obtained from 7-8 independent experiments and the data were expressed as mean protein amount relative

to WT at each timepoint. Statistical significance was determined in GraphPad Prism 8 (GraphPad Software Incorporated, La Jolla, CA, USA) using a one-sample t-test (mean, 100; two-tailed). A p-value < 0.05 was considered significant.

2.5 Plaque expansion assay

Three full loops of *Klebsiella aerogenes* were collected using an inoculating loop and resuspended in KK2 buffer. 25 µL of KK2 buffer containing *Klebsiella aerogenes* were deposited onto SM plates two days prior to conducting the assay. Cells were harvested in the mid-log phase of growth and washed thrice with KK2 buffer to remove any remaining HL5 media. Cells (0.1 x 10^6 cells total) were resuspended in KK2 buffer and deposited onto the center of the *Klebsiella aerogenes* lawn. Plaques were captured at the indicated time points using a Leica EZ4W stereomicroscope equipped with an internal 5MP CMOS camera (Leica Microsystems Incorporated, Concord, ON, CA). The diameters of fully formed plaques were quantified using ImageJ/Fiji. Results were obtained from 4 biological replicates averaged from 2 technical replicates. Statistical significance was assessed in GraphPad Prism 8 (GraphPad Software Incorporated, La Jolla, CA, USA) using two-way ANOVA followed by Bonferroni's multiple comparison test. A p-value < 0.05 was considered significant.

2.6 Aggregation and mound size analyses

The aggregation assay was performed as described previously with minor modifications (Huber, 2017). For the aggregation assay, cells (6 x 10^6 cells total) harvested from mid-log phase of growth were deposited into separate wells of a 6-well dish. Cells were allowed to adhere to the surface of the dish for 1 hour after which time they were washed two times with KK2 buffer, and

then starved in 1 mL of fresh KK2 buffer. Cells were imaged at the indicated times with a Nikon Ts2R-FL inverted microscope equipped with a Nikon 10 Digital Sight Qi2 monochrome camera (Nikon Canada Incorporated Instruments Division, Mississauga, ON, CA). Mounds that formed were imaged the following day and the areas were quantified using ImageJ/Fiji. Results were obtained from 3 independent experiments and placed into different ranges of mound area. Data were presented as the mean % of total mounds analyzed. Statistical significance was assessed in GraphPad Prism 8 (GraphPad Software Incorporated, La Jolla, CA, USA) using two-way ANOVA followed by Bonferroni's multiple comparison test. A p-value < 0.05 was considered significant.

A conditioned buffer (CB) swap experiment was conducted to test the effect of proteins secreted by WT cells on the aggregation of *mfsd8*$^{-}$ cells. Briefly, after cells were deposited into separate wells of a 6-well dish and allowed to adhere for 1 hour, WT cells were starved for 2 hours in 1.5 mL of KK2 buffer. The CB of WT cells was gently collected and spun down to remove any cells remaining in the CB. *mfsd8*$^{-}$ cells were submerged in either KK2 buffer (control) or CB collected from starving WT cells. Like the aggregation assay, cells were imaged at the indicated times with a Nikon Ts2R-FL inverted microscope equipped with a Nikon 10 Digital Sight Qi2 monochrome camera (Nikon Canada Incorporated Instruments Division, Mississauga, ON, CA).

2.7 Cell-substrate adhesion assay

Cell-substrate adhesion was assessed using a previously described method with minor modifications (Huber et al., 2016; Huber & Mathavarajah, 2018b). Cells (6×10^6 cells total) were deposited into separate wells of a 6-well dish and allowed to adhere for 1 hour after which time cells were washed twice with KK2 buffer and starved in fresh KK2 buffer for 4 hours. After 4

hours, cells were shaken at 150 rpm for 30 minutes. Samples of CB (1500 µL) were collected and cells in CB were counted using a hemocytometer to determine cell dissociation. Cells remaining on the dish were also lysed and protein concentrations of the lysates were quantified using the Qubit Protein Assay Kit and Qubit 2.0 Fluorometer (Thermo Fisher Scientific, Whitby, ON, CA). Results were obtained from 9 independent experiments. Statistical significance was assessed in GraphPad Prism 8 (GraphPad Software Inc., La Jolla, CA, USA) using one-way ANOVA followed by Bonferroni's multiple comparison test. A p-value < 0.05 was considered significant.

2.8 Multicellular developmental assay

Multicellular development on nitrocellulose filters was performed as described previously (Huber et al., 2014). A black gridded nitrocellulose filter (0.45 mm pore size) (Sigma-Aldrich Canada Co., Oakville, ON, CA) was placed on top of four Whatman #3 cellulose filters (GE Healthcare Life Sciences, Mississauga, ON, CA) that were soaked in KK2 buffer in a 60 mm x 15 mm Petri dish. Growth phase cells were washed twice with KK2 buffer and 25 µL of 30 x 10^6 cells/mL (750,000 cells total) were deposited onto the nitrocellulose filters. Dishes were placed on a wet paper towel, wrapped with plastic wrap and aluminium foil, and incubated in a drawer for 10-12 hours to create a dark humidity chamber for development. Plates were taken out at indicated time points and developmental structures were imaged using a Leica EZ4W stereomicroscope equipped with an internal 5MP CMOS camera (Leica Microsystems Incorporated, Concord, ON, CA). The number of mounds formed in each cell line was counted after 10-12 hours of development. Statistical significance was assessed in GraphPad Prism 8 (GraphPad Software Inc., La Jolla, CA, USA) using one-way ANOVA followed by Bonferroni's multiple comparison test. The percentage of morphological structures per cell droplet was quantified at the indicated time

points. Statistical analysis was determined using the non-parametric Kruskal-Wallis test followed by the Dunn multiple comparisons test. Developmental structures that formed outside the spot of deposition after 24 hours of development were also noted. Statistical significance was assessed using one-way ANOVA followed by Bonferroni's multiple comparison test. Data were collected from 7 biological replicates averaged from 2 technical replicates. A p-value < 0.05 was considered significant.

2.9 Enzyme activity assays

To assess various enzyme activities, cells were grown in HL5 overnight to confluency in 60 mm × 15 mm Petri dishes (9×10^6 cells total). Growth-phase cells and cells starved for 4 hours or 8 hours in KK2 buffer were then lysed with lysis buffer (50 mM MES pH 6.53, 0.1% NP40) unless indicated otherwise (Phillips & Gomer, 2015). The CB was also collected at these time points. Protein concentrations of WC lysates were quantified and 150 µg of protein was used for the enzyme assays described below. Samples of CB were standardized against protein concentrations of the WC lysates. The protocol for the enzyme assays carried out in this study are summarized in Table 3.

To assay the activity of β-glucosidase, lysates were added to 18 µL of 10 mM of p-Nitrophenyl- β-D-glucopyranoside (Sigma-Aldrich Canada, Oakville, ON, CA) in 50 mM acetate buffer (pH 5.0) (Coston & Loomis, 1969). To assay the activity of α-mannosidase, lysates were added to 18 µL of 5 mM of 4-Nitrophenyl-α-D-mannopyranoside (Sigma-Aldrich Canada, Oakville, ON, CA) in 5 mM acetate buffer (pH 5.0) (Loomis, 1970). Samples were incubated for 45 minutes at 35 °C after which time an equal volume of 1 M sodium carbonate was added to quench the reactions. To assay the activity of β-galactosidase, lysates were added to 36 µL of 5 mM

of *o*-Nitrophenyl-β-D-galactopyranoside (Sigma-Aldrich Canada, Oakville, ON, CA) in 100 mM citrate buffer (pH 4.0) (Maruhn, 1976). To assay the activity of α-galactosidase, lysates were added to 18 µL of 2 mM of 4-Nitrophenyl-α-D-galactopyranoside (Sigma-Aldrich Canada, Oakville, ON, CA) in sodium citrate/phosphate buffer (pH 4.5) (Kilpatrick & Stirling, 1976). Samples were then incubated for 45 minutes at 37 °C after which time an equal volume of AMP/HCl or 1 M sodium glycinate (pH 10.4) were added to quench the reactions for the activities of β-galactosidase and α-galactosidase respectively. To assay the activity of β-N-glucosaminidase, lysates were added to 75 µL of 7 mM of 4-Nitrophenyl N-acetyl-β-D-glucosaminide (Sigma-Aldrich Canada, Oakville, ON, CA) in 100 mM acetate buffer (pH 5.0). Samples were then incubated for 5 minutes at 35 °C after which time an equal volume of 1 M sodium carbonate was added to quench the reactions (Huber & Mathavarajah, 2018a; Loomis, 1969). The quenched reactions were then deposited into a 96-well black clear bottom plate and the amount of cleaved substrate was measured using a BioTek Synergy HTX plate reader (BioTek Instruments Incorporated, Winooski, VT, USA). p-Nitrophenyl-β-D-glucopyranoside (substrate for β-glucosidase) and 4-Nitrophenyl α-D-mannopyranoside (substrate for α-mannosidase) were measured at 420 nm while *o*-Nitrophenyl-β-D-galactopyranoside (substrate for β-galactosidase), 4-Nitrophenyl-α-D-galactopyranoside (substrate for α-galactosidase) and 4-Nitrophenyl N-acetyl-β-D-glucosaminide (substrate for β-N-glucosaminidase) were measured at 405 nm.

To assess Ppt1 activity, lysates were added to 5 µL of 9 mM of 4-methylumbelliferyl-6-thio-β-D-glucopyranoside (Cayman Chemical, Ann Arbor, MI, USA) dissolved in McIlvaine phosphate/citric-acid buffer (pH 4) supplemented with 15 mM dithiothreitol and 0.375% Triton X-100. The reactions were incubated at 37 °C for 1 hour after which time they were boiled for 3

minutes at 95 °C (van Diggelen et al., 1999; Brand et al., 2018). Once the reactions were cooled, 2.75 µL of 2.5 M sodium hydroxide and 4 µL of 0.025 U/µL β-glucosidase (Sigma-Aldrich Canada, Oakville, ON, CA) were added to the reactions and incubated for another hour at 37°C. The reaction was terminated by adding 0.5 M Na_2CO_3/$NaHCO_3$ containing 0.025% Triton X-100 (pH 10.7). To assess Tpp1 activity, cells were lysed with Tpp1 lysis buffer (50 mM sodium phosphate buffer pH 6.5 with 0.5% NP40) and added to 80 µL of 200 µM Ala-Ala-Phe-7-amido-4-methylcoumarin (Sigma-Aldrich Canada, Oakville, ON, CA) dissolved in Tpp1 reaction buffer (150 mM NaCl, 100 mM sodium acetate, pH 4.5, 0.1% Triton X-100) (Stumpf et al., 2017). Reactions were incubated in the dark at 37 °C for 1 hour and then quenched by adding Tpp1 stop solution (150 mM NaCl, 100 mM sodium acetate, pH 4.3). A Cathepsin D Activity Fluorometric Assay kit was used to assess CtsD activity (BioVision, Milpitas, CA, USA). Briefly, cells were lysed with 100 µL of chilled CD Cell Lysis Buffer and incubated on ice for 10 minutes after which time cells were centrifuged for 5 minutes. 27.5 µg of clear cell lysate was added to 100 µL of CD Reaction Buffer mixed with 2 µL of CD substrate. Reactions were incubated at 37°C for 1 hour and 30 minutes. To assay CtsF activity, lysates were added to 0.5 µL of 25% HCl and 1 µL of 250 µg/mL pepsin. Reactions were incubated for 1 hour at 37°C after which time 0.24 µL of 0.5 mM Z-FR-AMC (BPS Bioscience, San Diego, CA, USA) followed by 5.76 µL dimethyl sulfoxide and 70 µL of 0.1 M sodium phosphate buffer containing 1mM ethylenediaminetetraacetic acid (EDTA) and 0.1% (v/v) polyethylene glycol (PEG) 6000 (pH = 6.5) were added to the reaction mixture. Reactions were incubated at 27 °C for 1 hour (Fonovič et al., 2004). Once the reactions were completed or quenched, the samples were then deposited into a 96-well black bottom plate and the fluorescence of each reaction was measured using a BioTek Synergy HTX microplate reader (excitation: 360 nm, emission: 460 nm) (BioTek Instruments Incorporated, Winooski, VT, USA).

The absorbance and fluorescence values for the experimental samples were corrected using a buffer control (i.e., lysis buffer for WC lysates and KK2 buffer for CB). These values were then normalized to WT for each independent experiment. Data were obtained from 4-19 independent experiments. Statistical significance was determined in GraphPad Prism 8 (GraphPad Software Incorporated, La Jolla, CA, USA) using the one-sample t-test (mean, 100; two-tailed). A p-value < 0.05 was considered significant.

Table 3. List of colorimetric and fluorometric substrates, reaction times and temperatures, and quenching solutions for measurement of enzymatic activities

Enzyme	Substrate	Supplier, Cat. No	Reaction time and temperature	Quenching solution	Wavelength for Absorbance/ Fluorescence	Reference
β-glucosidase	p-Nitrophenyl- β-D-glucopyranoside	Sigma, 487507	45 minutes at 35 °C	Sodium carbonate	Absorbance: 420 nm	Coston & Loomis, 1969
α-mannosidase	4-Nitrophenyl α-D-mannopyranoside	Sigma, N2127	45 minutes at 35 °C	Sodium carbonate	Absorbance: 420 nm	Loomis, 1970
β-galactosidase	*o*-Nitrophenyl-β-D-galactopyranoside	Sigma, 48712	45 minutes at 37 °C	AMP/HCl	Absorbance: 405 nm	Maruhn, 1976
α-galactosidase	4-Nitrophenyl-α-D-galactopyranoside	Sigma, N0877	45 minutes at 37 °C	Sodium glycinate (pH 10.4)	Absorbance: 405 nm	Kilpatrick & Stirling, 1976
β-N-glucosaminidase	4-Nitrophenyl N-acetyl-β-D-glucosaminide	Sigma, N8759	5 minutes at 35 °C	Sodium carbonate	Absorbance: 405 nm	Loomis, 1969; Huber & Mathavarajah, 2018
Palmitoyl-Protein Thioesterase 1 (Ppt1)	4-methylumbelliferyl-6-thio-β-D-glucopyranoside	Cayman Chemical, 19524-1	1 hour at 37 °C with substrate, Boiled for 3 minutes at 95 °C followed by 1 hour at 37 °C after addition of beta-glucosidase and NaOH	Na_2CO_3/$NaHCO_3$,0.025% Triton X-100 (pH 10.7)	Excitation: 360 nm, Emission: 460 nm	Diggelen et al., 1999; Brand et al., 2018
Tripeptidyl peptidase 1 (TPP1)	Ala-Ala-Phe-7-amido-4-methylcoumarin	Sigma, A3401	1 hour at 37 °C in the dark	150 mM NaCl, 100 mM sodium acetate (pH 4.3)	Excitation: 360 nm, Emission: 460 nm	Stumpf et al., 2017
Cathepsin D (CtsD)	CD substrate	BioVision, 10013-596	1 hour and 30 minutes at 37°C	None	Excitation: 360 nm, Emission: 460 nm	Protocol for this assay was specified in the kit
Cathepsin F (CtsF)	Z-FR-AMC	BPS Bioscience, 80350(BP)	1 hour at 37 °C with HCl and pepsin, 1 hour at 27 °C with substrate, DMSO and buffer	None	Excitation: 360 nm, Emission: 460 nm	Fonovič et al., 2004

2.10 SDS-PAGE and western blotting

Cells were lysed with NP40 lysis buffer supplemented with a Pierce™ protease inhibitor tablet (Thermo Fisher Scientific, Whitby, ON, CA). After protein quantification, WC lysates and samples of CM were diluted in a 1:1 ratio with 2x Laemmlli sample buffer (120 mM Tris-HCl, 4% sodium dodecyl sulfate, 20% glycerol, 0.004% bromophenol blue, 10% 2-mercaptoethanol, pH 6.8). Prior to gel loading, protein samples were either unheated or heated at 95°C for 5 minutes. Samples were then separated by SDS-PAGE and analyzed by western blotting via wet electroblotting method following a method previously described (Huber et al., 2014). Briefly, proteins were transferred to a Immun-Blot® PVDF membrane for 90 minutes at 90 V (Bio-Rad Laboratories Limited, Mississauga, ON, Canada). Membranes were then blocked with 5% milk dissolved in tris-buffered saline (TBS) and Tween 20 (TBST), followed by incubation of primary antibodies and secondary antibodies for 2 hours each. Protein bands were imaged using Clarity or Clarity Max enhanced chemiluminescence (ECL) and the ChemiDoc MP Imaging System (Bio-Rad Laboratories Limited, Mississauga, ON, Canada). Gels stained using the Pierce™ Silver Stain Kit were imaged using the Invitrogen iBright Imaging Systems (Thermo Fisher Scientific, Whitby, ON, CA).

2.11 Immunolocalization

Growth-phase cells (0.5×10^6 cells total) were deposited onto coverslips placed inside separate wells of a 12-well dish. After allowing cells to adhere for 1 hour, coverslips were submerged overnight in low-fluorescence HL5. The following day, cells were fixed by placing the coverslips in −80 °C methanol for 45 minutes using a previously described method (Hagedorn et al., 2006). Fixed cells were incubated in blocking buffer (KK2 buffer, 0.2% gelatin, 0.1% Triton

X-100) for 1 hour after which time cells were incubated in primary antibodies for 1 hour followed by secondary antibodies for 1 hour. Coverslips were then mounted onto slides using Prolong Gold Anti-Fade Reagent with DAPI (Fisher Scientific Company, Ottawa, ON, CA) and sealed with nail polish. Fixed cells were imaged using a Leica DM6000B microscope equipped with a Leica DFC350FX digital camera (Leica Microsystems Incorporated, Concord, ON, CA). Images were viewed with Leica Application Suite Advanced Fluorescence version 2.4.1 build 6384, and then merged with ImageJ/Fiji.

3. Results

3.1 Validation of an *mfsd8*$^{-}$ cell line expressing C-term GFP tagged Mfsd8

To further elucidate the role of Mfsd8 in *Dictyostelium, mfsd8*$^{-}$ cells were transformed with a vector expressing C-term GFP tagged Mfsd8 to generate *mfsd8*$^{-}$ + Mfsd8-GFP cells. When analyzed by western blotting, anti-GFP detected a smeared band around 75 kDa in lysates from *mfsd8*$^{-}$ cells expressing Mfsd8-GFP that were heated at 95℃ for 5 minutes. Interestingly, when samples were unheated, anti-GFP detected three bands: a faint band at 75 kDa, a strong band at 50 kDa, and another strong band between the 50 kDa and 75 kDa ladder bands in lysates from *mfsd8*$^{-}$ cells expressing Mfsd8-GFP (Fig 3A). In a prior study, Mfsd8 fused to GFP on either terminus appeared between the 50 kDa and 75 kDa ladder bands, which is in agreement with the observations on western blot shown in Fig 3A (Huber et al., 2020). All these bands were not seen in *mfsd8*$^{-}$ cells, which served as the control.

Next, the localization of Mfsd8-GFP in *mfsd8*$^{-}$ cells was determined using immunofluorescence microscopy. Mfsd8-GFP expressed in *mfsd8*$^{-}$ cells also showed a

localization pattern consistent to that of previous findings (Huber et al., 2020) (Fig 3B). In *Dictyostelium*, protein 80 (p80) is a putative copper transporter that localizes to late endosomes, while vacuolar ATPase subunit C (VatC), the ortholog of the C subunit of human V-ATPase, localizes to acidic compartments (e.g., contractile vacuoles, endosomes, lysosomes, etc.) (Journet et al., 1999; Ravanel et al., 2001). During growth, Mfsd8 co-localized to vesicular-like structures and punctate distributions in the cytoplasm marked by p80 and VatC, which appeared yellow in the merged images (Fig 3B). Combined, these observations verified the successful transformation and expression of Mfsd8-GFP in *mfsd8*$^{-}$ cells.

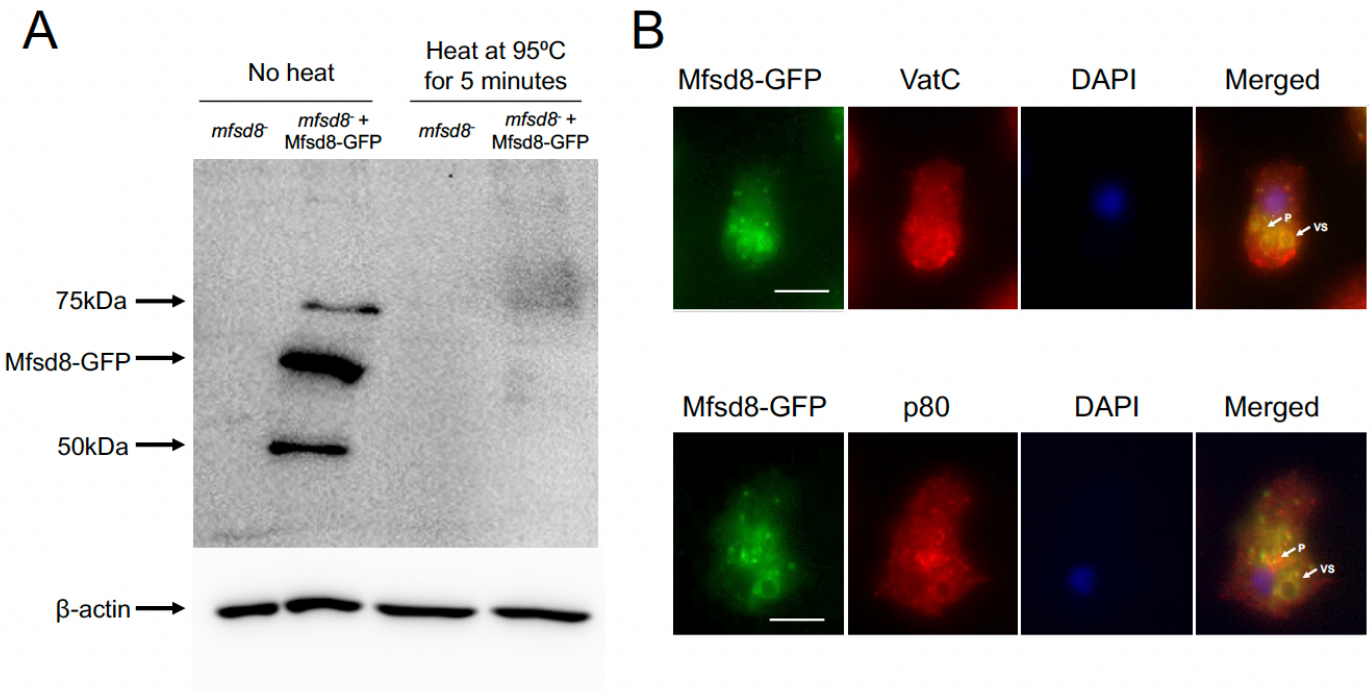

Figure 3. Validation of Mfsd8-GFP expression in *mfsd8*$^{-}$ + Mfsd8-GFP cells using immunofluorescence and western blotting. (A) Whole cell lysates (15 µg) from growth-phase *mfsd8*$^{-}$ cells and *mfsd8*$^{-}$ cells expressing Mfsd8-GFP were either heated or not heated prior to gel loading. All protein samples were separated by SDS-PAGE and analyzed by western blotting with anti-GFP and anti-β-actin (loading control). Molecular weight markers (in kDa) are shown to the left of the blot. (B) Growth-phase *mfsd8*$^{-}$ cells expressing Mfsd8-GFP (green) probed with anti-VatC or anti-p80 followed by anti-mouse Alexa 555 secondary antibodies (red). Cells were stained with DAPI to reveal nuclei (blue). Images were merged with ImageJ/Fiji. Scale bar = 5 µm. P, punctate. VS, vesicular.

3.2 *mfsd8*$^{-}$ cells are larger and show increased rates of proliferation and pinocytosis in liquid media

Since lysosomes play a vital role during *Dictyostelium* growth, the effect of *mfsd8*-deficiency on the rate of cell proliferation in HL5 was examined. Cells were deposited at the same density in flasks and grown in suspension for a period of 144 hours. During the first 72 hours of growth, *mfsd8*$^{-}$ cells proliferated at an increased rate, leading to a significantly greater cell density at the 72-hour timepoint compared to WT cells (Fig 4A). After 120 hours of growth, the proliferation rate of *mfsd8*$^{-}$ cells decreased and the cells attained a lower density compared to WT cells (Fig 4A). Introducing Mfsd8-GFP into *mfsd8*$^{-}$ cells significantly suppressed the enhanced proliferation of *mfsd8*$^{-}$ cells to a rate that is similar to that of WT cells (Fig 4A).

Since *Dictyostelium* cells ingest extracellular liquid nutrients through macropinocytosis during growth, I sought to assess whether the rate of pinocytosis was affected by *mfsd8*-deficiency (Hacker et al., 1997). Cells were incubated with FITC-dextran for a 120-minute period and the amount of intracellular fluorescence was measured every 15 minutes. Two-way ANOVA revealed significantly higher intracellular fluorescence in *mfsd8*$^{-}$ cells compared to WT starting at 45 minutes and continuing over the 120-minute incubation period with FITC-dextran (Fig 4B). Together, these results indicate that *mfsd8*$^{-}$ cells display an increased rate of pinocytosis compared to WT, suggesting that the enhanced proliferation rate observed in *mfsd8*$^{-}$ cells is in part due to its increased rate in liquid nutrient uptake.

Several studies done in *Dictyostelium* have correlated enhanced pinocytosis to increased cell size (Lim et al., 2005; Winckler et al., 2001). Indeed, after quantifying the area of each individual cell during growth, *mfsd8*$^{-}$ cell populations contained a smaller proportion of cells that have areas between the 100-200 μm^2 range (43 ± 1%) and a greater proportion of cells that have

areas >200 μm^2 (17 ± 1%) compared to WT cell populations (Fig 4D). *mfsd8*$^-$ cells were larger than WT cells, which could be a consequence of increased liquid nutrients uptake (Fig 4 C&D). Overall, these results suggest that Mfsd8 negatively regulates cell size as well as proliferation through pinocytosis during *Dictyostelium* growth.

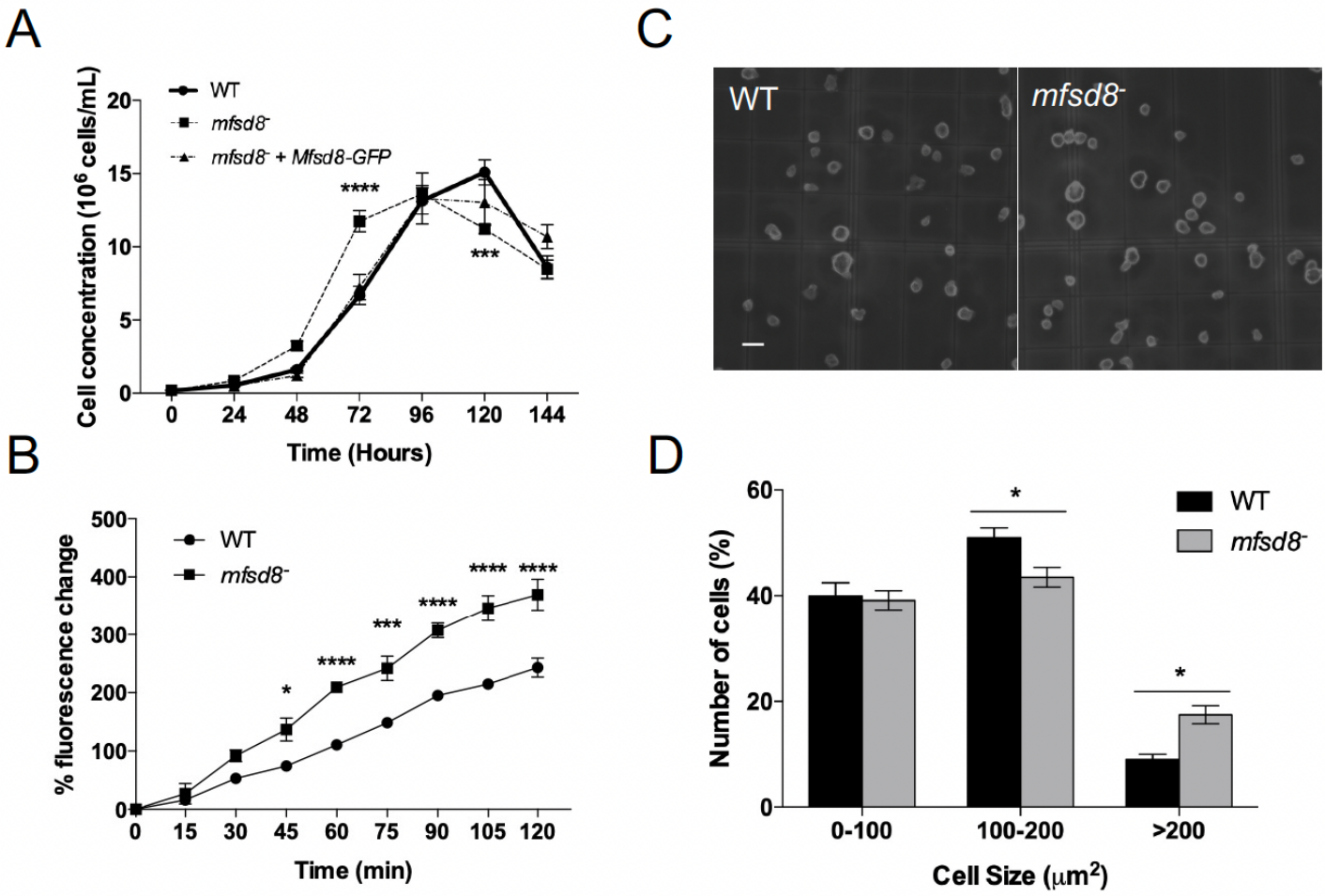

Figure 4. Effect of *mfsd8*-deficiency on cell proliferation, pinocytosis, and cell size during growth. (A) Proliferation of WT, *mfsd8*$^-$ and *mfsd8*$^-$ cells expressing Mfsd8-GFP in HL5 medium. Cell densities were measured every 24 hours for a period of 144 hours. Data presented as mean concentration (×10^6 cells/ml) ± SEM (n=5). (B) Effect of *mfsd8* knockout on the intracellular accumulation of FITC-dextran as a measurement for pinocytotic rate. Cells were incubated in HL5 containing FITC-dextran for 120 minutes. Cells were collected, washed, lysed and the intracellular fluorescence of the lysates was measured every 15 minutes. Data presented as mean % fluorescence change ± SEM (n=3). (C) Effect of *mfsd8* knockout on cell size. Growth phase WT and *mfsd8*$^-$ cells were deposited into a hemocytometer and imaged. (D) Area quantification of each individual cell using ImageJ/Fiji. Data was placed into different ranges of cell area and expressed as mean % of total cells analyzed ± SEM (n=3). Scale bar = 20 μm. Statistical significance was assessed using two-way ANOVA followed by Bonferroni post-hoc analysis. Two-way ANOVA revealed a significant effect of *mfsd8*-deficiency on the cell proliferation, pinocytosis, and cell size. *p-value < 0.05, ***p-value < 0.001 and ****p-value < 0.0001 vs. WT at the indicated time points.

3.3 *mfsd8*$^-$ cells show decreased extracellular levels of 60 kDa AprA during growth and altered protein secretion

To gain insight into the possible mechanisms by which *mfsd8* deficiency leads to increased proliferation, the intracellular and extracellular levels of autocrine proliferation repressor A (AprA) were examined. AprA functions extracellularly to repress cell proliferation in *Dictyostelium* (Brock & Gomer, 2005). WC lysates and CM from WT and *mfsd8*$^-$ cells were collected at the 24-, 48- and 72-hour time points (Fig 6A). When analyzed by western blotting, anti-AprA strongly detected a protein band at 60 kDa and weakly detected a protein band at 55 kDa protein intracellularly and extracellularly, which were similar to the molecular weights of AprA observed in previous studies (Brock & Gomer, 2005; Huber et al., 2014) (Fig 5A&B).

After 24 and 72 hours of axenic growth, the amounts of 60 kDa AprA in *mfsd8*$^-$ WC lysates were reduced by 21 ± 4% and 21 ± 3%, respectively, compared to WT (Fig 5A). However, there was no significant difference between cell lines in the intracellular amount of 55 kDa AprA at all the timepoints. In samples of CM, 60 kDa AprA was reduced by 43 ± 12% and 35 ± 7% at the 24 and 48-hour time points, respectively, in *mfsd8*$^-$ compared to WT (Fig 5B). In contrast, a significantly higher extracellular amount of 55 kDa AprA was observed in *mfsd8*$^-$ relative to WT at the 72-hour time point (174 ± 26%) (Fig 5B). Furthermore, when gels containing samples of CM were silver-stained, global protein levels were higher in *mfsd8*$^-$ CM compared to WT CM at the 24 and 72-hour timepoints by 5± 2% and 19 ± 3% respectively, indicating an overall increase of protein secretion at those timepoints in *mfsd8*$^-$ cells (Fig 6). Taken together, these data indicate that *mfsd8* deficiency alters the levels of protein(s) that are involved in regulating proliferation, which leads to an overall increased rate of proliferation.

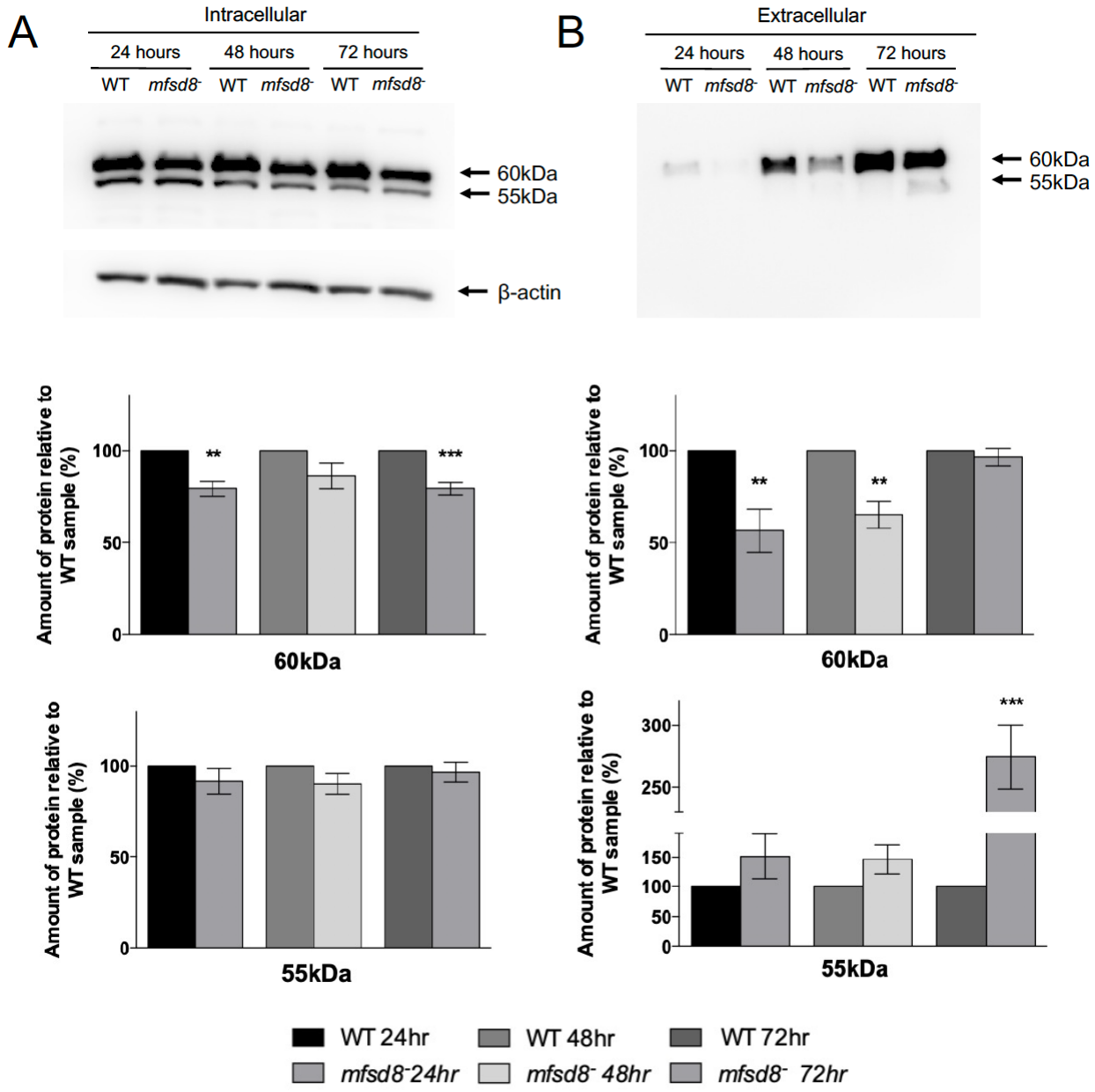

Figure 5. Effect of *mfsd8*-deficiency on the intracellular and extracellular levels of AprA during growth. WT and *mfsd8*$^{-}$ cells were grown in HL5, harvested and lysed after 24, 48 and 72 hours of growth. Proliferation curve can be found in Fig 6A. (A) Whole cell lysates (15 µg) were separated by SDS-PAGE and analyzed by western blotting with anti-AprA and anti-β-actin (loading control). Intracellular AprA protein levels were normalized against beta-actin levels. (B) For extracellular protein levels of AprA, samples of conditioned growth media (CM) were standardized against cell number. Equal volume of sample of CM were separated by SDS-PAGE and analyzed by western blotting with anti-AprA. Identified bands of whole cell lysates and samples of CM were quantified with ImageJ/Fiji. Molecular weight markers (in kDa) are shown to the right of each blot. Data in all plots presented as mean amount of protein relative to WT at each timepoint (%) ± SEM (n=7). Statistical significance was determined using a one-sample t-test (mean, 100; two-tailed) vs. WT. **p-value<0.01 and ***p-value<0.001 vs. WT at the indicated time points.

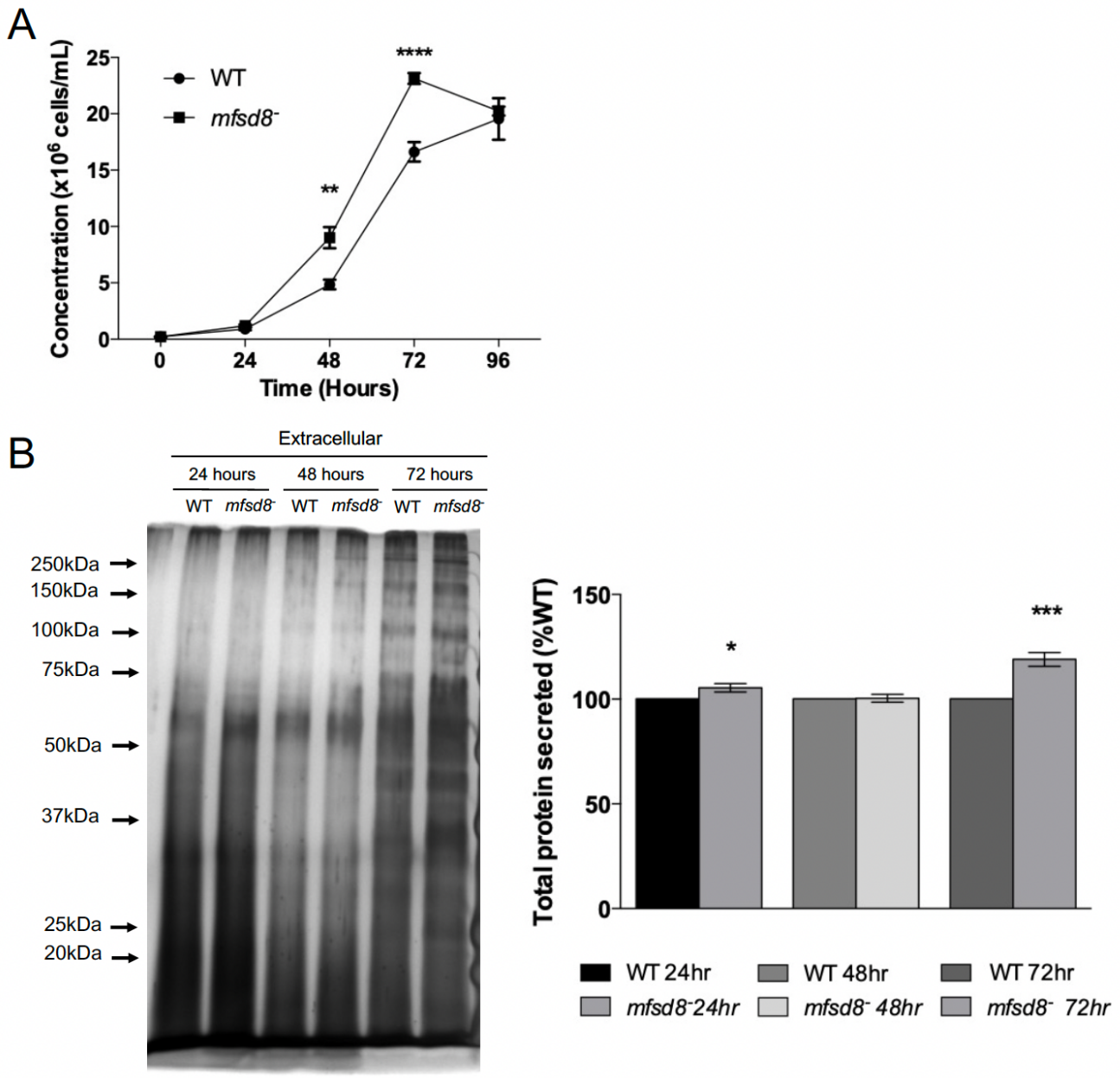

Figure 6. Effect of *mfsd8*-deficiency on global protein secretion during growth. (A) WT and *mfsd8*$^-$ cells were grown axenically in HL5 medium. Cell densities were measured every 24 hours for a period of 96 hours. Cells and conditioned media were collected at the 24-, 48- and 72-hour timepoints to assess for AprA levels and global protein secretion. Data presented as mean concentration ($\times 10^6$ cells/mL) ± SEM (n=3). Statistical significance was assessed using two-way ANOVA followed by Bonferroni post-hoc analysis. Two-way ANOVA revealed a significant effect of *mfsd8*-deficiency on the cell proliferation. **p-value<0.05 and ****p-value<0.0001 vs. WT at the indicated time points. **(B)** WT and *mfsd8*$^-$ cells were grown in HL5 and samples of conditioned media (CM) were harvested after 24, 48 and 72 hours of growth. Samples of CM were standardized against cell number. Equal volumes of CM were separated by SDS-PAGE and silver-stained. The intensity of each lane was quantified with ImageJ/Fiji. Molecular weight markers (in kDa) are shown to the left of the blot. Data presented as mean amount of protein relative to WT at each timepoint (%) ± SEM (n=8). Statistical significance was determined using the one-sample t-test (mean, 100; two-tailed) vs. WT. *p-value < 0.05 and ***p-value < 0.001 vs. WT at the indicated time points

3.4 *mfsd8*$^{-}$ cells form plaques on bacterial lawns at a faster rate

Given that lysosomes play a role in phagocytosis, I tested whether *mfsd8*$^{-}$ cells would recapitulate the same phenotype on bacteria lawn as seen in liquid media. Cell lines were plated on bacterial lawns and plaque formation was monitored at the indicated time points. Once the plaque was fully cleared, its diameter was measured (Fig 7). Two-way ANOVA revealed that *mfsd8*$^{-}$ cells formed plaques in a shorter period of time relative to WT cells (Fig 7). After 32 hours of growth, fully cleared plaques were observed in *mfsd8*$^{-}$ cells, while WT plaques were only beginning to clear (Fig 7). Partially cleared plaques were seen in *mfsd8*$^{-}$ + Mfsd8-GFP cells after 32 hours of growth (Fig 7). At 48 hours, fully cleared plaques were observed in all cell lines. At 48 and 72 hours, the plaques formed by *mfsd8*$^{-}$ cells were bigger than those formed by WT (Fig 7). The expansion of *mfsd8*$^{-}$ plaques was partially rescued to a rate close to that of WT when Mfsd8-GFP was introduced in *mfsd8*$^{-}$ cells (Fig 7). The increased rate of *mfsd8*$^{-}$ plaque growth could be explained by the increased proliferation of *mfsd8*$^{-}$ cells. However, these results could also signal a role for Mfsd8 in regulating phagocytosis.

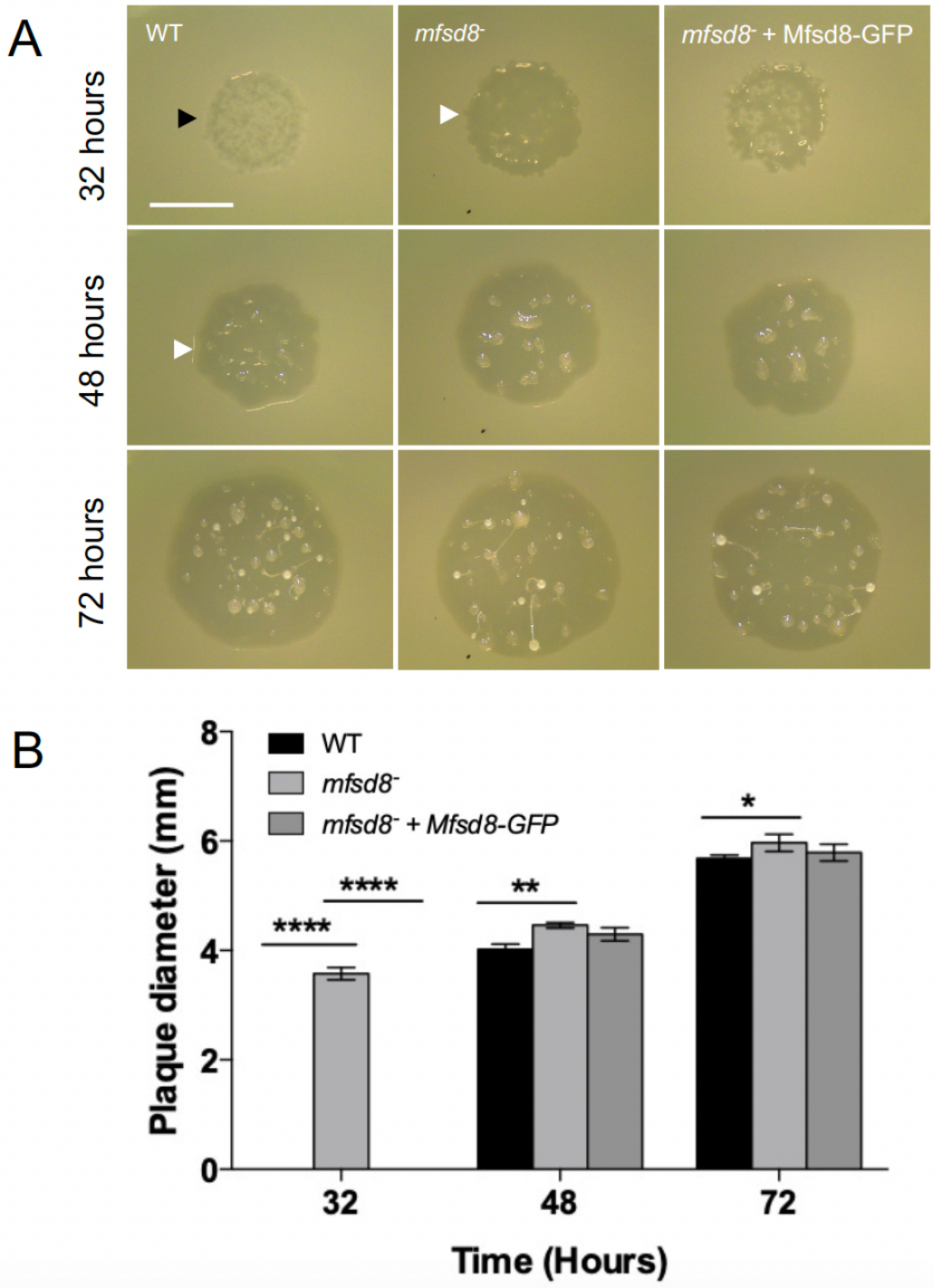

Figure 7. Effect of *mfsd8*-deficiency on plaque expansion on bacteria lawns. (A) WT, *mfsd8*$^-$ and *mfsd8*$^-$ cells expressing Mfsd8-GFP were harvested, washed with KK2 buffer and deposited onto bacteria lawns. Plaques formed were imaged at the indicated time points. White arrow indicates fully cleared plaque. Black arrow indicates plaque that has not been cleared. (B) Diameters of fully cleared plaques were quantified at the indicated time points using ImageJ/Fiji. Data presented as diameter of plaque ± SEM (n=4). Statistical significance was assessed using two-way ANOVA followed by Bonferroni post-hoc analysis. Two-way ANOVA revealed a significant effect of genotype on plaque expansion. *p-value < 0.05, **p-value < 0.01 and ****p-value < 0.0001 vs. WT at the indicated time points. Scale bar =20 μm.

3.5 *mfsd8*$^-$ cells display delayed aggregation and a greater proportion of *mfsd8*$^-$ cells form smaller-sized mounds

Based on the increase in *mfsd8* expression during the early stages of development, I reasoned that early multicellular development may be affected by the absence of *mfsd8*. When *Dictyostelium* cells are submerged in starvation buffer, the progress of development terminates at the mound stage, which allows us to closely examine the morphological and structural changes of aggregating cells. When cells were deposited into 6-well dishes and starved, there was no obvious difference between WT and *mfsd8*$^-$ cells after 6 hours. Aggregation was observed after 8 hours of starvation for WT cells and 10 hours for *mfsd8*$^-$ cells (Fig 8). *mfsd8*$^-$ cells expressing Mfsd8-GFP aggregated with timing relatively close to that of WT (Fig 8). In addition, there were no significant morphological differences between cell lines (Fig 8). Furthermore, when mound areas were quantified the following day, there were significantly more *mfsd8*$^-$ mounds formed that are within the 1000-1999 μm^2 area range, compared to WT mounds, indicating that *mfsd8*$^-$ cells formed more mounds that were smaller in size (Fig 9). Expression of Mfsd8-GFP in *mfsd8*$^-$ cells partially suppressed the aberrant formation of *mfsd8*$^-$ mounds.

To explore the possible role of secretion in *mfsd8*$^-$ phenotypes during the early stages of development, I tested the ability of CB from starving WT cells to restore the timing of aggregation of *mfsd8*$^-$ cells. Since previous work showed that loss of *mfsd8* delayed aggregation by 2 hours, after 2 hours of starvation, the CB of WT cells was collected and added to freshly prepared *mfsd8*$^-$ cells. There was a subtle rescue of the delayed aggregation when *mfsd8*$^-$ cells were submerged in CB from starving WT cells (Fig 10). At 8 hours of starvation, WT cells submerged in KK2 buffer were aggregating towards a common aggregation center while *mfsd8*$^-$ cells conditioned in WT CB

were only starting to aggregate (Fig 10). Likewise, at 10 hours, aggregation was slightly delayed between *mfsd8*$^{-}$ cells conditioned in WT CB and WT, however, aggregation of *mfsd8*$^{-}$ cells submerged in WT CB was more advanced than that of *mfsd8*$^{-}$ cells submerged in KK2 buffer. Collectively, like growth, these results indicate that *mfsd8* deficiency impacts the secretion of proteins or factors that are essential during the early stages of development, ultimately contributing to a delay in aggregation.

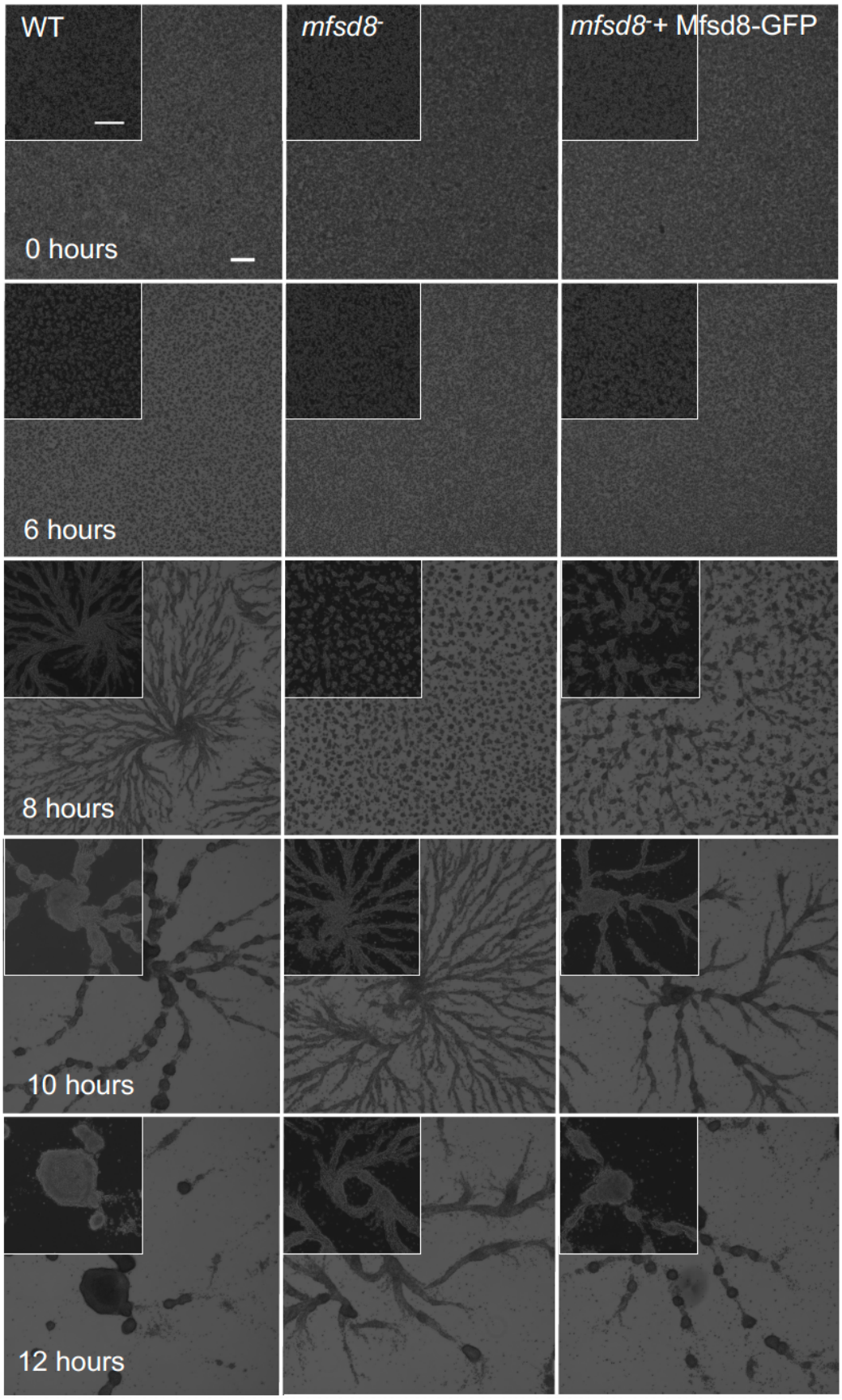

Figure 8. Effect of *mfsd8*-deficiency on aggregation. WT, *mfsd8*$^{-}$ and *mfsd8*$^{-}$ cells expressing Mfsd8-GFP were submerged in KK2 buffer and imaged at the indicated timepoints. Scale bar = 250 µm, n= 6

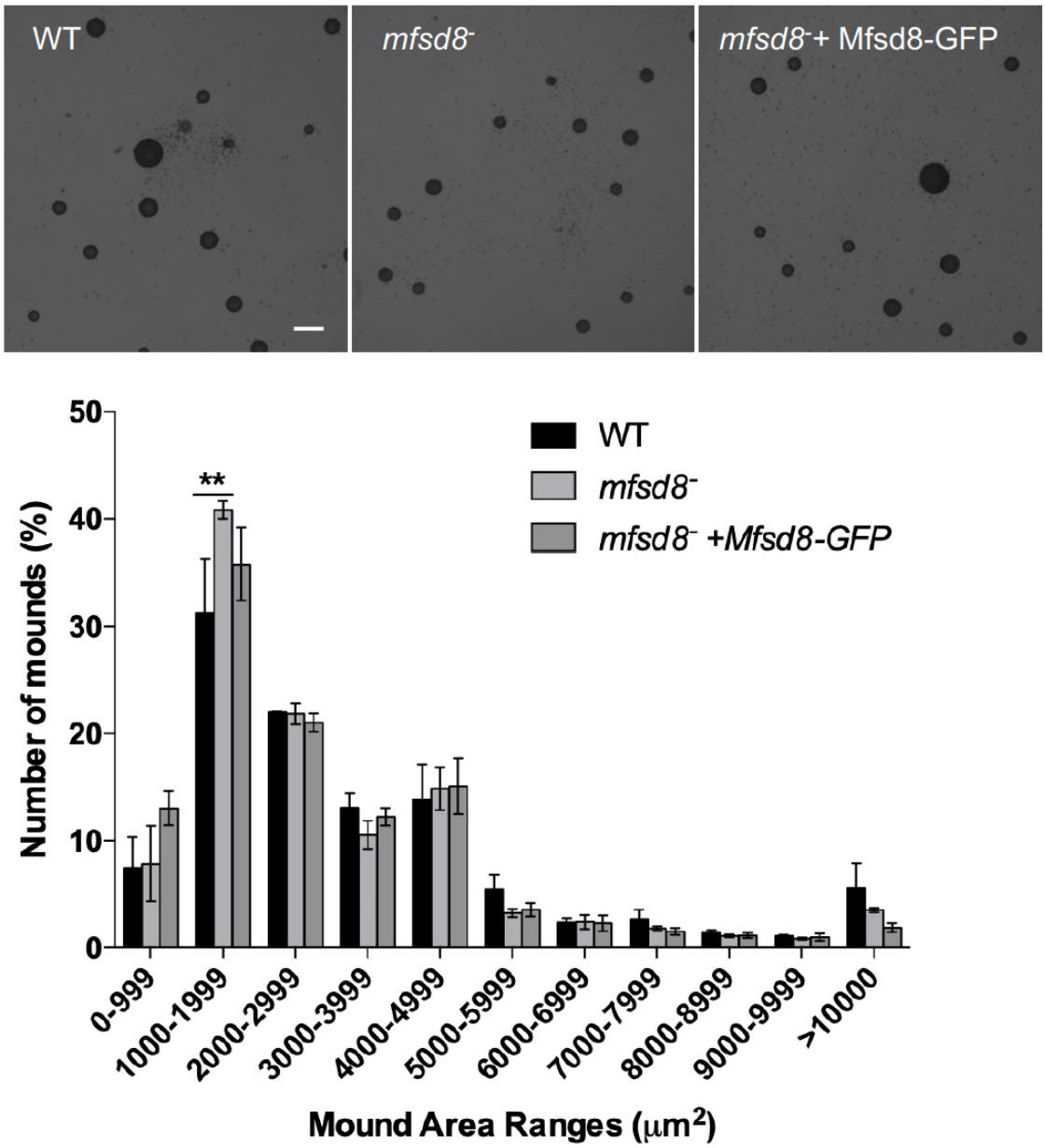

Figure 9. Effect of *mfsd8*-deficiency on mound formation. (A) WT, *mfsd8*$^{-}$ and *mfsd8*$^{-}$ cells expressing Mfsd8-GFP were submerged in KK2 buffer. Mounds were imaged the following day and their areas were quantified using ImageJ/Fiji. Data presented as % total of mounds analyzed ± SEM (n=3). Statistical significance was assessed using two-way ANOVA followed by Bonferroni post-hoc analysis. Two-way ANOVA revealed a significant effect of genotype on mound size. *p-value < 0.05 vs. WT at the indicated ranges. Scale bar =250 μm.

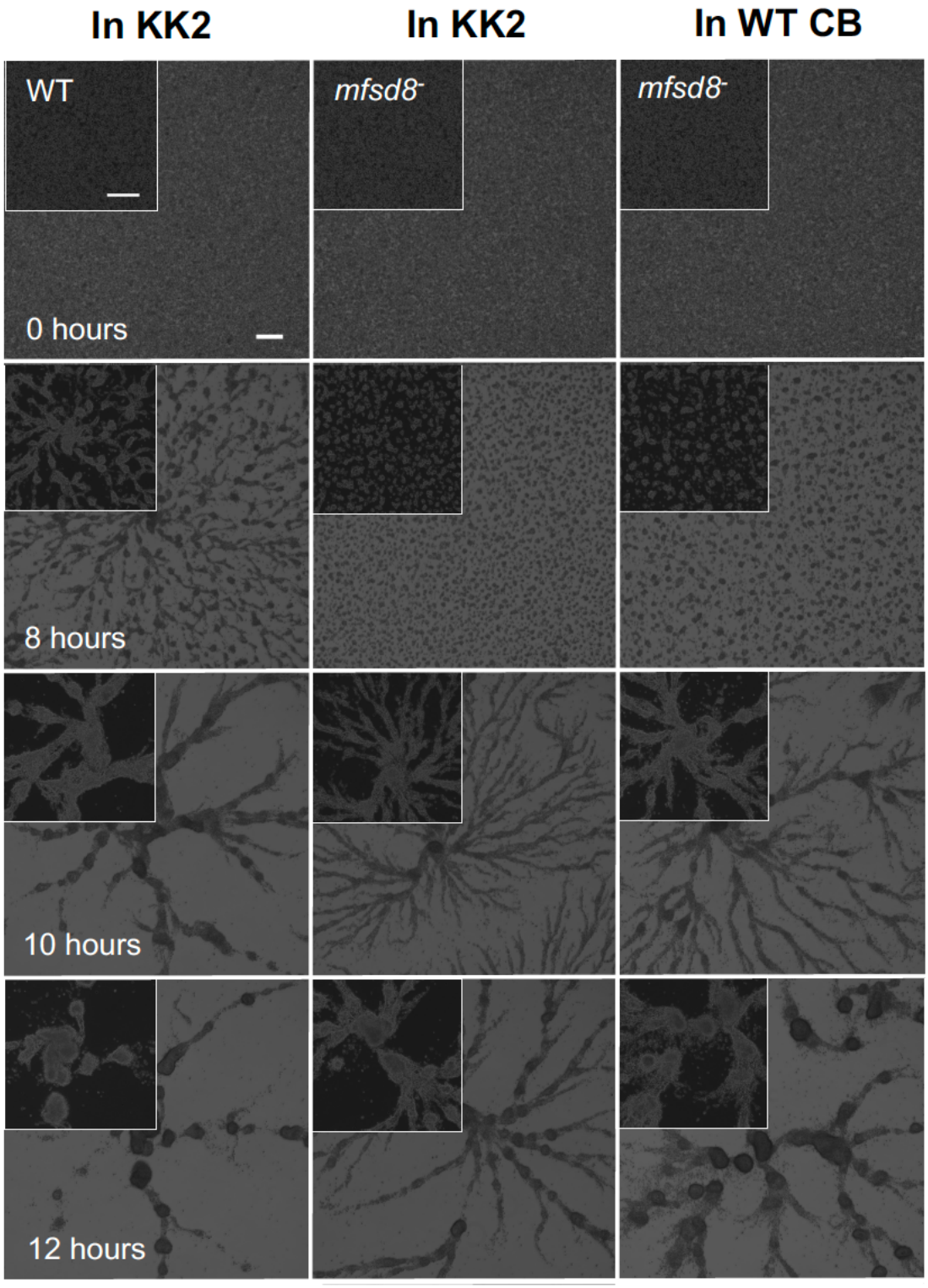

Figure 10. Effect of conditioned buffer on the aggregation of *mfsd8*⁻ cells. WT cells were submerged in KK2 buffer for 2 hours, after which time, the conditioned buffer (CB) of starving WT cells was collected. WT and *mfsd8*⁻ cells were submerged in either KK2 buffer or WT CB and imaged at the indicated timepoints. Scale bar = 250 µm, n= 9

3.6 *mfsd8*$^{-}$ cells display reduced cell-substrate adhesion during the early stages of development

During the first few hours of development, cell-substrate adhesion decreases dramatically to facilitate the migration of cells towards an aggregation center (Tarantola et al., 2014). Given that there was a delay in aggregation in *mfsd8*$^{-}$ cells, I examined whether there were defects in cell-substrate adhesion when *mfsd8* is lost (Tarantola et al., 2014). *mfsd8* deficiency caused more cells to detach from plates relative to WT cells by ~60% (Fig 11A). In agreement with these results, when protein concentration of the lysates was analyzed, a marked decrease (~30%) in protein concentration in *mfsd8*$^{-}$ lysates was observed when compared to WT lysates, indicating that fewer *mfsd8*$^{-}$ cells remained on the dish (Fig 11B). The aberrant phenotype was partially restored to WT levels when Mfsd8-GFP was introduced into *mfsd8*$^{-}$ cells. Combined, these data suggest that the reduced cell-substrate adhesion along with aberrant protein secretion during the early stages of development could contribute to the delay in aggregation of *mfsd8*$^{-}$ cells.

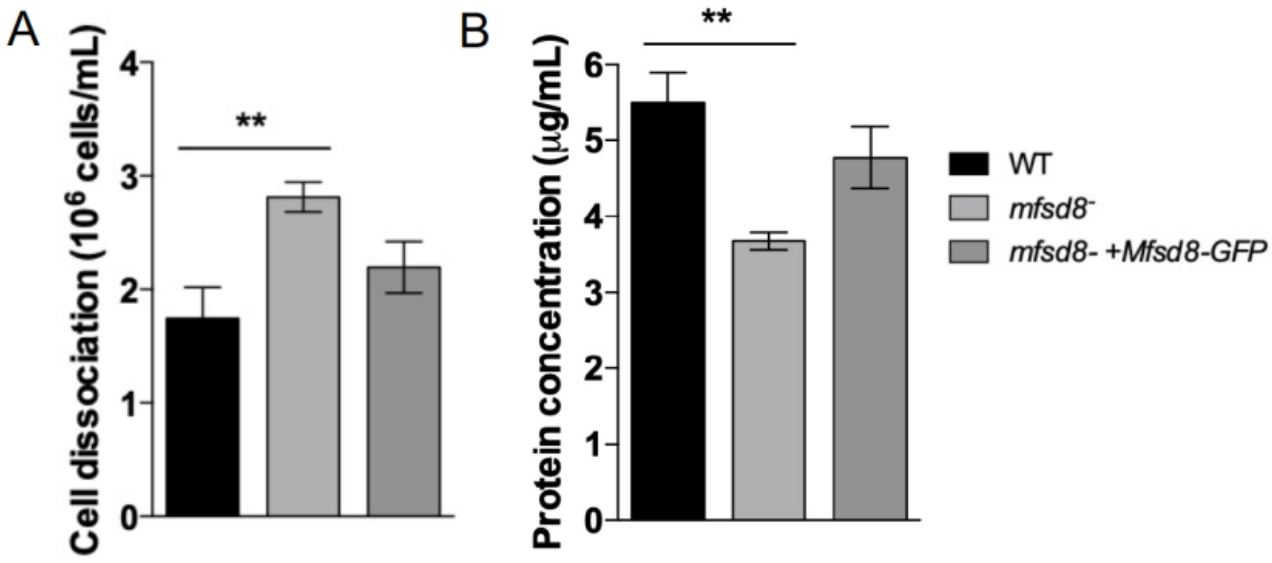

Figure 11. Effect of *mfsd8*-deficiency on cell-substrate adhesion. (A, B) WT, *mfsd8*$^{-}$ and *mfsd8*$^{-}$ cells expressing Mfsd8-GFP were submerged in KK2 buffer for 4 hours, after which time they were shaken at 150 rpm for 30 minutes. Samples of conditioned buffer were collected to measure cell dissociation while cells remaining on the dish were lysed to assess protein concentration. Data presented as cell dissociation and protein concentration ± SEM (n=9). Statistical significance was assessed using one-way ANOVA followed by Bonferroni post-hoc analysis. One-way ANOVA revealed a significant effect of genotype on cell substrate adhesion. **p-value < 0.01 vs. WT.

3.7 Loss of *mfsd8* alters the intracellular and extracellular activities of lysosomal enzymes

Deficiencies in lysosomal enzymes contribute to the onset of LSDs including the NCLs (summarized in Table 1). Besides their role in intracellular degradation, secreted lysosomal enzymes, such as alpha-mannosidase and N-Acetyl glucosaminidase, function to hydrolyze surface glycoproteins, thus reducing cell-substrate adhesion (Loomis et al., 2012; Tarantola et al., 2014). Furthermore, previous work revealed that NCL lysosomal enzymes, Cln5 and CtsD, are aberrantly secreted by *mfsd8*$^{-}$ cells after 4 hours of starvation (Huber et al., 2020). In mouse models of CLN7 disease, altered intracellular activities of some lysosomal enzymes were observed (Damme et al., 2014; Danyukova et al., 2018; von Kleist et al., 2019). Based on these findings, I assessed the intracellular and extracellular activities of lysosomal enzymes during growth and starvation in both WT and *mfsd8*$^{-}$ cells. During growth, an increase in the activities of β-glucosidase, α-mannosidase, N-Acetyl glucosaminidase, Ppt1 and CtsF by ~15% and a dramatic increase in the activity of α-galactosidase by ~60% were observed in *mfsd8*$^{-}$ WC lysates compared to WT, indicating the enhanced breakdown of sugar and lipid molecules (Fig 12).

In *Dictyostelium*, numerous studies have shown that lysosomal enzymes are secreted during the first 4 hours of starvation (Dimond et al., 1981; Ebert et al., 1990; Rossomando et al., 1978). In addition, *mfsd8* mRNA expression peaks after 8 hours of starvation (Fig 1A). For these reasons, I explored the activities of lysosomal enzymes at two timepoints: after 4 and 8 hours of starvation. After 4 hours of starvation, an increase in the activity of α-mannosidase by ~20% and a decrease in the activities of Ppt1 and CtsF by ~30% were observed in *mfsd8*$^{-}$ WC lysates compared to WT (Fig 12). In CB harvested after 4 hours of starvation, a pronounced 45% increase in the extracellular activity of β-glucosidase was seen in *mfsd8*$^{-}$ cells compared to WT. Likewise, an altered profile lysosomal enzyme activity after 8 hours of starvation was observed in *mfsd8*$^{-}$

cells. After 8 hours of starvation, *mfsd8* deficiency increased the intracellular activities of α-mannosidase by 6 ± 3% and decreased the intracellular activities of α-galactosidase, Ppt1 and Tpp1 by 15-24%. In CB harvested after 8 hours of starvation, a 25 ± 8% increase in the extracellular activity of N-Acetyl glucosaminidase was seen in *mfsd8*$^{-}$ cells compared to WT. These differences were statistically significant.

Based on the findings from previous work, only the extracellular activities of β-glucosidase, α-mannosidase and N-Acetyl glucosaminidase were examined since they were secreted rapidly and abundantly, while extracellular activities of other enzymes, such as β-galactosidase-2, were too low to be detected (Dimond et al., 1981; Ebert et al., 1990). Notably, although it was previously reported that Mfsd8 interacts with CtsD and increases the secretion of CtsD during starvation, these results indicate that *mfsd8* deficiency has no effect on its intracellular activity during both growth and starvation (Huber et al., 2020). Interestingly, loss of *mfsd8* affects the intracellular activity of Ppt1 at all three timepoints (Fig 12). Coupled with findings in mouse models of CLN7 disease, these results support a role of Mfsd8 in regulating the function of lysosomal enzymes during *Dictyostelium* growth and starvation.

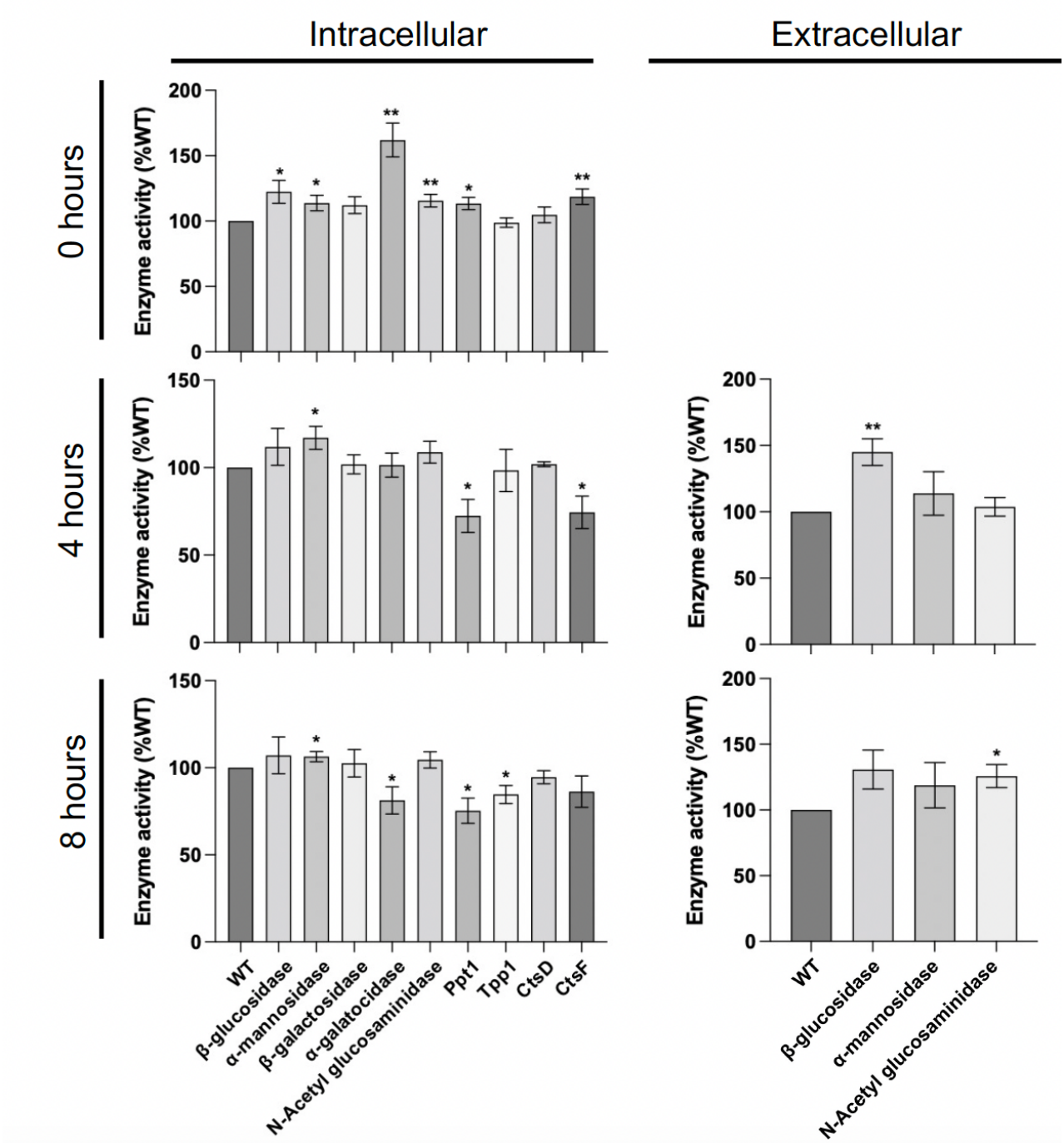

Figure 12. Effect of *mfsd8*-deficiency on the intracellular and extracellular activities of lysosomal enzymes during growth and development. Growth-phase, cells starved for 4 hours or 8 hours in KK2 buffer were collected and lysed to determine intracellular activities of lysosomal enzymes. The conditioned buffer of 4 hours and 8 hours starved cells were collected to determine extracellular activities of lysosomal enzymes. The activities of β-glucosidase,α-mannosidase, β-galactosidase, α-galactosidase, N-Acetyl glucosaminidase, palmitoyl thioesterase 1 (Ppt1), tripeptidyl peptidase 1 (Tpp1), cathepsin D (CtsD), and cathepsin F (CtsF) were assessed. Data presented as mean enzyme activity (% WT) ± SEM (n = 4–19). Statistical significance was determined using a one-sample t-test (mean, 100; two-tailed) vs. WT. *p-value<0.05 and **p-value<0.01 vs. WT

3.8 *mfsd8*$^{-}$ cells show a delay in tipped mound formation and a slug migration defect

Given the moderate increase in *mfsd8* expression after 20-24 hours of *Dictyostelium* development, the effect of *mfsd8*-deficiency on the mid to late stages of *Dictyostelium* development was investigated. Washed cells were deposited onto nitrocellulose membranes and allowed to develop in a dark humidity chamber overnight. Aligned with the observation on mound size in 6-well dishes, after 10-12 hours of development on nitrocellulose membranes, *mfsd8*$^{-}$ cells also formed more mounds that were visually smaller than those in WT (Fig 9 & 13B). Furthermore, after 12-14 hours of development, 15 ± 3% of WT structures had progressed to the tipped mound stage of development, whereas 2 ± 1% of *mfsd8*$^{-}$ structures formed tipped mounds, indicating a delay in tipped mound formation in *mfsd8*$^{-}$ cells (Fig 13C). Introducing Mfsd8-GFP into *mfsd8*$^{-}$ cells accelerated the delayed tipped mound development of *mfsd8*$^{-}$ cells to levels that were not significantly different from WT (Fig 13C).

By 14-16 hours, there were no significant differences between the numbers of fingers or slugs formed by WT and *mfsd8*$^{-}$ cells (Fig 13D). The fingers and slugs formed by *mfsd8*$^{-}$ cells appeared to be visually smaller compared to WT, which is consistent with the smaller mounds observed earlier in development (Fig 13A). Likewise, at 22 hours, the number of fruiting bodies formed by WT and *mfsd8*$^{-}$ cells were not significantly different from each other (Fig 14A). Intriguingly, expression of Mfsd8-GFP in *mfsd8*$^{-}$ cells significantly impacted the number of fruiting bodies formed by ~70 % when compared to both WT and *mfsd8*$^{-}$ cells (Fig 14A). In addition, after 24 hours, 25 ± 7% of *mfsd8*$^{-}$ developmental structures were found outside the spot of deposition compared to 39 ± 6% of WT developmental structures, indicating that slug migration was reduced in the absence of *mfsd8* (Fig 14B). The aberrant slug migration phenotype was partially restored to levels of WT in *mfsd8*$^{-}$ cells expressing Mfsd8-GFP (Fig 14B).

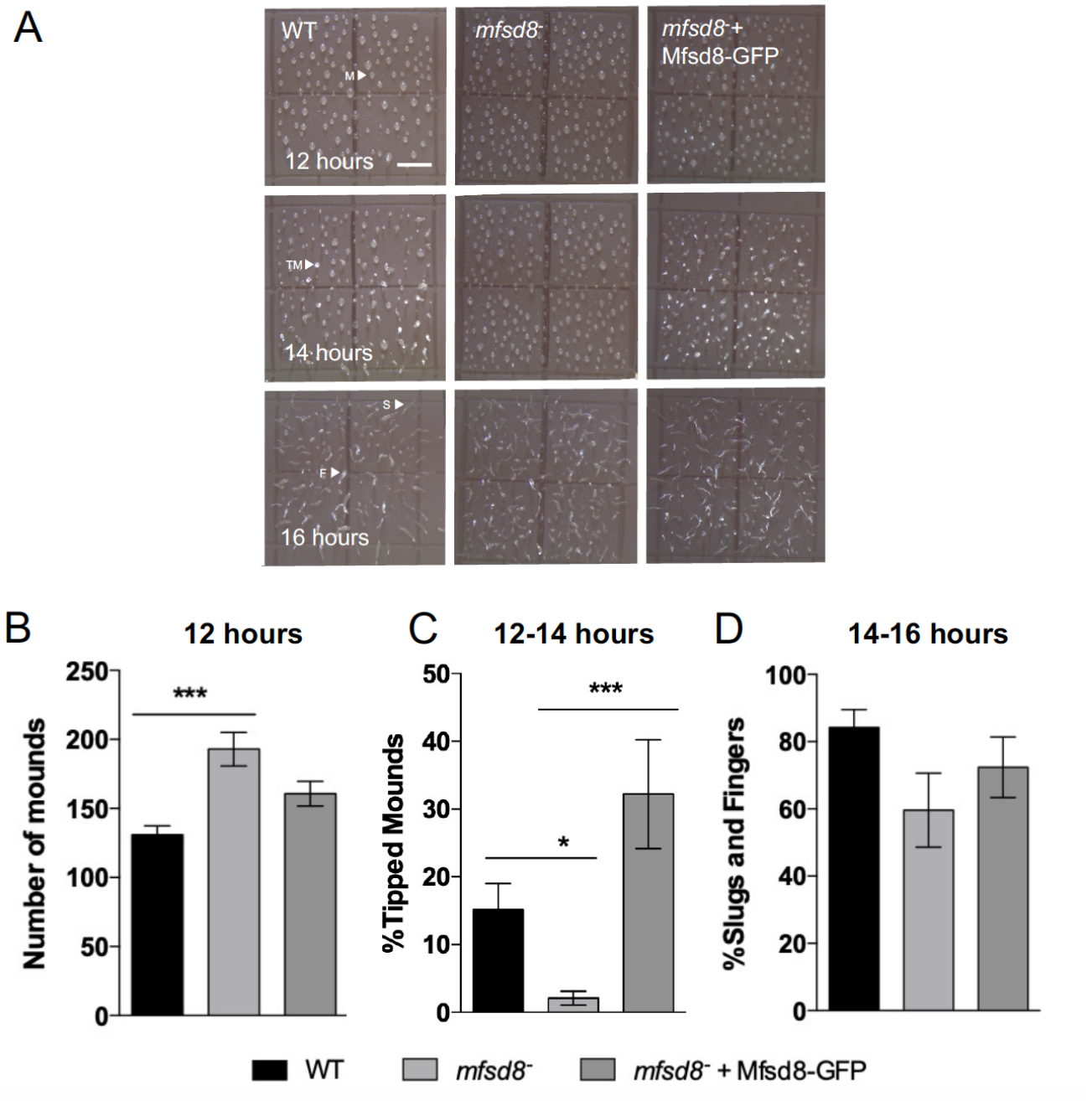

Figure 13. Effect of *mfsd8*-deficiency on mid-stage development. (A) WT, *mfsd8*$^-$ and *mfsd8*$^-$ cells expressing Mfsd8-GFP were developed on nitrocellulose membranes in a dark chamber and imaged at the indicated times. Images represent a top view of developing cells. (B) Quantification of the number of mounds observed after 10-12 hours of development. Data presented as mean total number of mounds formed ± SEM (n=7). Statistical significance was assessed using one-way ANOVA followed by Bonferroni's multiple comparison test. ***p-value < 0.001 vs. WT. (C) Quantification of the number of tipped mounds observed after 12-14 hours of development. Data presented as mean % tipped mounds ± (n=7). (D) Quantification of the number of fingers and slugs observed after 14-16 hours of development. Data presented as mean % fingers and slugs ± SEM (n=7). Statistical significance was assessed using the Kruskal-Wallis test followed by the Dunn multiple comparison test. *p-value < 0.05 and p-value < 0.001 vs. WT. Scale bar=0.2 µm. M, mound; TM, tipped-mound; F, finger; S, slug.

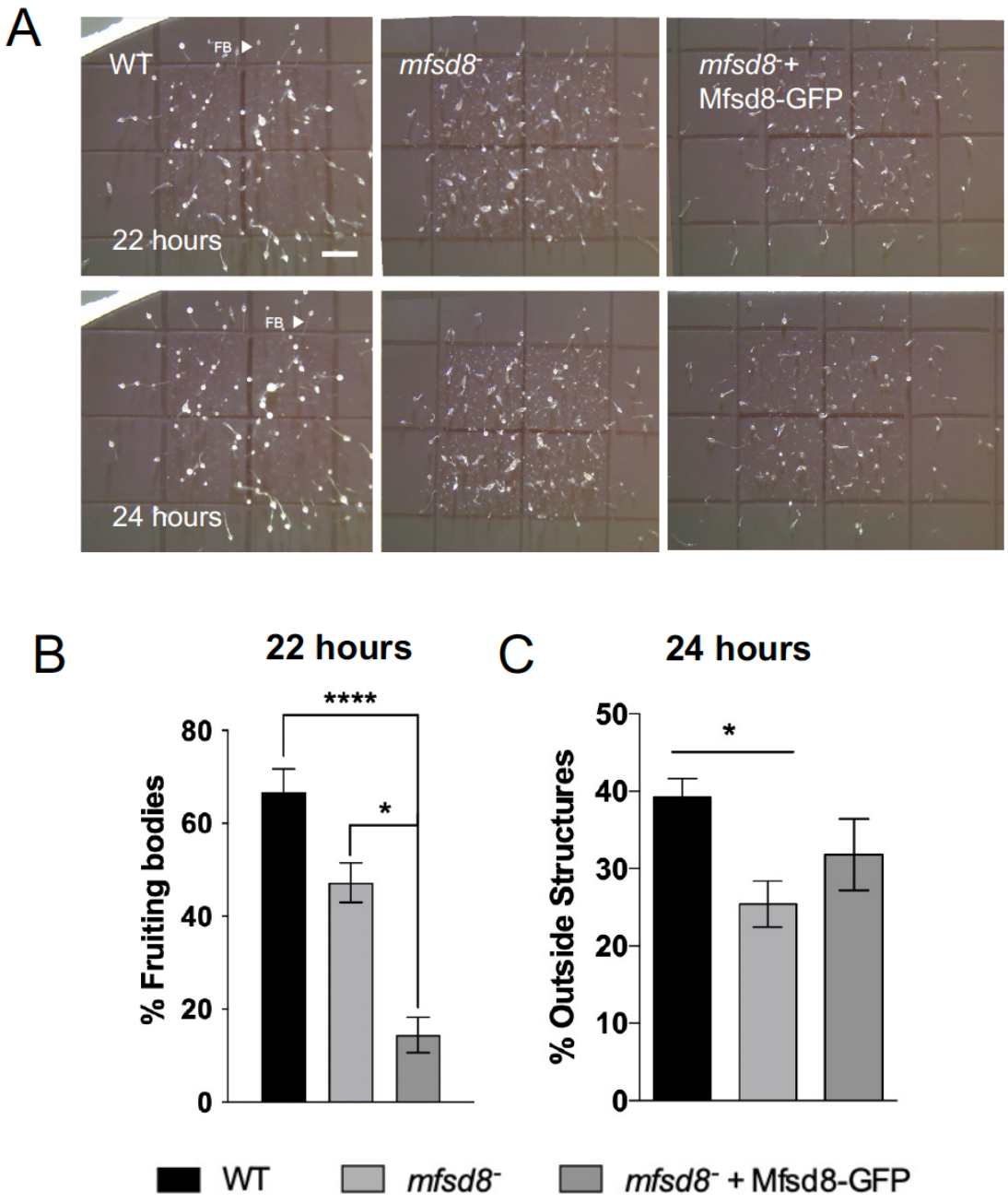

Figure 14. Effect of *mfsd8*-deficiency on late-stage development. (A) WT, *mfsd8*$^-$ and *mfsd8*$^-$ cells expressing Mfsd8-GFP were developed on nitrocellulose membranes in a dark chamber and imaged at the indicated times. Images represent a top view of developing cells. (B) Quantification of the number of fruiting bodies observed after 22 hours of development. Data presented as mean % fruiting bodies ± SEM (n=7). Statistical significance was assessed using the Kruskal-Wallis test followed by the Dunn multiple comparison test. *p-value < 0.05 and ****p-value < 0.0001 vs. WT. (C) Quantification of the number of developmental structures found outside the spot of deposition after 24 hours. Data presented as mean outside structures/total structures (%) ± SEM (n=7). Statistical significance was assessed using one-way ANOVA followed by the Bonferroni multiple comparison test. *p-value < 0.05 vs. WT. Scale bar=0.2 µm. FB, fruiting body.

Taken together, *mfsd8* deficiency led to a delay in mid-stage development of *Dictyostelium* and reduced slug migration during later developmental phases. Combined, these results indicate that Mfsd8 plays an important role in regulating late-stage development of *Dictyostelium.*

4. Discussion

Here, the roles of Mfsd8 during the growth and multicellular development of *Dictyostelium discoideum* were investigated. During growth, *mfsd8* deficiency enhanced proliferation, possibly through its role in modulating pinocytosis and lysosomal enzymatic activities. Furthermore, the rapid proliferation observed in *mfsd8*$^{-}$ cells correlated with decreased secretion of the 60 kDa AprA. Mfsd8 also appeared to play a role in maintaining cell size since there were a greater proportion of larger growth phase *mfsd8*$^{-}$ cells compared to WT. In addition, *mfsd8*$^{-}$ cells formed plaques on bacteria lawns in a shorter period of time compared to WT cells. During early multicellular development, *mfsd8* deficiency reduced cell-substrate adhesion and altered the intracellular and extracellular activities of several lysosomal enzymes, ultimately leading to a delay in aggregation. Interestingly, the delay in aggregation was subtly suppressed when *mfsd8*$^{-}$ cells were submerged in CB harvested from starving WT cells, suggesting defects in protein secretion when *mfsd8* is absent. Following aggregation, *mfsd8*$^{-}$ cells formed a greater number of mounds that are smaller in size compared to WT. Lastly, a delay in tipped mound formation and reduced slug migration were observed when *mfsd8* is absent in the late stage of *Dictyostelium* development. Additionally, the expression of Mfsd8-GFP in *mfsd8*$^{-}$ cells was able to either successfully or partially rescue *mfsd8*-deficiency phenotypes except for fruiting body formation. In total, these findings strongly support a role for Mfsd8 in regulating *Dictyostelium* growth and multicellular developmental through lysosomal-associated functions (Fig 15).

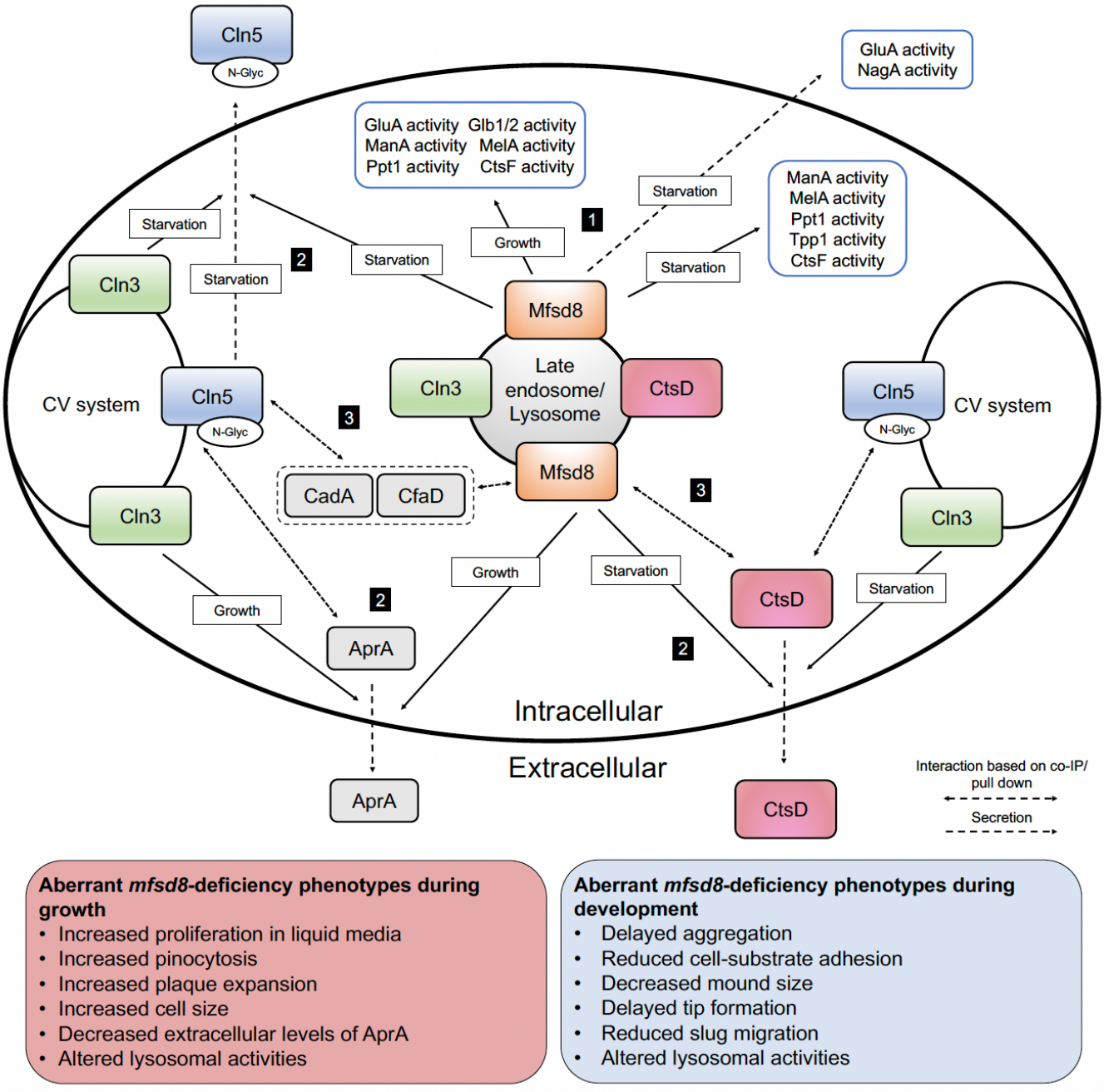

Figure 15. Graphical summary of the role of Mfsd8 in *Dictyostelium*. An overview of the functions and interactions of Mfsd8 with other NCL proteins during growth and starved (development) conditions in *Dictyostelium*. Mfsd8, Cln3 and CtsD localize to the late endosome/lysosome while Cln3 and Cln5 localize to the contractile vacuole (CV) system in *Dictyostelium*. (1) During growth, Mfsd8 influences the intracellular activities of lysosomal enzymes GluA, ManA, Glb1/2, MelA, Ppt1 and CtsF. During early stages of development, Mfsd8 regulates the activities of lysosomal enzymes ManA, MelA, Ppt1, Tpp1 and CtsF within the cell. Whereas, Mfsd8 mediates the extracellular activities of lysosomal enzymes GluA and NagA during the first few hours of development. (2) Mfsd8 and Cln3 influences the secretion of AprA during growth and Cln5 and CtsD during starvation. (3) Mfsd8 and Cln5 interact with CadA, CfaD and CtsD. Cln5 also interacts with AprA.

4.1 Mfsd8-GFP localizes to compartments of the endocytic system in *mfsd8*$^{-}$ cells

To generate the recovery cell line, *mfsd8*$^{-}$ cells were transformed with a plasmid expressing Mfsd8 with GFP fused to the C-terminus and its expression was verified through immunolocalization and western blotting. Immunolocalization showed that, akin to mammalian models, *Dictyostelium* Mfsd8-GFP expressed in *mfsd8*$^{-}$ cells localizes to endocytic compartments, such as acidic intracellular compartments and late endosomes (Huber et al., 2020; Sharifi et al., 2010; Steenhuis et al., 2010). Coupled with findings from previous studies in *Dictyostelium* and mammalian models, these results indicate that the localization of Mfsd8 is conserved in *Dictyostelium*, which further supports the use of *Dictyostelium* as a model for studying CLN7 disease (Huber et al., 2020; Sharifi et al., 2010; Steenhuis et al., 2010).

For the western blotting analysis, when protein samples were heated at 95 °C for 5 minutes, anti-GFP detected a smeared band in *mfsd8*$^{-}$ + Mfsd8-GFP lysates, possibly due to the multi-spanning transmembrane structure of Mfsd8. A recent study showed heating protein samples prior to gel loading induces aggregation of transmembrane proteins (Tsuji, 2020). These aggregated transmembrane proteins failed to migrate through the separating gel, compromising the detection of the protein on the western blot (Tsuji, 2020). In contrast, unheated protein samples allowed for the detection of these transmembrane proteins (Tsuji, 2020). Accordingly, when the samples were unheated, anti-GFP strongly detected a band that appeared between 50 kDa and 75 kDa, which corresponds to the apparent molecular weight of Mfsd8-GFP that was reported in a previous study (Huber et al., 2020). As discussed in Huber et al. (2020) and Steenhuis et al. (2010), the band appeared lower than the expected molecular weight (82 kDa), possibly due to the hydrophobic nature of Mfsd8.

Two immunoreactive bands in *mfsd8*$^{-}$ + Mfsd8-GFP lysates were seen around 50 kDa and 75 kDa, which were not observed in the previous study (Huber et al., 2020) (Fig 3A). Although there is evidence showing that the human MFSD8 is proteolytically cleaved, recent findings indicate that *Dictyostelium* N-term GFP tagged Mfsd8 (GFP-Mfsd8) is not proteolytically processed, however, this does not rule out the possibility that the endogenous Mfsd8 may be processed (Huber et al., 2020; Steenhuis et al., 2012). The discrepancy in the western blots may be due to the processing and stability differences between the N-term and C-term GFP tagged to Mfsd8. In support of this, *Dictyostelium* Mfsd8-GFP was detected at a lower molecular weight and in reduced amounts when compared to GFP-Mfsd8 (Huber et al., 2020). Similarly, in HEK293 human embryonic kidney cells, although the bands appear at the same molecular weight, the intensity of CLN7-GFP bands were lower compared to GFP-CLN7 bands (Steenhuis et al., 2010). Furthermore, an increase in the intensity of CLN7-GFP bands was observed when cells were treated with aspartic and cysteine protease inhibitors, indicating that CLN7-GFP is present in lower amounts due to degradation by lysosomal proteases (Steenhuis et al., 2010). Nevertheless, coupled with the immunolocalization data, both analyses confirm the expression of Mfsd8-GFP in *mfsd8*$^{-}$ cells.

4.2 The role of Mfsd8 during growth

During growth, Mfsd8 interacts with proteins involved in many biological processes including metabolic and biosynthetic processes, transport, cytokinesis, and development (Huber et al., 2020). In this study, it was revealed that *mfsd8*$^{-}$ cells display an increased rate of proliferation in liquid media during the first 72 hours of growth. Based on these results, it suggests that nutrients become increasingly depleted to fuel the initial enhanced rate of proliferation in *mfsd8*$^{-}$ cells, and

subsequently led to a significant decrease in cell density after 120 hours of growth. Likewise, when grown on bacterial lawns, *mfsd8*$^{-}$ cells form plaques in a shorter period of time. These abnormal phenotypes were partially suppressed by introducing Mfsd8-GFP into *mfsd8*$^{-}$ cells. Together, along with findings from the Mfsd8 interactome data, these results indicate a regulatory role of Mfsd8 during *Dictyostelium* growth (Huber et al., 2020).

Late endosomes and lysosomes play key roles in degrading endocytosed material to simple metabolites, thereby providing nutrients essential for cell growth and function (Pillay et al., 2002; Tjelle et al., 1996). *Dictyostelium* cells endocytose extracellular liquid nutrients through pinocytosis, while bacteria are ingested by phagocytosis (Journet et al., 2011; Rosel et al., 2012). Mfsd8 has been shown to participate in the macropinocytosis pathway of *Dictyostelium* (Journet et al., 2011). Accordingly, *mfsd8*$^{-}$ cells display an increase in the rate of pinocytosis, suggesting that the rapid proliferation could be in part due to its increased uptake of liquid nutrients.

Endocytic processes, namely pinocytosis and phagocytosis, are highly dependent on cytoskeletal elements, such as actin and microtubules, for proper membrane invagination and transportation of vesicles (Kumari et al., 2010; Mooren et al., 2012). Through pull-down assays, it was revealed that *Dictyostelium* Mfsd8 interacts with transport proteins and proteins that localize to endocytic vesicles and the cytoskeleton (i.e., actin 10 and V-ATPase subunit B) (Huber et al., 2020). In addition, in cerebellar cells derived from a *Cln7*-deficient mouse, loss of *Cln7* impaired the trafficking of late endosomes and lysosomes independently of microtubule organization (von Kleist et al., 2019). Based on these findings, it is possible that Mfsd8 may be involved in actin polymerization and intracellular trafficking, leading to an increase in pinocytotic rate. Thus, future studies should explore its role in these processes in *Dictyostelium*. Combined, it is reasonable to

suggest that Mfsd8 plays a role in regulating proliferation through its localization to endocytic compartments.

Besides pinocytosis, aberrant proliferation in liquid media may also be caused by abnormal levels of extracellular signals that serve to modulate the rate of proliferation (Brock & Gomer, 2005; Huber et al., 2014). In *Dictyostelium,* AprA is a secreted factor that binds to the G protein-coupled receptor GrIH to slow proliferation (Brock & Gomer, 2005; Tang et al., 2018). To date, studies have identified several components in the AprA-activated proliferation inhibition signal transduction pathway (Bakthavatsalam et al., 2009; Bakthavatsalam et al., 2014; Herlihy et al., 2013; Phillips & Gomer, 2010; Phillips & Gomer, 2014; Phillips et al., 2011). Extracellular AprA accumulates in parallel with cell density, which corroborates with the observation on the western blots (Brock & Gomer, 2005; Huber et al., 2014). The intracellular amounts of 60 kDa AprA were markedly reduced in *mfsd8*$^{-}$ cells at the 24 and 72-hour time points compared to WT. Whereas, the extracellular levels of 60 kDa AprA were significantly decreased in *mfsd8*$^{-}$ cells compared to WT cells at the 24 and 48-hour time points. Notably, based on our proliferation curve that showed a significant increase in proliferation at the 48 and 72-hour time points, there appears be a delay in cellular response to extracellular AprA on cell proliferation. Together, since the decrease of intracellular AprA does not fully account for the decrease of extracellular AprA observed in *mfsd8*$^{-}$ cells, these results suggest that Mfsd8 regulates proliferation by facilitating both the synthesis and secretion of AprA. Contrary to the levels of 60 kDa AprA, there was a dramatic increase in the extracellular levels of 55 kDa AprA in *mfsd8*$^{-}$ cells compared to WT at the 72-hour time point. The decrease in extracellular levels of 60 kDa AprA levels and increase in extracellular levels 55 kDa AprA were also observed in the *Dictyostelium* model of CLN3 disease, another NCL subtype (Huber et al., 2014). Since the extracellular 55 kDa AprA levels increase with cell density, it may

be indicative of the high cell density attained by cells and could potentially serve as a caution signal on limited nutrient availability (Brock & Gomer, 2005). Nevertheless, future work should verify this hypothesis and examine whether the decreased intracellular amounts of AprA in *mfsd8*$^{-}$ cells are the result of altered *aprA* gene expression or translation.

In contrast to a reduction in AprA secretion, loss of *mfsd8* increases total protein secretion during growth, indicating that these proteins may function extracellularly to regulate proliferation. For example, counting factor associated protein D (CfaD), which has been identified as a Mfsd8-interactor, is also secreted and functions to slow proliferation in an autocrine manner (Bakthavatsalam et al., 2008; Huber et al., 2020). Interestingly, it was shown that CfaD interacts with AprA and both proteins are required to inhibit proliferation (Bakthavatsalam et al., 2008; Choe et al., 2009). Furthermore, lysosomal enzymes are secreted abundantly during axenic growth and their amounts increase in parallel with cell density (Dimond et al., 1981). Hence, future studies should consider identifying these proteins and elucidating their roles in relation to the regulatory function of Mfsd8 during growth. In total, the increased pinocytosis along with altered protein secretion may contribute to the proliferation defect observed in *mfsd8*$^{-}$ cells.

In addition to repressing cell proliferation, AprA coordinates cytokinesis in mitosis and helps to reduce the formation of multinucleated cells (Brock & Gomer, 2005). Furthermore, many studies have also correlated reduced cytokinesis and enhanced pinocytosis to increased cell size (Adachi, 2001, Lim et al., 2005; Winckler et al., 2001). Decreased cytokinesis was also observed in *Dictyostelium* models of CLN3 and CLN5 disease, which are other NCL subtypes (McLaren et al., 2021; Mathavarajah et al., 2018). Furthermore, the Mfsd8 interactome also identified several proteins that are involved in cytokinesis during growth, including Actin-10 and Ras-like protein RasG, supporting a possible role of Mfsd8 in cytokinesis (Huber et al., 2020; Tuxworth et al.,

1997). In line with these studies, *mfsd8*$^{-}$ cells appeared larger than WT, possibly due to the increase in nutrient uptake and subsequent impaired cytokinesis caused by the decrease in AprA levels. Hence, further studies investigating the role of Mfsd8 in cytokinesis and related processes are warranted.

When grown on bacterial lawns, *mfsd8*$^{-}$ cells form plaques in a shorter period of time. Interestingly, *aprA*$^{-}$ cells displayed abnormal phenotypes that closely mirror those in *mfsd8*$^{-}$ cells (Table 4). Loss of *aprA* increases the rate of proliferation for cells grown in liquid media as well as on bacterial lawns (Brock & Gomer, 2005). Thus, the increase in plaque expansion seen in *mfsd8*$^{-}$ cells could also be attributed to decreased secretion of AprA. However, these results do not indicate whether the loss of *mfsd8* affects the proliferation rate of cells that are grown on bacteria, thus further work exploring the mechanism(s) underlying this phenotype is required.

Previous work reported that 61% of the Mfsd8-interactors possess catalytic activity during growth (Huber et al., 2020). Further western blot analyses confirmed the interaction between GFP-Mfsd8 and the aspartic protease, CtsD (Huber et al., 2020). Here, loss of *mfsd8* increases the intracellular activities of several lysosomal enzymes, namely β-glucosidase, α-mannosidase, α-galactosidase, and N-Acetyl glucosaminidase. The activities of two NCL-related lysosomal enzymes, Ppt1 and CtsF were also increased in *mfsd8*$^{-}$ WC lysates. Interestingly, the intracellular activity of CtsD was not affected by *mfsd8*-deficiency, indicating that Mfsd8 may bind to CtsD without affecting its proteolytic activity. Nonetheless, the altered activities of lysosomal enzymes may contribute to the increased proliferation and size of *mfsd8*$^{-}$ cells, as there are more nutrients available to fuel cell proliferation and growth due to the rapid breakdown of macromolecules.

Huber et al. (2020) showed that Mfsd8 interacts with proteins that have been linked to Cln3 function, namely CfaD. This is further supported by similar growth defects in *cln3* and *mfsd8*

knockout cells (i.e., increased proliferation rate and decreased extracellular levels of AprA), which supports the hypothesis that NCL proteins may participate in common or convergent pathways (Huber et al., 2014) (Table 4, Fig 15). Therefore, coupled with similar aberrant growth phenotypes between *aprA*$^{-}$ and *mfsd8*$^{-}$ cells, future work should assess the ability of Cln3 and/or AprA to recover *mfsd8*-deficiency phenotypes. Of note, TOR signaling was recently tied to the function of Tpp1, an ortholog of human TPP1, in *Dictyostelium.* Smith et al. (2019) found that overexpression of Rheb, an upstream regulator of TORC1, rescued the slow growth defects caused by the loss of *tpp1A,* suggesting that Tpp1 may work upstream of Rheb and TOR. Given that TORC1 is a master regulator of cell growth, it would be informative to examine if the rapid proliferation of *mfsd8*$^{-}$ cells is caused by attenuated TORC1 signalling. Collectively, during growth, Mfsd8 negatively regulates proliferation and cell size through lysosome-related functions such as protein secretion, pinocytosis, and lysosomal enzyme activity.

Table 4. Summary of aberrant phenotypes of *Dictyostelium* knockout mutants related to Mfsd8 function. Green indicates upregulation while red indicated downregulation.

	tpp1A^{-}	*cln3*$^{-}$	*cln5*$^{-}$	*mfsd8*$^{-}$	*ctsD*$^{-}$	*aprA*$^{-}$	*crlA*$^{-}$
Cell proliferation in liquid media					No effect		
Cytokinesis	N/A				N/A		N/A
Pinocytosis		No effect	No effect		No effect	N/A	N/A
Cell substrate adhesion	N/A				N/A	N/A	N/A
Timing of aggregation/streaming						N/A	No effect
Mound size			No effect		N/A		
Timing of mid-stage development					N/A	N/A	
Slug migration	No effect		No effect		N/A	N/A	N/A
Timing of late-stage development	No effect			No effect	No effect	N/A	No effect

4.3 The role of Mfsd8 during the early stages of multicellular development

mfsd8 mRNA expression increases during the early stages of development and reaches peak levels after 8 hours. Expression then decreases dramatically during mid-stages of development and increases slightly between 20 to 24 hours, which coincides with terminal differentiation and fruiting body formation. Aligned with its expression, during starvation, Mfsd8-interactors are linked to several developmental processes, including adhesion, aggregation, chemotaxis, and fruiting body formation (Huber et al., 2020).

In this study, loss of *mfsd8* delayed aggregation by approximately 2 hours. Moreover, submerging *mfsd8*$^-$ cells in CB harvested from starving WT cells subtly restored the timing of aggregation to WT levels. Taken together, coupled with the ability of Mfsd8-GFP expression to rescue the delayed aggregation in *mfsd8*$^-$ cells, these results support the regulatory role of Mfsd8 in processes involved in aggregation, specifically secretion. Intriguingly, delayed aggregation has also been observed in *Dictyostelium cln3, cln5* and *ctsD* knockout cells (Journet et al., 1999; Huber et al., 2017; McLaren et al., 2021) (Table 4).

Cell-substrate adhesion decreases during the first 8 hours of *Dictyostelium* development, which facilitates the migration and aggregation of cells (Tarantola et al., 2014). Consistent with *cln3* and *cln5* knockout cells, loss of *mfsd8* also reduces cell substrate adhesion and consequently delays aggregation (Huber & Mathavarajah, 2018b, Huber et al., 2016). Introducing Mfsd8-GFP into *mfsd8*$^-$ cells partially reverts this aberrant phenotype to levels that were similar to WT, indicating a role of Mfsd8 in regulating cell adhesion.

Accumulated data suggest that secreted lysosomal enzymes regulate cell-substrate adhesion (Dimond et al., 1981; Rossomando et al.,1978). Furthermore, aberrant aggregation was seen in 80% of secretory mutants (Ebert et al., 1990). Thus, these data suggest that the secretion

of lysosomal enzymes may be compromised in the absence of *mfsd8*. In support of this, loss of *mfsd8* increases the secretion of lysosomal enzymes Cln5 and CtsD (Huber et al., 2020). Aligned with its role in protein secretion, *mfsd8*$^{-}$ cells display an increase in the extracellular activities of β-glucosidase after 4 hours of starvation and N-Acetyl glucosaminidase after 8 hours of starvation. Although the extracellular function of β-glucosidase has not been clearly identified, Loomis et al (2012) showed that incubation of cells with α-mannosidase, but not β-galactosidase, reduces cell-substrate adhesion as it functions to cleave surface oligosaccharides. A marked reduction of cell-substrate adhesion was also reported when cells were treated with N-Acetyl glucosaminidase (Tarantola et al., 2014). However, altered extracellular activities of α-mannosidase or N-Acetyl glucosaminidase were not observed after *mfsd8*$^{-}$ cells were starved for 4 hours. Instead, at 8 hours, the increase in extracellular activity of N-Acetyl glucosaminidase in *mfsd8*$^{-}$ cells may lead to more detached cells, affecting the signalling between cells and subsequently delaying the aggregation of *mfsd8*$^{-}$ cells. Nevertheless, these results do not exclude the possibility that other secreted lysosomal enzymes or mechanisms may be altered in *mfsd8*$^{-}$ cells causing the decrease in cell substrate adhesion.

Besides lysosomal enzymes, *Dictyostelium* cells also secrete a variety of proteins and molecules that are required for development (Brock & Gomer, 1999; Consalvo et al., 2019; Loomis, 2014; Loomis, 2015; Yuen, 1995). Upon starvation, *Dictyostelium* cells secrete the glycoprotein conditioned media factor (CmfA) (Gomer et al., 1991). As CmfA accumulates and reaches a threshold concentration, it stimulates the expression of developmental genes (e.g., spore coat protein, CotB) and activates cAMP signal transduction (Brazill et al., 1998, Deery & Gomer, 1999; Van Haastert et al., 1996). The starved cells secrete pulses of cAMP, attracting neighboring cells to chemotactically aggregate towards a common aggregation center and form a mound

(Loomis, 2015; Yuen, 1995). Accordingly, *cmfA* mutant strains fail to aggregate due to their inability to produce cAMP (Yuen, 1995). Based on these studies, disruption of cAMP signal transduction may also delay the aggregation in *mfsd8*$^{-}$ cells and should be explored in future studies. Together, along with the ability of CB from starving WT cells to subtly restore the timing of aggregation of *mfsd8*$^{-}$ cells, these results suggest that, like growth, Mfsd8 also regulates the secretion of proteins that are necessary for proper development.

In addition to its role in modulating protein secretion, Mfsd8 also influences the activities of lysosomal enzymes intracellularly. Within cells, loss of *mfsd8* increases the activity of α-mannosidase after 4 and 8 hours of development and decreases the activity of α-galactosidase after 8 hours. Altered enzymatic activities may be caused by changes in the amounts of enzymes present within cells. In agreement with this, the lysosomal proteome of *Cln7* knockout mouse embryonic fibroblasts (MEFs) showed altered amounts of several soluble lysosomal proteins, while the amounts of lysosomal membrane proteins were not affected (Danyukova et al., 2018). When tested for enzymatic activities, like *Dictyostelium mfsd8*$^{-}$ cells, *Cln7* knockout MEFs displayed a 1.5-fold increase in the activity of α-mannosidase, while the enzymatic activities of β-hexosaminidase and β-galactosidase were unchanged (Danyukova et al., 2018). In contrast, Damme et al. (2014) reported unaltered activity of α-mannosidase in protein extracts generated from the cerebral cortex and liver of aged *Cln7*-depleted mice. The discrepancy between these findings could be due to differences in cell type or tissue examined in the studies. Of note, a decrease in the activities of NCL lysosomal enzymes Ppt1, Tpp1 and CtsF, were observed, during starvation (Fig 12). The combined decrease in their activities could lead to an accumulation of their respective substrate, causing lysosomal dysfunction and contributing synergistically to NCL pathogenesis. Consistent with these results, the intracellular amounts of PPT1, CLN5 and CTSD were reduced in human

CLN7 knockout haploid (HAP1) cells (Danyukova et al., 2018). Importantly, the depletion of intracellular Cln5 has been consistently observed in neuronal and non-neuronal cell types derived from *Cln7* knockout mice as well as *Dictyostelium* (Danyukova et al., 2018; Huber et al., 2020; von Kleist et al., 2019). Taken together, these studies corroborate with the data presented in this study showing that the degradative capacity of lysosomes are compromised in the absence of *mfsd8*. Nonetheless, to gain insights into the mechanisms underlying the altered enzymatic activities, future research should examine the effect of *mfsd8*-deficiency on the expression, translation, and post-translational modifications of these enzymes in *Dictyostelium*.

Attenuated enzymatic activities are indicative of lysosomal dysfunction, specifically aberrant autophagy, which has been implicated in many neurodegenerative diseases and LSDs, including the NCLs (Brandenstein et al., 2016; Cao et al., 2006; McLaren et al., 2021; Nah et al., 2015; Raben et al., 2009; Settembre et al., 2008). Recent studies revealed that loss of *cln5* compromises autophagy in mammalian and *Dictyostelium* models (Adams et al., 2019; McLaren et al., 2021; Yasa et al., 2020). Likewise, in mammals, the function of Mfsd8 has also been linked to autophagy. In brain tissues of 10-month-old *Cln7* knockout mice, loss of *Cln7* impaired autophagy as indicated by the accumulation of protein aggregates and polyubiquitinated proteins (Brandenstein et al., 2016). Similarly, another study done in mouse cortical neurons showed that loss of *Cln7* compromises the autophagic clearance of brain mitochondria, resulting in the accumulation of high reactive oxygen species (ROS)-generating mitochondria that ultimately contributes to CLN7 pathogenesis (Lopez-Fabeul et al., 2020). In contrast to these findings, cultured cerebellar cells derived from $Cln7^{-/-}$ mice and $Cln7^{-/-}$ MEFs demonstrated efficient autophagic machinery even in the absence of *Cln7* (Danyukova et al., 2018; von Kleist et al., 2019). Autophagy was also largely intact in a *Drosophila* model of CLN7 disease (Connolly et al.,

2019). Combined, these studies indicate that impaired autophagy may become more apparent as the disease progresses or worsens (i.e., 10-month-old tissue samples).

Contrasting findings were also reported on the link between Mfsd8 and mTORC1 reactivation, however, the authors noted that the differences were attributed to the cell types used (i.e., neuronal vs non-neuronal cells) (von Kleist et al., 2019). Contrary to findings in neuronal cerebellar cells, attenuated mTORC1 reactivation was observed when *Cln7* knockout MEFs were starved for prolonged periods, which subsequently compromises the reformation of new lysosomes (Danyukova et al., 2018; von Kleist et al., 2019). Thus, there is mounting evidence to support a role for MFSD8 in regulating lysosomal-associated functions including mTORC1 signaling and autophagy. Perturbations in these processes may lead to the developmental defects seen in *Dictyostelium mfsd8* knockout cells. Thus, future research should ascertain whether the role of Mfsd8 is conserved in these processes and how they relate to the observed defects.

During *Dictyostelium* development, cells undergo autophagy to obtain simple metabolites that are required for cell survival, maintenance of cellular homeostasis, aggregation, morphogenesis and terminal differentiation (Mesquita et al., 2017). Hence, optimal autophagy is required for development as loss of autophagy genes, such as *atg1* and *atg6*, abolish aggregation and negatively affect the mid-to-late stages of development (Mesquita et al., 2017; Mizushima et al., 2011; Otto et al., 2004). It is reasonable to suggest that the delayed aggregation of *mfsd8*$^{-}$ cells may be due to aberrant autophagy, specifically the altered activities of lysosomal enzymes. Together, these studies highlight the need to investigate the link between autophagic mechanisms and the abnormal phenotypes observed in *Dictyostelium mfsd8* knockout cells.

Like CmfA, as cells aggregate, they secrete a protein complex known as counting factor (CF) that regulates mound formation (typically 10^5 cells) (Brock & Gomer, 1999). Countin, which

is a part of the CF complex, plays a role in regulating the size of aggregates (Brock & Gomer, 1999). Disruption of the genes involved in the CF result in the formation of fewer aggregates that are larger in size compared to WT (Brock et al., 2003; Brock et al., 2006). When cells were developed on dishes or nitrocellulose membranes, *mfsd8*$^{-}$ cells consistently formed a greater number of mounds that were smaller in size relative to WT cells, which resembles the phenotype displayed by cells that oversecrete CF (i.e., *smlA*$^{-}$ cells) (Brock & Gomer, 1999). Based on this, the aberrant mound formation in *mfsd8*$^{-}$ cells could be related to higher levels of secreted CF. Further investigation is needed to delineate the possible role of Mfsd8 in CF function such as analyzing the intracellular and extracellular levels of CF via western blotting in *mfsd8*$^{-}$ cells. Collectively, consistent with its expression, Mfsd8 mediates early development processes including aggregation, cell-substrate adhesion, protein secretion as well as the formation and regulation of mound size, possibly via autophagic pathways.

4.4 The effect of *mfsd8* deficiency during the mid to late stages multicellular development

Following impaired aggregation, *mfsd8*$^{-}$ cells produced smaller mounds with delayed tip formation and this phenotype was rescued when Mfsd8-GFP was introduced into *mfsd8*$^{-}$ cells. Intriguingly, precocious tip development was reported in *tpp1A*$^{-}$, *cln3*$^{-}$, and *cln5*$^{-}$ cells, indicating that perhaps Mfsd8 regulates tipped mound formation via a pathway that is distinct from the one involving Tpp1, Cln3, and Cln5 (Huber et al., 2014; McLaren et al., 2021; Phillips and Gomer, 2015) (Table 4). As development progresses, *mfsd8*$^{-}$ cells formed fingers and slugs at a rate that were relatively close to WT. *mfsd8*$^{-}$ slugs appeared to be visually smaller than WT slugs, a direct consequence of the smaller mounds that formed. Furthermore, *mfsd8*$^{-}$ slugs appeared to travel a much shorter distance than WT slugs as most of the developmental structures at 24 hours remained

close to the spot of deposition as opposed to WT. In contrast, an increase in migration was observed for *cln3* slugs (Huber et al., 2014) (Table 4). Like fingers and slug formation, *mfsd8* deficiency had no effect on the timing of fruiting body formation, however, overexpression of Mfsd8-GFP in *mfsd8*$^{-}$ cells severely impacted fruiting body formation. Likewise, loss of *cln3* or *cln5* accelerated the formation of fruiting bodies, with the latter arising due to aberrant autophagy (McLaren et al., 2021) (Table 4).

The early to mid-developmental delay of *mfsd8*$^{-}$ cells could possibly be due to the inability of cells to generate, sense or secrete extracellular signals that are critical for aggregation, determining mound size, and tip development. As the tipped mound forms, the apical tip serves as a source of continuous cAMP production and acts as an organizer that coordinates subsequent morphogenesis and cell differentiation (Siegert & Weijer, 1991, Siegert & Weijer, 1992). Cell differentiation is initiated during aggregation, forming two distinct cell populations, pre-stalk cells and pre-spore cells (Firtel, 1995). The differentiated cells are then sorted within the tipped mounds through differential chemotaxis towards cAMP source, where the pre-spore cells, which become less sensitive to cAMP pulses, are found in the body of the mounds, while the pre-stalk cells become localized at the tip (Firtel, 1995). Several components of the cAMP signaling pathway are preferentially expressed within the tipped mound to facilitate the sorting of precursor cells. Among these components is the cAMP receptor CarB, which is preferentially expressed in pre-stalk cells and has been shown to mediate cell sorting during tip formation (Saxe et al. 1993). Strains lacking *carB* did not develop past the mound stage and only developed a tip after an extended period of time (Saxe et al., 1993). While proteins such as the G-protein α5 (Gα5) subunit are not expressed specifically in pre-spore or pre-stalk cells, loss of *gα5*, like *mfsd8*$^{-}$ cells, also delayed anterior tip formation, while overexpression of *gα5* caused precocious tip morphogenesis (Hadwiger et al.,

1996). Seemingly, given that *cln3*$^{-}$ and *cln5*$^{-}$ cells show opposite phenotypes compared to *mfsd8* and *gα5* mutants, these results suggest that NCL proteins may participate in the Gα5-mediated signal transduction pathway but in a contrasting manner. Furthermore, since Gα5-mediated signal transduction pathway has been hypothesized to modulate cAMP levels and cAMP signaling underlies multiple development processes including aggregation and tip development, these results strongly support a possible defect in cAMP signaling in *mfsd8*$^{-}$ cells (Hadwiger et al., 1996). Intriguingly, delayed anterior tip formation has also been reported in knockout mutants of cAMP receptor-like protein, *crlA*$^{-}$, and the phenotype arose independently of cAMP chemotaxis, indicating that there are pathways other than those stimulated by cAMP that regulate tip formation (Raisley et al., 2004). In support of this, recent work showed that CrlA and Gα5 function in separate signaling pathways to regulate developmental processes (Villines & Hadwiger, 2017). Thus, future work should investigate the role of NCL proteins in both cAMP-dependent and independent pathways in the context of tip formation.

Interestingly, like *mfsd8*$^{-}$ cells, a number of mutant strains lacking membrane proteins also displayed delayed tip development, including the family of ATP-binding cassette (ABC) transporters and G protein-coupled receptors (i.e., CrlA). These results aligned with the role of Mfsd8 as a transporter. Several members of the family of ABC transporters have been identified as Mfsd8-interactors during both growth and starved conditions (Huber et al., 2020). ABC transporters export a wide variety of molecules, including lipids, peptides, amino acids, carbohydrates, ions, and signaling molecules, while utilizing ATP hydrolysis (Dean & Annilo, 2005). Like NCL proteins, ABC transporters localize to multiple membranes, namely the plasma membrane, and those found in the ER, Golgi complex, endosomes, and multivesicular bodies (Dean & Annilo, 2005). While most of the *abc* transporter mutants showed subtle developmental

defects, mutations in some of the *abc* genes resulted in delayed tipped aggregate formation and a reduction in spore formation (Miranda et al., 2013). Further evidence indicates that several genes of the *abc* family play an important role in cell sorting and spore differentiation through signal processing and export (Good et al., 2003; Miranda et al., 2013). For example, autophagy regulates the unconventional secretion of Acyl Coenzyme A binding protein (AcbA), the precursor of spore differentiation factor 2 (SDF-2) (Duran et al., 2010). Genes of the *abcB* family, namely *tagC*, which is primarily expressed in pre-stalk cells, serves to process the diffusible AcbA protein into SDF-2, thereby facilitating spore cell differentiation (Anjard et al., 1998). Together, these studies suggest that Mfsd8 may bind to and subsequently influence the function of these transporters. Coupled with the delay in *mfsd8*$^{-}$ tip formation, the studies discussed above indicate that Mfsd8 may play an important role in cell differentiation.

As development progresses, the tip of the mound starts to elongate, to form a finger and, eventually, a migrating slug (Mathavarajah et al., 2017). Consistent with a dramatic decrease of *mfsd8* expression in mid-development, the number of fingers and slugs formed between all three cell lines around 14-16 hours were comparable, indicating that, unlike Cln3 and Cln5, Mfsd8 is not involved in the temporal regulation of finger and slug formation (Table 4). The ability of *mfsd8*$^{-}$ cells to proceed through tip development indicates the presence of other mechanisms in overcoming the temporary delay in development. Interestingly, this similar phenotype was seen in *crlA* knockout cells, whereby mutant aggregates proceed to form slugs and fruiting bodies with no overt delays or aberrant morphological phenotypes following delayed tip development (Raisley et al., 2004) (Table 4). Taken together, these studies suggest that Mfsd8 and CrlA may be involved in a shared or related pathway.

Migration in *mfsd8*$^{-}$ slugs was greatly curtailed compared to WT slugs and expression of Mfsd8-GFP in *mfsd8*$^{-}$ slugs was able to partially reverse the phenotype. Several knockout mutants that display a decrease in slug migration have been described, including mutants for genes important for cytoskeletal organization, ammonia sensing, calcium signaling, and the components involved in the regulation of glycogen synthase kinase 3 (GSK3) signalling (Ginsburg et al., 1995; Schilde et al., 2004; Singleton et al., 2006; Tsujioka et al., 2004). In support of this, STRING analysis of Mfsd8-interactors revealed that binding partners of Mfsd8 are involved in pathways that regulate cell polarity and movement, ion transporters and glucose metabolism during starvation (Huber et al., 2020). These data strongly support the involvement of Mfsd8 in these processes.

Dictyostelium developmental processes, such as cell motility, aggregation and differentiation, is mediated by various signal transduction pathways including calcium signalling pathways (Newell et al., 1995; O' Day et al., 2020). For instance, during the multicellular slug stage, anteriorly located pre-stalk cells have substantially higher levels of calcium than the pre-spore cells in the posterior and the spatial gradient of calcium within the slug induces downstream cell differentiation processes (Azhar et al., 1995; Schaap et al., 1996). Furthermore, calcium signalling is also crucial for slug migration since the increased in slug migration in *cln3*$^{-}$ cells can be suppressed through the chelation of calcium (Huber et al., 2014). Based on these studies, the decrease in slug migration in *mfsd8* knockout cells may potentially be attributed to defects in the calcium signalling pathways. In line with this hypothesis, several studies have tied the role of Cln7 to glucose metabolism and calcium signalling. *Cln7*$^{\Delta ex2}$ mice cortical neurons failed to sequester calcium ions, which subsequently led to a high glycolytic flux caused by the stabilization and upregulation of the pro-glycolytic 6-phosphofructo-2-kinase/fructose-2,6-bisphosphatase-3

(PFKFB3) (Lopez-Fabeul et al., 2020). PFKFB3-promoted glycolytic flux in *Cln7*$^{\Delta ex2}$ neurons is stimulated by the excess neuronal mitochondria ROS and underlies the histopathological hallmarks observed in CLN7 disease as PFKFB3 inhibition was able to revert these hallmarks (Lopez-Fabeul et al., 2020). In addition, another study found that Mfsd8 mRNA levels were downregulated in response to prolonged glucose starvation but returned to normal levels after subsequent glucose refeeding in both mouse primary cortex cultures and adult flies, indicating a possible role of Mfsd8 in sensing glucose availability (Ceder et al., 2020). Taken together, it would be informative to elucidate the pathways discussed above in relation to the function of Mfsd8 during *Dictyostelium* development.

At 22 hours, most of the WT cells had differentiated into fruiting bodies but there was no significant effect of *mfsd8* deficiency on the timing of fruiting body formation. Intriguingly, the overexpression of Mfsd8-GFP in *mfsd8*$^{-}$ cells had a pronounced effect on the formation of fruiting bodies. These data indicate that abnormally high levels of Mfsd8 reduce the ability of cells to form proper fruiting bodies, hence the regulation of *mfsd8* expression is pivotal for fruiting body formation. Moreover, since there is an evolutionary advantage for efficient spore formation (i.e., optimal spore dispersal), there may be an underlying compensatory mechanism in place when *mfsd8* is absent as there were no significant effect on fruiting body formation in *mfsd8*$^{-}$ cells compared to WT. Overall, these data strongly support a role of Mfsd8 in regulating late development processes, specifically tip formation and slug migration.

5.0 Conclusion

Mfsd8 plays a pleiotropic role during *Dictyostelium* growth and development via lysosomal functions (Fig 15). During growth, Mfsd8 functions as a negative regulator of proliferation and cell size. During development, Mfsd8 also regulates aggregation, cell-substrate adhesion, mound morphogenesis, tip formation and slug migration. In addition, Mfsd8 influences the secretion of proteins and lysosomal enzymes during growth and the early stages of *Dictyostelium* development. Coupled with observation of aberrant *mfsd8*-deficiency phenotypes that are indicative of lysosomal dysfunction, my hypothesis stating that *Dictyostelium* Mfsd8 plays a critical role in regulating lysosomal function was supported. Cellular and developmental processes in *Dictyostelium* were affected due to altered lysosomal function caused by *mfsd8* deficiency. Nevertheless, more work is required to elucidate the mechanisms underlying the role of Mfsd8 in *Dictyostelium* in relation to lysosomal functions (e.g., TOR signaling, autophagy, lysosomal size, and lysosomal pH). Aberrant phenotypes observed in cells lacking *mfsd8* are also seen in other *Dictyostelium* NCL models, further implying that these proteins function in shared pathways, in an antagonistic or non-antagonistic manner (Table 4). Hence, future studies should also investigate the ability of the expression of these NCL genes in rescuing *mfsd8*-deficiency phenotypes. Overall, findings in this study have provided novel insight into the role of Mfsd8 in *Dictyostelium*, which could be translated to mammalian cell models and hopefully contribute to the development of a treatment for CLN7 disease.

6.0 References

Adachi H. (2001). Identification of proteins involved in cytokinesis of *Dictyostelium*. *Cell Structure and Function*, *26*(6), 571–575. https://doi.org/10.1247/csf.26.571

Adams, J., Feuerborn, M., Molina, J. A., Wilden, A. R., Adhikari, B., Budden, T., & Lee, S. Y. (2019). Autophagy–lysosome pathway alterations and alpha-synuclein up-regulation in the subtype of neuronal ceroid lipofuscinosis, CLN5 disease. *Scientific Reports*, *9*(1). https://doi.org/10.1038/s41598-018-36379-z

Anjard, C., Chang, W. T., Gross, J., & Nellen, W. (1998). Production and activity of spore differentiation factors (SDFs) in *Dictyostelium. Development (Cambridge, England)*, *125*(20), 4067–4075.

Ashwini, A., D'Angelo, A., Yamato, O., Giordano, C., Cagnotti, G., Harcourt-Brown, T., Mhlanga-Mutangadura, T., Guo, J., Johnson, G. S., & Katz, M. L. (2016). Neuronal ceroid lipofuscinosis associated with an MFSD8 mutation in Chihuahuas. *Molecular Genetics and Metabolism*, *118*(4), 326–332. https://doi.org/10.1016/j.ymgme.2016.05.008

Azhar, M., Saran, S., & Nanjundiah, V. (1995) Spatial gradients of calcium in the slug of *Dictyostelium discoideum. Current Science, 68* (3), 337-342.

Bagshaw, R. D., Mahuran, D. J., & Callahan, J. W. (2005). Lysosomal membrane proteomics and biogenesis of lysosomes. *Molecular Neurobiology*, *32*(1), 27–41. https://doi.org/10.1385/MN:32:1:027

Bakthavatsalam, D., Brock, D. A., Nikravan, N. N., Houston, K. D., Hatton, R. D., & Gomer, R. H. (2008). The secreted *Dictyostelium* protein CfaD is a chalone. *Journal of Cell Science*, *121*(Pt 15), 2473–2480. https://doi.org/10.1242/jcs.026682

Bakthavatsalam, D., Choe, J. M., Hanson, N. E., & Gomer, R. H. (2009). A *Dictyostelium* chalone uses G proteins to regulate proliferation. *BMC Biology*, *7*, 44. https://doi.org/10.1186/1741-7007-7-44

Bakthavatsalam, D., White, M. J., Herlihy, S. E., Phillips, J. E., & Gomer, R. H. (2014). A retinoblastoma orthologue is required for the sensing of a chalone in *Dictyostelium discoideum*. *Eukaryotic Cell*, *13*(3), 376–382. https://doi.org/10.1128/EC.00306-13

Beck-Wödl, S., Harzer, K., Sturm, M., Buchert, R., Rieß, O., Mennel, H. D., Latta, E., Pagenstecher, A., & Keber, U. (2018). Homozygous TBC1 domain-containing kinase (TBCK) mutation causes a novel lysosomal storage disease - a new type of neuronal ceroid lipofuscinosis (CLN15)?. *Acta Neuropathologica Communications*, *6*(1), 145. https://doi.org/10.1186/s40478-018-0646-6

Bonam, S. R., Wang, F., & Muller, S. (2019). Lysosomes as a therapeutic target. *Nature Reviews. Drug discovery*, *18*(12), 923–948. https://doi.org/10.1038/s41573-019-0036-1

Brand, S., Roy, S., Schröder, P., Rathmer, B., Roos, J., Kapoor, S., Patil, S., Pommerenke, C., Maier, T., Janning, P., Eberth, S., Steinhilber, D., Schade, D., Schneider, G., Kumar, K., Ziegler, S., & Waldmann, H. (2018). Combined proteomic and in silico target identification reveal a role for 5-Lipoxygenase in developmental signaling pathways. *Cell Chemical Biology*, *25*(9), 1095–1106.e23. https://doi.org/10.1016/j.chembiol.2018.05.016

Brandenstein, L., Schweizer, M., Sedlacik, J., Fiehler, J., & Storch, S. (2016). Lysosomal dysfunction and impaired autophagy in a novel mouse model deficient for the lysosomal membrane protein Cln7. *Human Molecular Genetics*, *25*(4), 777–791. https://doi.org/10.1093/hmg/ddv615

Brazill, D. T., Lindsey, D. F., Bishop, J. D., & Gomer, R. H. (1998). Cell density sensing mediated by a G protein-coupled receptor activating phospholipase C. *The Journal of Biological Chemistry*, *273*(14), 8161–8168. https://doi.org/10.1074/jbc.273.14.8161

Brock, D. A., & Gomer, R. H. (1999). A cell-counting factor regulating structure size in *Dictyostelium*. *Genes & Development*, *13*(15), 1960–1969. https://doi.org/10.1101/gad.13.15.1960

Brock, D. A., & Gomer, R. H. (2005). A secreted factor represses cell proliferation in *Dictyostelium*. *Development (Cambridge, England)*, *132*(20), 4553–4562. https://doi.org/10.1242/dev.02032

Brock, D. A., Hatton, R. D., Giurgiutiu, D. V., Scott, B., Jang, W., Ammann, R., & Gomer, R. H. (2003). CF45-1, a secreted protein which participates in *Dictyostelium* group size regulation. *Eukaryotic Cell, 2*(4), 788–797. https://doi.org/10.1128/EC.2.4.788-797.2003

Brock, D. A., van Egmond, W. N., Shamoo, Y., Hatton, R. D., & Gomer, R. H. (2006). A 60-kilodalton protein component of the counting factor complex regulates group size in *Dictyostelium discoideum. Eukaryotic Cell, 5*(9), 1532–1538. https://doi.org/10.1128/EC.00169-06

Buratta, S., Tancini, B., Sagini, K., Delo, F., Chiaradia, E., Urbanelli, L., & Emiliani, C. (2020). Lysosomal exocytosis, exosome release and secretory autophagy: The autophagic- and endo-lysosomal systems go extracellular. *International Journal of Molecular Sciences*, *21*(7), 2576. https://doi.org/10.3390/ijms21072576

Burns, R. A., Livi, G. P., & Dimond, R. L. (1981). Regulation and secretion of early developmentally controlled enzymes during axenic growth in *Dictyostelium discoideum*. *Developmental Biology*, *84*(2), 407–416. https://doi.org/10.1016/0012-1606(81)90409-7

Cao, Y., Espinola, J. A., Fossale, E., Massey, A. C., Cuervo, A. M., MacDonald, M. E., & Cotman, S. L. (2006). Autophagy is disrupted in a knock-in mouse model of juvenile neuronal ceroid lipofuscinosis. *The Journal of Biological Chemistry*, *281*(29), 20483–20493. https://doi.org/10.1074/jbc.M602180200

Cárcel-Trullols, J., Kovács, A. D., & Pearce, D. A. (2015). Cell biology of the NCL proteins: What they do and don't do. *Biochimica et Biophysica Acta*, *1852*(10 Pt B), 2242–2255. https://doi.org/10.1016/j.bbadis.2015.04.027

Ceder, M. M., Lekholm, E., Klaesson, A., Tripathi, R., Schweizer, N., Weldai, L., Patil, S., & Fredriksson, R. (2020). Glucose availability alters gene and protein expression of several newly classified and putative solute carriers in mice cortex cell culture and *D. melanogaster. Frontiers in Cell and Developmental Biology,* 8, 579. https://doi.org/10.3389/fcell.2020.00579

Choe, J. M., Bakthavatsalam, D., Phillips, J. E., & Gomer, R. H. (2009). *Dictyostelium* cells bind a secreted autocrine factor that represses cell proliferation. *BMC Biochemistry*, *10*, 4. https://doi.org/10.1186/1471-2091-10-4

Connolly, K. J., O'Hare, M. B., Mohammed, A., Aitchison, K. M., Anthoney, N. C., Taylor, M. J., Stewart, B. A., Tuxworth, R. I., & Tear, G. (2019). The neuronal ceroid lipofuscinosis protein cln7 functions in the postsynaptic cell to regulate synapse development. *Scientific Reports*, *9*(1). https://doi.org/10.1038/s41598-019-51588-w

Consalvo, K. M., Rijal, R., Tang, Y., Kirolos, S. A., Smith, M. R., & Gomer, R. H. (2019). Extracellular signaling in *Dictyostelium*. *The International Journal of Developmental Biology*, *63*(8-9-10), 395–405. https://doi.org/10.1387/ijdb.190259rg

Coston, M. B., & Loomis, W. F., Jr (1969). Isozymes of beta-glucosidase in *Dictyostelium discoideum*. *Journal of Bacteriology*, *100*(3), 1208–1217. https://doi.org/10.1128/jb.100.3.1208-1217.1969

Damme, M., Brandenstein, L., Fehr, S., Jankowiak, W., Bartsch, U., Schweizer, M., Hermans-Borgmeyer, I., & Storch, S. (2014). Gene disruption of Mfsd8 in mice provides the first animal model for CLN7 disease. *Neurobiology of Disease*, *65*, 12–24. https://doi.org/10.1016/j.nbd.2014.01.003

Danyukova, T., Ariunbat, K., Thelen, M., Brocke-Ahmadinejad, N., Mole, S. E., & Storch, S. (2018). Loss of CLN7 results in depletion of soluble lysosomal proteins and impaired mTOR reactivation. *Human Molecular Genetics*, *27*(10), 1711–1722. https://doi.org/10.1093/hmg/ddy076

Dean, M., & Annilo, T. (2005). Evolution of the ATP-binding cassette (ABC) transporter superfamily in vertebrates. *Annual Review of Genomics and Human Genetics*, *6*, 123–142. https://doi.org/10.1146/annurev.genom.6.080604.162122

Deery, W. J., & Gomer, R. H. (1999). A putative receptor mediating cell-density sensing in *Dictyostelium*. *The Journal of Biological Chemistry*, *274*(48), 34476–34482. https://doi.org/10.1074/jbc.274.48.34476

Dimond, R. L., Brenner, M., & Loomis, W. F., Jr (1973). Mutations affecting N-acetylglucosaminidase *in Dictyostelium discoideum*. *Proceedings of the National Academy of*

Sciences of the United States of America, *70*(12), 3356–3360. https://doi.org/10.1073/pnas.70.12.3356

Dimond, R. L., Burns, R. A., & Jordan, K. B. (1981). Secretion of lysosomal enzymes in the cellular slime mold, *Dictyostelium discoideum*. *The Journal of Biological Chemistry*, *256*(13), 6565–6572.

Duran, J. M., Anjard, C., Stefan, C., Loomis, W. F., & Malhotra, V. (2010). Unconventional secretion of Acb1 is mediated by autophagosomes. *The Journal of Cell Biology*, *188*(4), 527–536. https://doi.org/10.1083/jcb.200911154

Ebert, D. L., Jordan, K. B., & Dimond, R. L. (1990). Lysosomal enzyme secretory mutants of *Dictyostelium discoideum*. *Journal of Cell Science*, *96 (Pt 3)*, 491–500.

Elleder, M., Kousi, M., Lehesjoki, A.E., Mole, S.E., Siintola, E., & Topcu, M. (2011) Chapter 11: CLN7. In: S. Mole, R. Williams, H. Goebel, (Eds), The Neuronal Ceroid Lipofuscinoses (Batten Disease) 2nd ed. (pp. 176-188). Oxford: OUP Oxford

Faix, J., Linkner, J., Nordholz, B., Platt, J. L., Liao, X. H., & Kimmel, A. R. (2013). The application of the Cre-loxP system for generating multiple knock-out and knock-in targeted loci. *Methods in Molecular Biology (Clifton, N.J.)*, *983*, 249–267. https://doi.org/10.1007/978-1-62703-302-2_13

Faller, K. M., Bras, J., Sharpe, S. J., Anderson, G. W., Darwent, L., Kun-Rodrigues, C., Alroy, J., Penderis, J., Mole, S. E., Gutierrez-Quintana, R., & Guerreiro, R. J. (2016). The Chihuahua dog: A new animal model for neuronal ceroid lipofuscinosis CLN7 disease?. *Journal of Neuroscience Research*, *94*(4), 339–347. https://doi.org/10.1002/jnr.23710

Ferguson S. M. (2019). Neuronal lysosomes. *Neuroscience letters*, *697*, 1–9. https://doi.org/10.1016/j.neulet.2018.04.005

Fey, P., Dodson, R. J., Basu, S., & Chisholm, R. L. (2013). One stop shop for everything *Dictyostelium*: dictyBase and the Dicty Stock Center in 2012. *Methods in Molecular Biology (Clifton, N.J.)*, *983*, 59–92. https://doi.org/10.1007/978-1-62703-302-2_4

Fey, P., Kowal, A. S., Gaudet, P., Pilcher, K. E., & Chisholm, R. L. (2007). Protocols for growth and development of *Dictyostelium discoideum*. *Nature Protocols*, *2*(6), 1307–1316. https://doi.org/10.1038/nprot.2007.178

Firtel, R. A. (1995). Integration of signaling information in controlling cell-fate decisions in *Dictyostelium*. *Genes & Development*, *9*(12), 1427–1444. https://doi.org/10.1101/gad.9.12.1427

Fonovič, M., Brömme, D., Turk, V., & Turk, B. (2004). Human cathepsin F: expression in baculovirus system, characterization and inhibition by protein inhibitors. *Biological Chemistry*, *385*(6), 505–509. https://doi.org/10.1515/BC.2004.059

Francione, L. M., Annesley, S. J., Carilla-Latorre, S., Escalante, R., & Fisher, P. R. (2011). The *Dictyostelium* model for mitochondrial disease. *Seminars in Cell & Developmental Biology*, *22*(1), 120–130. https://doi.org/10.1016/j.semcdb.2010.11.004

Fu, W., & Hall, M. N. (2020). Regulation of mTORC2 Signaling. *Genes*, *11*(9), 1045. https://doi.org/10.3390/genes11091045

Gaudet, P., Pilcher, K. E., Fey, P., & Chisholm, R. L. (2007). Transformation *of Dictyostelium discoideum* with plasmid DNA. *Nature Protocols, 2*(6), 1317–1324. https://doi.org/10.1038/nprot.2007.179

Ginsburg, G. T., Gollop, R., Yu, Y., Louis, J. M., Saxe, C. L., & Kimmel, A. R. (1995). The regulation of *Dictyostelium* development by transmembrane signalling. *The Journal of Eukaryotic Microbiology*, *42*(3), 200–205. https://doi.org/10.1111/j.1550-7408.1995.tb01565.x

Gomer, R. H., Yuen, I. S., & Firtel, R. A. (1991). A secreted 80 x 10(3) Mr protein mediates sensing of cell density and the onset of development in *Dictyostelium. Development (Cambridge, England)*, *112*(1), 269–278.

Good, J. R., Cabral, M., Sharma, S., Yang, J., Van Driessche, N., Shaw, C. A., Shaulsky, G., & Kuspa, A. (2003). TagA, a putative serine protease/ABC transporter of *Dictyostelium* that is required for cell fate determination at the onset of development. *Development (Cambridge, England), 130*(13), 2953–2965. https://doi.org/10.1242/dev.00523

Guo, J., O'Brien, D. P., Mhlanga-Mutangadura, T., Olby, N. J., Taylor, J. F., Schnabel, R. D., Katz, M. L., & Johnson, G. S. (2015). A rare homozygous *MFSD8* single-base-pair deletion and frameshift in the whole genome sequence of a Chinese Crested dog with neuronal ceroid lipofuscinosis. *BMC Veterinary Research*, *10*, 960. https://doi.org/10.1186/s12917-014-0181-z

Hacker, U., Albrecht, R., & Maniak, M. (1997). Fluid-phase uptake by macropinocytosis in *Dictyostelium*. *Journal of Cell Science*, *110 (Pt 2)*, 105–112.

Hadwiger, J. A., Natarajan, K., & Firtel, R. A. (1996). Mutations in the *Dictyostelium* heterotrimeric G protein alpha subunit G alpha5 alter the kinetics of tip morphogenesis. *Development (Cambridge, England)*, *122*(4), 1215–1224.

Hagedorn, M., Neuhaus, E. M., & Soldati, T. (2006). Optimized fixation and immunofluorescence staining methods for *Dictyostelium* cells. *Methods in Molecular Biology (Clifton, N.J.)*, *346*, 327–338. https://doi.org/10.1385/1-59745-144-4:327

Haltia M. (2006). The neuronal ceroid-lipofuscinoses: from past to present. *Biochimica et Biophysica Acta*, *1762*(10), 850–856. https://doi.org/10.1016/j.bbadis.2006.06.010

Herlihy, S. E., Tang, Y., & Gomer, R. H. (2013). A *Dictyostelium* secreted factor requires a PTEN-like phosphatase to slow proliferation and induce chemorepulsion. *PloS One*, *8*(3), e59365. https://doi.org/10.1371/journal.pone.0059365

Hu, Y.B., Dammer, E., Ren, R.J. & Wang, G. (2015) The endosomal-lysosomal system: from acidification and cargo sorting to neurodegeneration. *Translation Neurodegeneration,* 4, 18. https://doi.org/10.1186/s40035-015-0041-1

Huber, R. J., Myre, M. A., & Cotman, S. L. (2014). Loss of Cln3 function in the social amoeba *Dictyostelium discoideum* causes pleiotropic effects that are rescued by human CLN3. *PloS One, 9*(10), e110544. https://doi.org/10.1371/journal.pone.0110544

Huber R. J. (2016). Using the social amoeba *Dictyostelium* to study the functions of proteins linked to neuronal ceroid lipofuscinosis. *Journal of Biomedical Science*, *23*(1), 83. https://doi.org/10.1186/s12929-016-0301-0

Huber R. J. (2017). Loss of Cln3 impacts protein secretion in the social amoeba *Dictyostelium*. *Cellular Signalling*, *35*, 61–72. https://doi.org/10.1016/j.cellsig.2017.03.022

Huber R. J. (2020). Molecular networking in the neuronal ceroid lipofuscinoses: insights from mammalian models and the social amoeba *Dictyostelium discoideum*. *Journal of Biomedical Science*, *27*(1), 64. https://doi.org/10.1186/s12929-020-00653-y

Huber, R. J., & Mathavarajah S. (2018a). Cln5 is secreted and functions as a glycoside hydrolase in *Dictyostelium*. *Cellular Signalling 42*, 236-248. https://doi.org/10.1016/j.cellsig.2017.11.001

Huber, R. J., & Mathavarajah, S. (2018b). Secretion and function of Cln5 during the early stages of *Dictyostelium* development. *Biochimica et Biophysica Acta- Molecular Cell Research*, *1865*(10), 1437–1450. Advance online publication. https://doi.org/10.1016/j.bbamcr.2018.07.017

Huber, R. J., Mathavarajah, S., & Yap, S. Q. (2020). Mfsd8 localizes to endocytic compartments and influences the secretion of Cln5 and cathepsin D in *Dictyostelium*. *Cellular Signalling*, *70*, 109572. https://doi.org/10.1016/j.cellsig.2020.109572

Huber, R. J., Myre, M. A., & Cotman, S. L. (2017). Aberrant adhesion impacts early development in a *Dictyostelium* model for juvenile neuronal ceroid lipofuscinosis. *Cell Adhesion & Migration*, *11*(4), 399–418. https://doi.org/10.1080/19336918.2016.1236179

Jia, R., & Bonifacino, J. S. (2019). Lysosome Positioning Influences mTORC2 and AKT Signaling. *Molecular Cell*, *75*(1), 26–38.e3. https://doi.org/10.1016/j.molcel.2019.05.009

Journet, A., Chapel, A., Jehan, S., Adessi, C., Freeze, H., Klein, G., & Garin, J. (1999). Characterization of *Dictyostelium discoideum* cathepsin D. *Journal of Cell Science*, *112 (Pt 21)*, 3833–3843.

Journet, A., Klein, G., Brugière, S., Vandenbrouck, Y., Chapel, A., Kieffer, S., Bruley, C., Masselon, C., & Aubry, L. (2012). Investigating the macropinocytic proteome of *Dictyostelium* amoebae by high-resolution mass spectrometry. *Proteomics*, *12*(2), 241–245. https://doi.org/10.1002/pmic.201100313

Kilpatrick, D. C., & Stirling, J. L. (1976). Properties and developmental regulation of an alpha-d-galactosidase from *Dictyostelium discoideum*. *The Biochemical Journal*, *158*(2), 409–417. https://doi.org/10.1042/bj1580409

Kosta, A., Roisin-Bouffay, C., Luciani, M. F., Otto, G. P., Kessin, R. H., & Golstein, P. (2004). Autophagy gene disruption reveals a non-vacuolar cell death pathway in *Dictyostelium*. *The Journal of Biological Chemistry*, *279*(46), 48404–48409. https://doi.org/10.1074/jbc.M408924200

Kousi, M., Siintola, E., Dvorakova, L., Vlaskova, H., Turnbull, J., Topcu, M., Yuksel, D., Gokben, S., Minassian, B. A., Elleder, M., Mole, S. E., & Lehesjoki, A. E. (2009). Mutations in CLN7/MFSD8 are a common cause of variant late-infantile neuronal ceroid lipofuscinosis. *Brain: A Journal of Neurology*, *132*(Pt 3), 810–819. https://doi.org/10.1093/brain/awn366

Kumari, S., Mg, S., & Mayor, S. (2010). Endocytosis unplugged: multiple ways to enter the cell. *Cell Research*, *20*(3), 256–275. https://doi.org/10.1038/cr.2010.19

Laplante, M., & Sabatini, D. M. (2009). mTOR signaling at a glance. *Journal of Cell Science*, *122*(Pt 20), 3589–3594. https://doi.org/10.1242/jcs.051011

Levi, S., Polyakov, M., & Egelhoff, T. T. (2000). Green fluorescent protein and epitope tag fusion vectors for *Dictyostelium discoideum*. *Plasmid*, *44*(3), 231–238. https://doi.org/10.1006/plas.2000.1487

Lim, C. J., Zawadzki, K. A., Khosla, M., Secko, D. M., Spiegelman, G. B., & Weeks, G. (2005). Loss of the *Dictyostelium* RasC protein alters vegetative cell size, motility and endocytosis. *Experimental Cell Research*, *306*(1), 47–55. https://doi.org/10.1016/j.yexcr.2005.02.002

Lopez-Fabuel, I., Garcia-Macia, M., Buondelmonte, C., Burmistrova, O., Bonora, N., Morant-Ferrando, B., Alonso-Batan, P., Vicente-Gutierrez, C., Jimenez-Blasco, D., Quintana-Cabrera, R., Fernandez, E., Sharaireh, A., Guevara-Ferrer, M., Fitzpatrick, L., Thompton, C.D., McKay, T.R., Storch, S., Medina, D.L., Mole, S.E., Fedichev, P.O., Almeida, A., & Bolaños, J.P. (2020). Mitochondrial collapse links PFKFB3-promoted glycolysis with CLN7/MFSD8 neuronal ceroid lipofuscinosis pathogenesis. bioRxiv. https://doi.org/10.1101/2020.10.20.345314

Loomis W. F. (2014). Cell signaling during development of *Dictyostelium*. *Developmental Biology*, *391*(1), 1–16. https://doi.org/10.1016/j.ydbio.2014.04.001

Loomis W. F. (2015). Genetic control of morphogenesis in *Dictyostelium. Developmental Biology, 402*(2), 146–161. https://doi.org/10.1016/j.ydbio.2015.03.016

Loomis W. F., Jr (1969). Acetylglucosaminidase, an early enzyme in the development of *Dictyostelium discoideum*. *Journal of Bacteriology*, *97*(3), 1149–1154. https://doi.org/10.1128/jb.97.3.1149-1154.1969

Loomis, W. F. (1970). Developmental regulation of α-Mannosidase in *Dictyostelium discoideum. Journal of Bacteriology*, *103*(2), 375–381. https://doi.org/10.1128/jb.103.2.375-381.1970

Loomis, W. F., Fuller, D., Gutierrez, E., Groisman, A., & Rappel, W. J. (2012). Innate non-specific cell substratum adhesion. *PloS One*, *7*(8), e42033. https://doi.org/10.1371/journal.pone.0042033

Maniak M. (2011). *Dictyostelium* as a model for human lysosomal and trafficking diseases. *Seminars in Cell & Developmental Biology*, *22*(1), 114–119. https://doi.org/10.1016/j.semcdb.2010.11.001

Maruhn D. (1976). Rapid colorimetric assay of beta-galactosidase and N-acetyl-beta-glucosaminidase in human urine. *Clinica Chimica Acta- International Journal of Clinical Chemistry*, *73*(3), 453–461. https://doi.org/10.1016/0009-8981(76)90147-9

Mathavarajah, S., Flores, A., & Huber, R. J. (2017). *Dictyostelium discoideum*: A model system for cell and developmental biology. *Current Protocols Essential Laboratory Techniques*, *15*(1). https://doi.org/10.1002/cpet.15

Mathavarajah, S., McLaren, M. D., & Huber, R. J. (2018). Cln3 function is linked to osmoregulation in a *Dictyostelium* model of Batten disease. *Biochimica et Biophysica Acta-Molecular Basis of Disease*, *1864*(11), 3559–3573. https://doi.org/10.1016/j.bbadis.2018.08.013

McBride, J. L., Neuringer, M., Ferguson, B., Kohama, S. G., Tagge, I. J., Zweig, R. C., Renner, L. M., McGill, T. J., Stoddard, J., Peterson, S., Su, W., Sherman, L. S., Domire, J. S., Ducore, R. M., Colgin, L. M., & Lewis, A. D. (2018). Discovery of a CLN7 model of Batten disease in non-human primates. *Neurobiology of Disease*, *119*, 65–78. https://doi.org/10.1016/j.nbd.2018.07.013

McLaren, M. D., Mathavarajah, S., Kim, W. D., Yap, S. Q., & Huber, R. J. (2021). Aberrant autophagy impacts growth and multicellular development in a *Dictyostelium* knockout model of CLN5 disease. *Frontiers in Cell and Developmental Biology*, *9*, 657406. https://doi.org/10.3389/fcell.2021.657406

Mesquita, A., Cardenal-Muñoz, E., Dominguez, E., Muñoz-Braceras, S., Nuñez-Corcuera, B., Phillips, B. A., Tábara, L. C., Xiong, Q., Coria, R., Eichinger, L., Golstein, P., King, J. S., Soldati, T., Vincent, O., & Escalante, R. (2017). Autophagy in *Dictyostelium*: Mechanisms, regulation and disease in a simple biomedical model. *Autophagy*, *13*(1), 24–40. https://doi.org/10.1080/15548627.2016.1226737

Miranda, E. R., Zhuchenko, O., Toplak, M., Santhanam, B., Zupan, B., Kuspa, A., & Shaulsky, G. (2013). ABC transporters in *Dictyostelium discoideum* development. *PloS One*, *8*(8), e70040. https://doi.org/10.1371/journal.pone.0070040

Mizushima, N., Yoshimori, T., & Ohsumi, Y. (2011). The role of Atg proteins in autophagosome formation. *Annual Review of Cell and Developmental Biology*, *27*, 107–132. https://doi.org/10.1146/annurev-cellbio-092910-154005

Mole, S. E., & Cotman, S. L. (2015). Genetics of the neuronal ceroid lipofuscinoses (Batten disease). *Biochimica et Biophysica Acta*, *1852*(10 Pt B), 2237–2241. https://doi.org/10.1016/j.bbadis.2015.05.011

Monteith, A. J., Vincent, H. A., Kang, S., Li, P., Claiborne, T. M., Rajfur, Z., Jacobson, K., Moorman, N. J., & Vilen, B. J. (2018). mTORC2 activity disrupts lysosome acidification in systemic lupus erythematosus by impairing caspase-1 cleavage of Rab39a. *Journal of Immunology (Baltimore, Md.: 1950)*, *201*(2), 371–382. https://doi.org/10.4049/jimmunol.1701712

Mony, V. K., Benjamin, S., & O'Rourke, E. J. (2016). A lysosome-centered view of nutrient homeostasis. *Autophagy*, *12*(4), 619–631. https://doi.org/10.1080/15548627.2016.1147671

Moore, S. J., Buckley, D. J., MacMillan, A., Marshall, H. D., Steele, L., Ray, P. N., Nawaz, Z., Baskin, B., Frecker, M., Carr, S. M., Ives, E., & Parfrey, P. S. (2008). The clinical and genetic epidemiology of neuronal ceroid lipofuscinosis in Newfoundland. *Clinical Genetics*, *74*(3), 213–222. https://doi.org/10.1111/j.1399-0004.2008.01054.x

Mooren, O. L., Galletta, B. J., & Cooper, J. A. (2012). Roles for actin assembly in endocytosis. *Annual Review of Biochemistry*, *81*, 661–686. https://doi.org/10.1146/annurev-biochem-060910-094416

Mohammed, A., O'Hare, M. B., Warley, A., Tear, G., & Tuxworth, R. I. (2017). In vivo localization of the neuronal ceroid lipofuscinosis proteins, CLN3 and CLN7, at endogenous expression levels. *Neurobiology of Disease, 103*, 123–132. https://doi.org/10.1016/j.nbd.2017.03.015

Mukherjee, A. B., Appu, A. P., Sadhukhan, T., Casey, S., Mondal, A., Zhang, Z., & Bagh, M. B. (2019). Emerging new roles of the lysosome and neuronal ceroid lipofuscinoses. *Molecular neurodegeneration, 14*(1), 4. https://doi.org/10.1186/s13024-018-0300-6

Myre, M. A. , Huber, R. J. & O'Day, D. H. (2018). Functional analysis of proteins involved in neurodegeneration using the model organism *Dictyostelium*: Alzheimer's, Huntington's and Batten disease. In W. E.Crusio & R. T Gerlai (Eds.), *Molecular-Genetic and Statistical Techniques for Behavioral and Neural Research* (pp. 491–518). Elsevier, San Diego, CA.

Nah, J., Yuan, J., & Jung, Y. K. (2015). Autophagy in neurodegenerative diseases: from mechanism to therapeutic approach. *Molecules and Cells*, *38*(5), 381–389. https://doi.org/10.14348/molcells.2015.0034

Newell, P. C., Malchow, D., & Gross, J. D. (1995). The role of calcium in aggregation and development of *Dictyostelium. Experientia, 51*(12), 1155–1165. https://doi.org/10.1007/bf01944733

O'Day, D. H., Mathavarajah, S., Myre, M. A., & Huber, R. J. (2020). Calmodulin-mediated events during the life cycle of the amoebozoan *Dictyostelium discoideum. Biological reviews of the Cambridge Philosophical Society, 95*(2), 472–490. https://doi.org/10.1111/brv.12573

Otto, G. P., Wu, M. Y., Kazgan, N., Anderson, O. R., & Kessin, R. H. (2003). Macroautophagy is required for multicellular development of the social amoeba *Dictyostelium discoideum*. *The Journal of Biological Chemistry*, *278*(20), 17636–17645. https://doi.org/10.1074/jbc.M212467200

Otto, G. P., Wu, M. Y., Kazgan, N., Anderson, O. R., & Kessin, R. H. (2004). *Dictyostelium* macroautophagy mutants vary in the severity of their developmental defects. *The Journal of Biological Chemistry*, *279*(15), 15621–15629. https://doi.org/10.1074/jbc.M311139200

Pao, S. S., Paulsen, I. T., & Saier, M. H., Jr (1998). Major facilitator superfamily. *Microbiology and Molecular Biology Reviews*, *62*(1), 1–34. https://doi.org/10.1128/MMBR.62.1.1-34.1998

Persaud-Sawin, D. A., Mousallem, T., Wang, C., Zucker, A., Kominami, E., & Boustany, R. M. (2007). Neuronal ceroid lipofuscinosis: a common pathway?. *Pediatric Research*, *61*(2), 146–152. https://doi.org/10.1203/pdr.0b013e31802d8a4a

Phillips, J. E., & Gomer, R. H. (2010). The ROCO kinase QkgA is necessary for proliferation inhibition by autocrine signals in *Dictyostelium discoideum*. *Eukaryotic Cell*, *9*(10), 1557–1565. https://doi.org/10.1128/EC.00121-10

Phillips, J. E., & Gomer, R. H. (2014). The p21-Activated Kinase (PAK) family Member PakD is required FOR chemorepulsion and proliferation inhibition by autocrine signals in *Dictyostelium discoideum*. *PLoS One*, *9*(5). https://doi.org/10.1371/journal.pone.0096633

Phillips, J. E., & Gomer, R. H. (2015). Partial genetic suppression of a loss-of-function mutant of the neuronal ceroid lipofuscinosis-associated protease TPP1 in *Dictyostelium discoideum*. *Disease Models & Mechanisms*, *8*(2), 147–156. https://doi.org/10.1242/dmm.018820

Phillips, J. E., Huang, E., Shaulsky, G., & Gomer, R. H. (2011). The putative bZIP transcription factor BzpN slows proliferation and functions in the regulation of cell density by autocrine signals in *Dictyostelium*. PloS One, 6(7), e21765. https://doi.org/10.1371/journal.pone.0021765

Pillay, C. S., Elliott, E., & Dennison, C. (2002). Endolysosomal proteolysis and its regulation. *The Biochemical Journal*, *363*(Pt 3), 417–429. https://doi.org/10.1042/0264-6021:3630417

Platt F. M. (2018). Emptying the stores: lysosomal diseases and therapeutic strategies. *Nature Reviews Drug discovery*, *17*(2), 133–150. https://doi.org/10.1038/nrd.2017.214

Platt, F. M., d'Azzo, A., Davidson, B. L., Neufeld, E. F., & Tifft, C. J. (2018). Lysosomal storage diseases. *Nature reviews Disease Primers*, *4*(1), 27. https://doi.org/10.1038/s41572-018-0025-4

Puertollano R. (2014). mTOR and lysosome regulation. *F1000prime Reports*, *6*, 52. https://doi.org/10.12703/P6-52

Raben, N., Shea, L., Hill, V., & Plotz, P. (2009). Monitoring autophagy in lysosomal storage disorders. *Methods in Enzymology*, *453*, 417–449. https://doi.org/10.1016/S0076-6879(08)04021-4

Radke, J., Stenzel, W., & Goebel, H. H. (2015). Human NCL Neuropathology. *Biochimica et Biophysica Acta*, *1852*(10 Pt B), 2262–2266. https://doi.org/10.1016/j.bbadis.2015.05.007

Raisley, B., Zhang, M., Hereld, D., & Hadwiger, J. A. (2004). A cAMP receptor-like G protein-coupled receptor with roles in growth regulation and development. *Developmental Biology*, *265*(2), 433–445. https://doi.org/10.1016/j.ydbio.2003.09.035

Ravanel, K., de Chassey, B., Cornillon, S., Benghezal, M., Zulianello, L., Gebbie, L., Letourneur, F., & Cosson, P. (2001). Membrane sorting in the endocytic and phagocytic pathway of *Dictyostelium discoideum*. *European Journal of Cell Biology*, *80*(12), 754–764. https://doi.org/10.1078/0171-9335-00215

Rivero, F., & Maniak, M. (2006). Quantitative and microscopic methods for studying the endocytic pathway. *Methods in Molecular Biology (Clifton, N.J.)*, *346*, 423–438. https://doi.org/10.1385/1-59745-144-4:423

Rosel, D., Khurana, T., Majithia, A., Huang, X., Bhandari, R., & Kimmel, A. R. (2012). TOR complex 2 (TORC2) in *Dictyostelium* suppresses phagocytic nutrient capture independently of TORC1-mediated nutrient sensing. *Journal of Cell Science*, *125*(Pt 1), 37–48. https://doi.org/10.1242/jcs.077040

Rosenberg, J. B., Chen, A., Kaminsky, S. M., Crystal, R. G., & Sondhi, D. (2019). Advances in the treatment of neuronal ceroid lipofuscinosis. *Expert Opinion on Orphan Drugs*, *7*(11), 473–500. https://doi.org/10.1080/21678707.2019.1684258

Rossomando, E. F., Maldonado, B., Crean, E. V., & Kollar, E. J. (1978). Protease secretion during onset of development in *Dictyostelium discoideum*. *Journal of Cell Science*, *30*, 305–318.

Rot, G., Parikh, A., Curk, T., Kuspa, A., Shaulsky, G., & Zupan, B. (2009). Dictyexpress: A *Dictyostelium discoideum* gene expression database with an explorative data analysis web-based interface. *BMC Bioinformatics*, *10*(1). https://doi.org/10.1186/1471-2105-10-265

Saier, M. H., Jr, Reddy, V. S., Tsu, B. V., Ahmed, M. S., Li, C., & Moreno-Hagelsieb, G. (2016). The Transporter Classification Database (TCDB): recent advances. *Nucleic Acids Research*, *44*(D1), D372–D379. https://doi.org/10.1093/nar/gkv1103

Saxe, C. L., 3rd, Ginsburg, G. T., Louis, J. M., Johnson, R., Devreotes, P. N., & Kimmel, A. R. (1993). CAR2, a prestalk cAMP receptor required for normal tip formation and late development of *Dictyostelium discoideum*. *Genes & Development*, *7*(2), 262–272. https://doi.org/10.1101/gad.7.2.262

Saxton, R. A., & Sabatini, D. M. (2017). mTOR Signaling in Growth, Metabolism, and Disease. *Cell*, *168*(6), 960–976. https://doi.org/10.1016/j.cell.2017.02.004

Schaap, P., Nebl, T., & Fisher, P. R. (1996). A slow sustained increase in cytosolic Ca2+ levels mediates stalk gene induction by differentiation inducing factor in *Dictyostelium. The EMBO Journal, 15*(19), 5177–5183.

Schilde, C., Araki, T., Williams, H., Harwood, A., & Williams, J. G. (2004). GSK3 is a multifunctional regulator of *Dictyostelium* development. *Development (Cambridge, England)*, *131*(18), 4555–4565. https://doi.org/10.1242/dev.01330

Schröder, B., Wrocklage, C., Pan, C., Jäger, R., Kösters, B., Schäfer, H., Elsässer, H. P., Mann, M., & Hasilik, A. (2007). Integral and associated lysosomal membrane proteins. *Traffic (Copenhagen, Denmark)*, *8*(12), 1676–1686. https://doi.org/10.1111/j.1600-0854.2007.00643.x

Schulz, A., Ajayi, T., Specchio, N., de Los Reyes, E., Gissen, P., Ballon, D., Dyke, J. P., Cahan, H., Slasor, P., Jacoby, D., Kohlschütter, A., & CLN2 Study Group (2018). Study of intraventricular cerliponase alfa for CLN2 Disease. *The New England Journal of Medicine*, *378*(20), 1898–1907. https://doi.org/10.1056/NEJMoa1712649

Schulz, A., Kohlschütter, A., Mink, J., Simonati, A., & Williams, R. (2013). NCL diseases - clinical perspectives. *Biochimica et Biophysica Acta*, *1832*(11), 1801–1806. https://doi.org/10.1016/j.bbadis.2013.04.008

Settembre, C., Fraldi, A., Jahreiss, L., Spampanato, C., Venturi, C., Medina, D., de Pablo, R., Tacchetti, C., Rubinsztein, D. C., & Ballabio, A. (2008). A block of autophagy in lysosomal storage disorders. *Human Molecular Genetics*, *17*(1), 119–129. https://doi.org/10.1093/hmg/ddm289

Sharifi, A., Kousi, M., Sagné, C., Bellenchi, G. C., Morel, L., Darmon, M., Hulková, H., Ruivo, R., Debacker, C., El Mestikawy, S., Elleder, M., Lehesjoki, A. E., Jalanko, A., Gasnier, B., & Kyttälä, A. (2010). Expression and lysosomal targeting of CLN7, a major facilitator superfamily transporter associated with variant late-infantile neuronal ceroid lipofuscinosis. *Human Molecular Genetics*, *19*(22), 4497–4514. https://doi.org/10.1093/hmg/ddq381

Siegert, F., & Weijer, C. J. (1991). Analysis of optical density wave propagation and cell movement in the cellular slime mould *Dictyostelium discoideum. Physica D: Nonlinear Phenomena*, *49*(1-2), 224–232. https://doi.org/10.1016/0167-2789(91)90210-z

Siegert, F., & Weijer, C. J. (1992). Three-dimensional scroll waves organize *Dictyostelium* slugs. *Proceedings of the National Academy of Sciences*, *89*(14), 6433–6437. https://doi.org/10.1073/pnas.89.14.6433

Siintola, E., Topcu, M., Aula, N., Lohi, H., Minassian, B. A., Paterson, A. D., Liu, X. Q., Wilson, C., Lahtinen, U., Anttonen, A. K., & Lehesjoki, A. E. (2007). The novel neuronal ceroid lipofuscinosis gene *MFSD8* encodes a putative lysosomal transporter. *American Journal of Human Genetics*, *81*(1), 136–146. https://doi.org/10.1086/518902

Singleton, C. K., Kirsten, J. H., & Dinsmore, C. J. (2006). Function of ammonium transporter A in the initiation of culmination of development in *Dictyostelium discoideum*. *Eukaryotic Cell*, *5*(7), 991–996. https://doi.org/10.1128/EC.00058-06

Smith, P. K., Sen, M. G., Fisher, P. R., & Annesley, S. J. (2019). Modelling of neuronal ceroid lipofuscinosis type 2 in *Dictyostelium discoideum* suggests That cytopathological outcomes Result from Altered TOR Signalling. *Cells*, *8*(5), 469. https://doi.org/10.3390/cells8050469

Søreng, K., Neufeld, T. P., & Simonsen, A. (2018). Membrane trafficking in autophagy. *International Review of Cell and Molecular Biology*, *336*, 1–92. https://doi.org/10.1016/bs.ircmb.2017.07.001

Steenhuis, P., Froemming, J., Reinheckel, T., & Storch, S. (2012). Proteolytic cleavage of the disease-related lysosomal membrane glycoprotein CLN7. *Biochimica et Biophysica Acta*, *1822*(10), 1617–1628. https://doi.org/10.1016/j.bbadis.2012.05.015

Steenhuis, P., Herder, S., Gelis, S., Braulke, T., & Storch, S. (2010). Lysosomal targeting of the CLN7 membrane glycoprotein and transport via the plasma membrane require a dileucine motif. *Traffic (Copenhagen, Denmark)*, *11*(7), 987–1000. https://doi.org/10.1111/j.1600-0854.2010.01073.x

Stumpf, M., Müller, R., Gaßen, B., Wehrstedt, R., Fey, P., Karow, M. A., Eichinger, L., Glöckner, G., & Noegel, A. A. (2017). A tripeptidyl peptidase 1 is a binding partner of the Golgi pH regulator (GPHR) in *Dictyostelium*. *Disease Models & Mechanisms*, *10*(7), 897–907. https://doi.org/10.1242/dmm.029280

Tang, Y., Wu, Y., Herlihy, S. E., Brito-Aleman, F. J., Ting, J. H., Janetopoulos, C., & Gomer, R. H. (2018). An autocrine proliferation repressor regulates *Dictyostelium discoideum* proliferation and chemorepulsion using the G protein-coupled receptor GrlH. *mBio*, *9*(1), e02443-17. https://doi.org/10.1128/mBio.02443-17

Tarantola, M., Bae, A., Fuller, D., Bodenschatz, E., Rappel, W. J., & Loomis, W. F. (2014). Cell substratum adhesion during early development of *Dictyostelium discoideum*. *PloS One*, *9*(9), e106574. https://doi.org/10.1371/journal.pone.0106574

Tjelle, T. E., Brech, A., Juvet, L. K., Griffiths, G., & Berg, T. (1996). Isolation and characterization of early endosomes, late endosomes and terminal lysosomes: their role in protein degradation. *Journal of Cell Science*, *109 (Pt 12)*, 2905–2914.

Trivedi, P. C., Bartlett, J. J., & Pulinilkunnil, T. (2020). Lysosomal biology and function: Modern view of cellular debris bin. *Cells*, *9*(5), 1131. https://doi.org/10.3390/cells9051131

Tsuji, Y. (2020). Transmembrane protein western blotting: Impact of sample preparation on detection of SLC11A2 (DMT1) and SLC40A1 (ferroportin). *PLoS One,* 15(7): e0235563. https://doi.org/10.1371/journal.pone.0235563

Tsujioka, M., Yoshida, K., & Inouye, K. (2004). Talin B is required for force transmission in morphogenesis of *Dictyostelium*. *The EMBO Journal*, *23*(11), 2216–2225. https://doi.org/10.1038/sj.emboj.7600238

Tuxworth, R. I., Cheetham, J. L., Machesky, L. M., Spiegelmann, G. B., Weeks, G., & Insall, R. H. (1997). *Dictyostelium* RasG is required for normal motility and cytokinesis, but not growth. *The Journal of Cell Biology*, *138*(3), 605–614. https://doi.org/10.1083/jcb.138.3.605

Uchikawa, T., Yamamoto, A., & Inouye, K. (2011). Origin and function of the stalk cell vacuole in *Dictyostelium*. *Developmental Biology*, *352*(1), 48–57. https://doi.org/10.1016/j.ydbio.2011.01.014

van Diggelen, O. P., Keulemans, J. L., Winchester, B., Hofman, I. L., Vanhanen, S. L., Santavuori, P., & Voznyi, Y. V. (1999). A rapid fluorogenic palmitoyl-protein thioesterase assay: pre- and postnatal diagnosis of INCL. *Molecular Genetics and etabolism*, *66*(4), 240–244. https://doi.org/10.1006/mgme.1999.2809

Van Haastert, P. J., Bishop, J. D., & Gomer, R. H. (1996). The cell density factor CMF regulates the chemoattractant receptor cAR1 in *Dictyostelium. The Journal of Cell Biology, 134*(6), 1543–1549. https://doi.org/10.1083/jcb.134.6.1543

Veltman, D. M., Akar, G., Bosgraaf, L., & Van Haastert, P. J. M. (2009). A new set of small, extrachromosomal expression vectors for *Dictyostelium discoideum*. *Plasmid*, *61*(2), 110–118. https://doi.org/10.1016/j.plasmid.2008.11.003

Villines, H.L. & Hadwiger, J.A. (2017). Do CrlA and Ga5 Function in the Same Pathway. *Research Reports from Life Science Freshmen Research Scholars, 3*(1).

von Kleist, L., Ariunbat, K., Braren, I., Stauber, T., Storch, S., & Danyukova, T. (2019). A newly generated neuronal cell model of CLN7 disease reveals aberrant lysosome motility and impaired cell survival. *Molecular Genetics and Metabolism*, *126*(2), 196–205. https://doi.org/10.1016/j.ymgme.2018.09.009

Wang, G. (2014). Basic genetics: The cell, mitosis and meiosis, and mendelian laws. In: S. Padmanabhan (Eds), *Handbook of Pharmacogenomics and Stratified Medicine* (pp. 29–40). Academic Press. https://doi.org/10.1016/b978-0-12-386882-4.00002-5

Williams, R.E. (2011) NCL incidence and prevalence data. In: S. Mole, R. Williams, H, Goebel, (Eds), *The Neuronal Ceroid Lipofuscinoses (Batten Disease) 2nd ed* (pp. 361-365). Oxford: OUP Oxford

Winckler, T., Trautwein, C., Tschepke, C., Neuhäuser, C., Zündorf, I., Beck, P., Vogel, G., & Dingermann, T. (2001). Gene function analysis by amber stop codon suppression: CMBF is a nuclear protein that supports growth and development of *Dictyostelium* amoebae. *Journal of Molecular Biology*, *305*(4), 703–714. https://doi.org/10.1006/jmbi.2000.4341

Yasa, S., Sauvageau, E., Modica, G., & Lefrancois, S. (2021). CLN5 and CLN3 function as a complex to regulate endolysosome function. *The Biochemical Journal*, *478*(12), 2339–2357. https://doi.org/10.1042/BCJ20210171

Yu, L., McPhee, C. K., Zheng, L., Mardones, G. A., Rong, Y., Peng, J., Mi, N., Zhao, Y., Liu, Z., Wan, F., Hailey, D. W., Oorschot, V., Klumperman, J., Baehrecke, E. H., & Lenardo, M. J. (2010). Termination of autophagy and reformation of lysosomes regulated by mTOR. *Nature*, *465*(7300), 942–946. https://doi.org/10.1038/nature09076

Yuen, I. S., Jain, R., Bishop, J. D., Lindsey, D. F., Deery, W. J., Van Haastert, P. J., & Gomer, R. H. (1995). A density-sensing factor regulates signal transduction in *Dictyostelium*. *Journal of Cell Biology*, *129*(5), 1251–1262. https://doi.org/10.1083/jcb.129.5.1251

7.0 Appendix

Additional publications not included in thesis

Huber, R. J., Mathavarajah, S., & Yap, S. Q. (2020). Mfsd8 localizes to endocytic compartments and influences the secretion of Cln5 and cathepsin D in *Dictyostelium. Cellular Signalling, 70*, 109572. https://doi.org/10.1016/j.cellsig.2020.109572

Kim, W. D., Yap, S. Q., & Huber, R. J. (2021). A proteomics analysis of calmodulin-binding proteins in *Dictyostelium discoideum* during the transition from unicellular Growth to multicellular development. *International Journal of Molecular Sciences, 22*(4), 1722. https://doi.org/10.3390/ijms22041722

Yap, S. Q., Mathavarajah, S., & Huber, R. J. (2021). The converging roles of Batten disease proteins in neurodegeneration and cancer. *iScience, 24*(4), 102337. https://doi.org/10.1016/j.isci.2021.102337

McLaren, M. D., Mathavarajah, S., Kim, W. D., Yap, S. Q., & Huber, R. J. (2021). Aberrant autophagy impacts growth and multicellular development in a *Dictyostelium* knockout model of CLN5 disease. *Frontiers in Cell and Developmental Biology,* 9, 657406. https://doi.org/10.3389/fcell.2021.657406